



HAL
open science

Modeling and design of 3D Imager IC

Vijayaragavan Viswanathan

► **To cite this version:**

Vijayaragavan Viswanathan. Modeling and design of 3D Imager IC. Other. Ecole Centrale de Lyon, 2012. English. NNT: 2012ECDL0022 . tel-00795558

HAL Id: tel-00795558

<https://theses.hal.science/tel-00795558>

Submitted on 28 Feb 2013

HAL is a multi-disciplinary open access archive for the deposit and dissemination of scientific research documents, whether they are published or not. The documents may come from teaching and research institutions in France or abroad, or from public or private research centers.

L'archive ouverte pluridisciplinaire **HAL**, est destinée au dépôt et à la diffusion de documents scientifiques de niveau recherche, publiés ou non, émanant des établissements d'enseignement et de recherche français ou étrangers, des laboratoires publics ou privés.

ECOLE CENTRALE DE LYON

ECOLE DOCTORALE Electronique, Electrotechnique, Automatique

Institut des Nanotechnologies de Lyon

Année : 2012

Thèse Numero :

Thèse

pour obtenir le grade de

DOCTEUR DE L'ECOLE CENTRALE DE LYON

Discipline : Electronique

présentée et soutenue par

Vijayaragavan VISWANATHAN

le Jeudi 6 Septembre 2012

Modeling and design of 3D Imager IC

Thèse dirigée par **Ian O'CONNOR**

JURY :

Luc HEBRARD	Professeur, InESS, Université de Strasbourg	Président
Yusuf LEBLEBICI	Professeur, Ecole Polytechnique Federale de Lausanne	Rapporteur
Patrick GARDA	Professeur, LIP6, Université Pierre et Marie Curie	Rapporteur
Olivier LE BRIZ	INGÉNIEUR, ST- Microelectronics	Examineur
Ian O'CONNOR	Professeur, Ecole Centrale de Lyon	Examineur
David NAVARRO	Maitre de Conference, Ecole Centrale de Lyon	Examineur
Lioua LABRAK	Post-doctorant, Ecole Centrale de Lyon	Examineur

To my parents and my wife

Acknowledgement

I would like to first and foremost thank my advisor Professor Ian O'Connor for his invaluable guidance, support, and for the encouragement he gave me during this thesis work. His valuable support, insightful comments have made my Ph.D life very memorable and enjoyable. Not only did he give me great advice for my research, but has been and is a great mentor for me. I truly appreciate it. I am thankful for the precious time spent on reviewing this thesis.

I am grateful to Dr.David Navarro for being my associate advisor. I am thankful for all the valuable time spend in discussion and to help me intellectually. I am grateful for the support he gave in using different tools and sharing knowledge on image sensors. I also thank Dr.Lioua Labrak who has been along with me all the time from the day I started the Ph.D. The numerous discussions and sharing of knowledge have made me stronger in the subject. I would like to thank both of them for reviewing this thesis.

I would like to show my gratitude for my colleagues at INL. I would especially like to thank Felipe Frantz who is always willing to share his knowledge. I thank him for the support he rendered all the time both at personal and professional level. I would also like to thank all the partners from the 3D-IDEAS project for the support during this project. My time at INL has intellectually and socially enriched by friends I have made. I thank all my former and current officemates Wan Du, Zhenfu, Nanhao, Zhen Li, Mihai Galos, Jabeur Kotb, Nataliya and Bo Wang. I also thank Laurent Carrel for the support. I would like to thank Patricia Dufaut, Nicole Durand, Sylvie Goncalves for their administrative support and making my stay at INL a pleasant one.

I would like to thank my extended family which I am lucky enough to have during these three years of stay in France. I am sure a word of thanks will not suffice for the amount of support they have given me. Especially I am indebted to Mr &Mrs. Berlier, Agnes Prat, Jean Francois Prat (Mamma & Pappa) and their family for making my stay a wonderful one. Ariane , Eric are one another family which I cannot forget at all times of my life. Thanks a lot. Massimo, Andrea, Meng, Aurelie, Remi, Jerome, Dawn, Franck, Peter, Pascale, Elisabeth, Joelle are few friends who made my stay a wonderful one. I wish to thank all my Indian friends in Lyon for the support and fun times had together. To name some of them Roy, Sudipta, Manjunath, Shwetha, Deepak, Preeti, Karthik. Thanks all.

Last but not the least, I owe my life to few people: Firstly, I would like to thank my better half and my dear wife Mamatha for her understanding, belief and support all these years. I thank her for being patient and supporting me all the time. I would like to thank my role model in life, my father and mother. Thanks to all the sacrifice you have made all these years for me to come up in life. I am here only because of them. I would like to thank my uncle and my all time support, Jayaraman for his kind support and love. I owe a big thanks to my beloved sisters and my aunt for being always with me. Also would like to thank all my in-laws who made my life a better one. To name a few Anjanamurthy, Dhanalakshmi, Asha, Rupesh, Ajay, Deepu, Nirmala, Geetha and all their family.

I would like to say a special thank you to Ananthanarayanan, P.V.Gopi, Pallavi Reddy, Jayakrishnan, Karthick, Anjali, Aparna, Naga, Ganesh without whom I must have not decided to pursue higher studies. Thanks to all!

Abstract

CMOS image sensor based on Active pixel sensor has considerably contributed to the imaging market and research interest in the past decade. Furthermore technology advancement has provided the capability to integrate more and more functionality into a single chip in multiple layers leading to a new paradigm, 3D integration. CMOS image sensor is one such application which could utilize the capability of 3D stacked architecture to achieve dedicated technologies in different layers, wire length reduction, less area, improved performances

This research work is focused mainly on the early stages of design space exploration using hierarchical approach and aims at reducing time to market. This work investigates the imager from the top-down design perspective. Methodical analysis of imager is performed to achieve high level of flexibility and modularity. Re-useable models are developed to explore early design choices throughout the hierarchy. Finally, pareto front (providing trade off solutions) methodology is applied to explore the operating range of individual block at system level to help the designer making his design choice. Furthermore the thermal issues which get aggravated in the 3D stacked chip on the performance of the imager are studied.

SystemC based thermal model is built to investigate the behavior of imager pixel matrix and to simulate the pixel matrix at high speed with acceptable accuracy compared to electrical simulations. The modular nature of the model makes simulations with future matrix extension straightforward. Validation of the thermal model with respect to electrical simulations is discussed. Finally an integrated design flow is developed to perform 3D floorplanning and to perform thermal analysis of the imager pixel matrix.

Contents

Acknowledgement.....	i
Abstract.....	iii
Contents.....	iv
List of Figures.....	vii
List of Tables.....	ix
Glossary.....	x
CHAPTER 1 - INTRODUCTION.....	1
1.1 Imager.....	1
1.1.1 The rise of the CMOS image sensor.....	3
1.1.2 CMOS Active Pixel Sensor.....	4
1.1.3 CMOS image sensor performance metrics.....	5
1.1.4 CMOS image sensor noise.....	6
1.2 3D technology.....	8
1.2.1 Trend.....	8
1.2.2 Opportunities.....	9
1.2.3 Issues.....	13
1.2.4 3D Imager.....	17
1.3 Research focus.....	17
1.3.1 Scalability - Technology.....	17
1.3.2 Simulation scalability– Pixel matrix.....	19
1.4 Key research contributions.....	20
1.5 Thesis outline.....	21
Bibliography.....	22
CHAPTER 2 - MODELING AND DESIGN.....	26
2.1 Introduction.....	26
2.2 System description.....	27
2.2.1 Pixel matrix.....	27
2.2.2 ADC.....	29
2.3 Methodology.....	30
2.3.1 Modeling.....	30
2.4 Parameter dependency graph.....	34
2.4.1 Formulation.....	34
2.4.2 Frames per second (FPS) dependency graph.....	36
2.4.3 Dynamic Range (DR) dependency graph.....	37
2.4.4 Signal to Noise Ratio (SNR) dependency graph.....	38

2.5	Abstraction	39
2.5.1	Segregation of abstractions	39
2.5.2	Formulation	41
2.6	Results	42
2.6.1	Pixel matrix	42
2.6.1.1	System level.....	42
2.6.1.2	Behavioral level.....	43
2.6.1.3	Accurate behavioral level	45
2.6.2	ADC - Results.....	46
2.6.2.1	System level.....	47
2.6.2.2	Behavioral level – DAC	50
2.6.2.3	Behavioral level - Comparator	51
2.7	Pareto-front methodology.....	53
2.7.1	Methodology.....	54
2.7.2	Pixel pareto-front - Results.....	55
2.8	Conclusion	58
	Bibliography	60

CHAPTER 3 - THERMAL-AWARE IMAGE SENSOR MODEL 62

3.1	Introduction	62
3.2	Thermal Model	63
3.2.1	Problems and requirements	63
3.2.2	Compact thermal model.....	64
3.2.3	Model development steps	65
3.3	Exhaustive data generation.....	67
3.3.1	Pixel behavior	67
3.3.2	Imager thermal model.....	68
3.3.3	Electrical simulations	69
3.4	Fitting	71
3.4.1	Types of fitting	71
3.4.2	Surface fitting	72
3.4.3	Volume fitting.....	74
3.5	Pre-Validation	77
3.5.1	Requirement.....	77
3.5.2	Preliminary results	79
3.5.3	Fitting order accuracy.....	81
3.6	Integrated simulation environment	87
3.6.1	SystemC.....	87
3.6.2	Image processing.....	88
3.6.3	SystemC-based pixel matrix model	89
3.6.4	Model integration.....	91
3.6.5	Simulation speed	91
3.7	Post-validation.....	94
3.7.1	Matrix simulation.....	94
3.7.2	Test case I (128*128 “lena”).....	95
3.7.3	Test case II (256*256 lena).....	97
3.7.4	Test case III (White picture)	99
3.8	Inference	102

Bibliography	103
CHAPTER 4 - 3D INTEGRATED DESIGN FLOW	105
4.1 Introduction	105
4.1.1 3D stacked chip	105
4.1.2 Integrated design flow	106
4.2 3D Floorplanning	108
4.2.1 Thermal floorplanning	108
4.2.2 Floorplanner algorithm	109
4.2.3 Floorplanner options	110
4.3 Thermal Simulation	113
4.3.1 Thermal-aware floorplanning	113
4.3.2 Two-phase algorithm	115
4.3.3 Thermal simulation options	117
4.4 3D Integrated design flow	119
4.4.1 Design flow characteristics	119
4.5 Results	121
4.5.1 Test cases	121
4.5.2 Test case I – Compact area	125
4.5.3 Testcase II – Minimizing temperature	128
4.5.4 Testcase III - Longer iteration	132
4.5.5 Testcase IV – UseHeuristics	136
4.6 Conclusion	140
Bibliography	144
CHAPTER 5 - CONCLUSION	146
5.1 Summary and discussion of achievements	146
5.2 Future perspectives	150
Appendix I – Surface fitting	152
Appendix II – Volume fitting	154
Appendix III – Tool I/O configuration	158
Publications	162

List of figures

FIGURE 1.1	IMAGING PIPELINE [1]	2
FIGURE 1.2	APS STRUCTURE	4
FIGURE 1.3	3D ROADMAP [16]	9
FIGURE 1.4	INTECONNECT DELAY [18]	10
FIGURE 1.5	2D VS 3D WIRELENGTH DISTRIBUTION [18]	10
FIGURE 1.6	3D IC FABRICATION PROCESS [19].....	11
FIGURE 1.7	HETEROGENEOUS INTEGRATION [22].....	12
FIGURE 2.1	IMAGER BLOCKS	27
FIGURE 2.2	3T APS STRUCTURE	28
FIGURE 2.3	SAR ARCHITECTURE[6]	29
FIGURE 2.4	DESIGN AND MODELING	31
FIGURE 2.5	PROBLEM FORMULATION	32
FIGURE 2.6	DESIGN HIERARCHY	33
FIGURE 2.7	PARAMETER DEPENDENCY GRAPH	35
FIGURE 2.8	FPS DEPENDENCY GRAPH	36
FIGURE 2.9	DYNAMIC RANGE DEPENDENCY GRAPH	37
FIGURE 2.10	SNR DEPENDENCY GRAPH	38
FIGURE 2.11	ABSTRACTION LEVELS.....	39
FIGURE 2.12	PIXEL MATRIX STRUCTURE	40
FIGURE 2.13	ABSTRACTION LEVEL INPUT/OUTPUTS.....	41
FIGURE 2.14	SYSTEM LEVEL COST FUNCTION OPTIMIZATION GRAPH.....	43
FIGURE 2.15	BEHAVIOR LEVEL COST FUNCTION OPTIMIZATION GRAPH.....	45
FIGURE 2.16	ACCURATE BEHAVIOR LEVEL COST FUNCTION OPTIMIZATION GRAPH	47
FIGURE 2.17	ADC SYSTEM LEVEL COST FUNCTION OPTIMIZATION GRAPH	49
FIGURE 2.18	ADC- BEHAVIORAL LEVEL COST FUNCTION OPTIMIZATION CURVE	53
FIGURE 2.19	PARAMETER SPACE (LEFT) AND PERFORMANCE SPACE (RIGHT)[19]	54
FIGURE 2.20	DYNAMIC RANGE EVOLUTION	56
FIGURE 2.21	SNR EVOLUTION	56
FIGURE 2.22	AREA EVOLUTION.....	57
FIGURE 2.23	PIXEL PARETO-FRONT.....	57
FIGURE 3.1	HOTSPOT MODEL [5]	64
FIGURE 3.2	BOTTOM-UP APPROACH	66
FIGURE 3.3	MODEL DEVELOPMENT PROCESS.....	66
FIGURE 3.4	(A) 3T-APS STRUCTURE (B) TIMING GRAPH	67
FIGURE 3.5	(A) CHARGE VS TIME (B) DISCHARGE VOLTAGE VS TEMPERATURE (@10MSINTEGRATION)	68
FIGURE 3.6	PIXEL SCHEMATIC WITH SIZED PARAMETERS	69
FIGURE 3.7	PARAMETRIC SIMULATION INPUT AND OUTPUT	70
FIGURE 3.8	SURFACE FITTING WITH TWO VARIABLES	74
FIGURE 3.9	PHOTODIODE DISCHARGE VOLTAGE	76
FIGURE 3.10	READOUT VOLTAGE	77
FIGURE 3.11	SIGNAL PATH OF PROPOSED MODEL	77
FIGURE 3.12	LIGHT INTENSITY VS GREY SCALE INTENSITY	78
FIGURE 3.13	PRE-VALIDATION MODEL VS SPICE SIMULATION.....	79
FIGURE 3.14	PRE-VALIDATION (T=300K, TINT=10MS)	80
FIGURE 3.15	PRE-VALIDATION (T=325K, TINT =10MS)	80
FIGURE 3.16	PRE-VALIDATION (T=350K, TINT =10MS)	81
FIGURE 3.17	AVERAGE ERROR AT 300K FOR VARIOUS VALUES OF INTEGRATION TIME	83
FIGURE 3.18	AVERAGE ERROR AT 350K FOR VARIOUS VALUES OF INTEGRATION TIME	83
FIGURE 3.19	AVERAGE ERROR ACROSS THE SYSTEM OPERATIONAL RANGE FOR VARIOUS ORDERS OF FITTING.....	84
FIGURE 3.20	READOUT VOLTAGE AT BRIGHT LIGHT AND 350K	85

FIGURE 3.21	AVERAGE ERROR AT 300K WITH READOUT THRESHOLD CRITERIA	86
FIGURE 3.22	AVERAGE ERROR AT 350K WITH READOUT THRESHOLD CRITERIA	86
FIGURE 3.23	AVERAGE ERROR FOR READOUT THRESHOLD VOLTAGE OVER ENTIRE SYSTEM RANGE	87
FIGURE 3.24	C++ BASED IMAGE CONVERSION	88
FIGURE 3.25	INTENSITY BASED HIS (LEFT), GREYSCALE (RIGHT).....	89
FIGURE 3.26	SYSTEMC MODEL BLOCK DIAGRAM.....	90
FIGURE 3.27	SYSTEMC MODEL SIMULATION TIME.....	92
FIGURE 3.28	SIMULATION TIME COMPARISON	93
FIGURE 3.29	POST VALIDATION STEPS AND USED TOOLS	95
FIGURE 3.30	POST VALIDATION AT T=300K AND TINT=8MS (AVERAGE ERROR = 139uV)	96
FIGURE 3.31	POST VALIDATION AT T=350K, TINT =10MS (AVERAGE ERROR = 101uV).....	97
FIGURE 3.32	POST VALIDATION AT T=300K, TINT=8MS (AVERAGE ERROR =20.55uV)	98
FIGURE 3.33	POST VALIDATION AT T=350K, TINT=10MS (AVERAGE ERROR =129.4uV)	99
FIGURE 3.34	POST VALIDATION AT T=300K, TINT=10MS (AVERAGE ERROR = 1.2MV).....	100
FIGURE 3.35	POST VALIDATION AT T=325K, TINT=10MS (AVERAGE ERROR =1.3MV)	100
FIGURE 3.36	ELECTRICAL SIMULATION (T=350K, TINT=10MS)	101
FIGURE 3.37	POST VALIDATION AT T=350K, TINT=10MS	102
FIGURE 4.1	3D STACKED CHIP.....	105
FIGURE 4.2	IMAGER THERMAL MODEL INPUT/OUTPUT	106
FIGURE 4.3	INTEGRATED DESIGN FLOWCHART	107
FIGURE 4.4	WORKFLOW [8].....	110
FIGURE 4.5	(A) NO SCALING (B) SCALED –DEFAULT (C) CENTERED [8]	112
FIGURE 4.6	SIMPLIFIED THERMAL MODEL [10].....	113
FIGURE 4.7	(A) VERTICAL HEAT FLOW MODEL (B)POWER DISTRIBUTION PROFILE THAT MINIMIZES TEMPERATURE	115
FIGURE 4.8	TWO-PHASE ALGORITHM AND THE SWITCHING CRITERIA	116
FIGURE 4.9	THERMAL PROFILE OF EACH LAYER ALONG A CROSS SECTION OF THE X-Y PLANE.....	116
FIGURE 4.10	(A) LAYER 0 (TOP) (B) LAYER 1 (BOTTOM)	118
FIGURE 4.11	3D INTEGRATED DESIGN FLOW	119
FIGURE 4.12	3D STACK – AMI33 – 4 LAYER STRUCTURE.....	121
FIGURE 4.13	“LENA” PICTURE INPUT TO IMAGER THERMAL MODEL.....	122
FIGURE 4.14	INPUT INTENSITY OF “WHITE PICTURE” TO IMAGER THERMAL MODEL.....	123
FIGURE 4.15	READOUT VOLTAGE - REFERENCE SIMULATION (TINT=10MS, TEMPERATURE=300K).....	123
FIGURE 4.16	READOUT VOLTAGE – REFERENCE SIMULATION (TINT=10MS, TEMPERATURE=300K)	124
FIGURE 4.17	TEST CASE 1 RESULT – THERMAL MAP	125
FIGURE 4.18	TESTCASE I RESULT – LENA PICTURE – READOUT VOLTAGE	126
FIGURE 4.19	TESTCASE I RESULT- WHITE PICTURE – READOUT VOLTAGE	127
FIGURE 4.20	TEST CASE I TEMPERATURE DISTRIBUTION.....	128
FIGURE 4.21	TEST CASE II RESULTS – THERMAL MAP.....	129
FIGURE 4.22	TESTCASE II RESULTS – LENA PICTURE – READOUT VOLTAGE.....	130
FIGURE 4.23	TESTCASE II RESULTS – WHITE PICTURE – READOUT VOLTAGE	131
FIGURE 4.24	TEST CASE II TEMPERATURE DISTRIBUTION.....	132
FIGURE 4.25	TEST CASE III RESULTS – THERMAL MAP.....	133
FIGURE 4.26	TESTCASE III RESULT – LENA PICTURE – READOUT VOLTAGE	134
FIGURE 4.27	TESTCASE III RESULT – WHITE PICTURE – READOUT VOLTAGE.....	135
FIGURE 4.28	TEST CASE III TEMPERATURE DISTRIBUTION.....	136
FIGURE 4.29	TEST CASE IV RESULTS – THERMAL MAP	137
FIGURE 4.30	TESTCASE IV RESULTS – LENA PICTURE – READOUT VOLTAGE.....	138
FIGURE 4.31	TESTCASE IV – WHITE PICTURE – READOUT VOLTAGE.....	139
FIGURE 4.32	TEST CASE IV TEMPERATURE DISTRIBUTION.....	140
FIGURE 4.33	TESTCASE RESULTS – AVERAGE ERROR	141
FIGURE 4.34	GRADIENT VS AREA	142
FIGURE 4.35	MAXIMUM TEMPERATURE VS AREA	142
FIGURE 5.1	HIGH LEVEL FLOW DIAGRAM	148

List of Tables

TABLE 1-1	TSV PARAMETER PROJECTIONS IN 2011 ITRS ROADMAP[20]	11
TABLE 2-1	SYSTEM LEVEL INPUT AND OUTPUTS	43
TABLE 2-2	BEHAVIOR LEVEL INPUT AND OUTPUT	44
TABLE 2-3	Pixel matrix - ACCURATE BEHAVIORAL LEVEL INPUT AND OUTPUT	46
TABLE 2-4	ADC SYSTEM LEVEL INPUT AND OUTPUT	49
TABLE 2-5	DAC OUTPUT AND INPUTS	52
TABLE 2-6	COMPARATOR INPUT AND OUTPUTS	52
TABLE 3-1	PARAMETRIC SIMULATION OPERATIONAL RANGE	70
TABLE 3-2	FITTING ORDER	75
TABLE 3-3	SIMULATION DATA – AVERAGE ERROR (IN VOLTS & IN %)	82
TABLE 3-4	SIMULATION TIME COMPARISON	93
TABLE 3-5	AVERAGE ERROR – 128*128 LENA PICTURE	96
TABLE 3-6	AVERAGE ERROR – 256*256 LENA PICTURE	98
TABLE 4-1	TEST CASES	122
TABLE 4-2	TEST CASE I – COMPACT AREA - REPORT	126
TABLE 4-3	COMPARATIVE RESULTS (REFERENCE VS TESTCASE I)	127
TABLE 4-4	TESTCASE II – MINIMIZATION TEMPERATURE - REPORT	130
TABLE 4-5	COMPARATIVE RESULTS (REFERENCE VS TESTCASE II)	131
TABLE 4-6	TESTCASE III – LONGER ITERATION WITH TEMPERATURE MINIMIZATION - REPORT	134
TABLE 4-7	COMPARATIVE RESULTS (REFERENCE VS TESTCASE III)	135
TABLE 4-8	TESTCASE IV – USEHEURISTICS - REPORT	138
TABLE 4-9	COMPARATIVE RESULTS (REFERENCE VS TESTCASE IV)	139
TABLE 4-10	AVERAGE ERROR	141

Glossary

CMOS Complimentary Metal Oxide Semiconductor

CISs CMOS Image Sensors

APS Active Pixel Sensor

ADC Analog-to-Digital Conversion

CCDs- Charged Coupled Devices

CDS - Correlated Double Sampling

ISP Image Signal Processor

ENOB Effective Number Of Bits

FPN Fixed Pattern Noise

MOS Metal-Oxide-Semiconductor

MSB Most Significant Bit

PPS Passive Pixel Sensor

PRNU Photo Response Non-Uniformity

QE Quantum Efficiency

SNR Signal-to-Noise Ratio

RAM Random Access Memory

SF Source Follower

AMS Austria Micro Systems

MP MegaPixel

DR Dynamic Range

SNR Signal to Noise ration

FPS Frames Per Second

FF Fill factor

3D-IC Three-Dimensional Integrated Circuit

Chapter 1

Introduction

In the past decade, semiconductor companies around the world started investing in the area of image sensors. On the technology point of view, CMOS Image Sensors (CIS) have become mature and attractive to produce in mass quantities. On the application point of view, CIS and its capability is utilized in various sectors pertaining to various application areas such as: commercial applications (toys, digital cameras, web cameras etc.), industrial sector (machine vision, automotive, quality control etc.), security sector (security cameras, motion detection, finger print ID, target tracking, spy cameras etc.) and it is also used in space applications. On the business point of view, the know-how in the IC design and fabrication process has increase the chance to be successful and meet the market demand on large array formats, high image quality, low cost, low power. Current technology advancement i.e 3D technology has advantage of small foot print imagers, dedicated technology (analog, digital etc.) for different layers is becoming more and more attractive because of cost and optimized performance. In this research work we will focus on the 3D imager IC.

In the section 1.1 we will see how an imager functions, the rise of CIS technology, CMOS APS structure, CIS performance metrics, CIS noise sources. Section 1.2 describes in detail the 3D technology trend, opportunities and issues. Section 1.3 describes in detail the research focus and followed by research contribution in section 1.4 and finally thesis outline is described in section 1.5.

1.1 Imager

An imager is an array of photosensitive devices that convert optical information into electronic signals. Firstly, the image scene is focused on the image sensor with the help of imaging optics. If the application requires it, a color filter array is placed during fabrication on top of

the image sensor arrays for color sensing. Because of the color filter, each pixel behind the filter array produces an electrical signal corresponding to one single color (red, green or blue). An analog-to-digital converter (ADC) is used to convert the generated signal into the digital domain for digital post processing such as color processing, image enhancement, data compression for storage, etc. The digital image data after the ADC block can also be fed back for auto exposure and auto focus followed by (Image Signal Processor) ISP for processing , color enhancement etc. as shown in Figure 1.1.

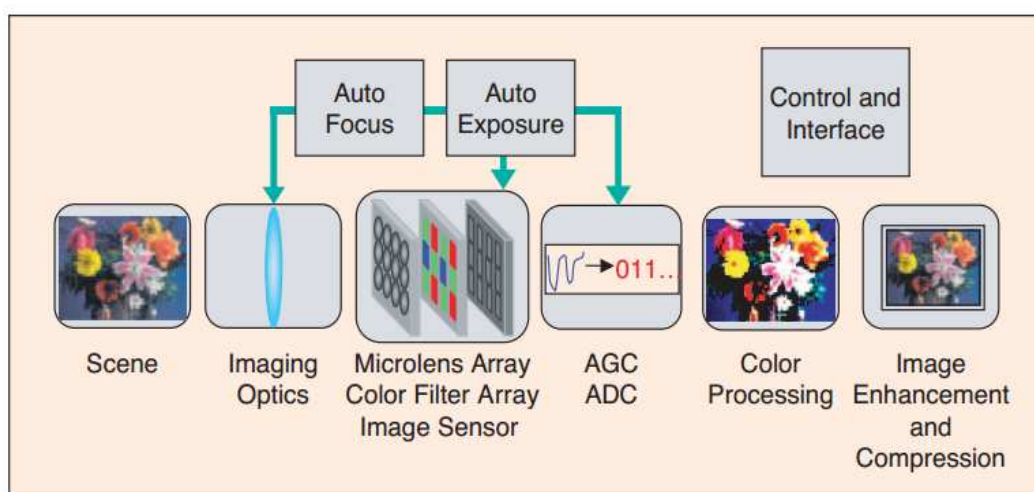


Figure 1.1 Imaging pipeline [1]

Visible spectrum imaging is the main target for consumer applications such as mobile phone cameras. Silicon, the cheap and widely-available material at the basis of the semiconductor industry, also happens to be highly suitable for visible spectrum imaging due to its high absorption in the visible range of light (i.e. the range of wavelengths over which the human eye is sensitive, around 390nm-750nm).

In the following sections, we focus on the drive behind the main (CMOS) technological implementation of consumer image sensors, and on the main performance metrics and limitations.

1.1.1 The rise of the CMOS image sensor

Over the past decade, developments in image sensor technology have brought a shift from Charge Coupled Devices (CCD) to Complementary Metal Oxide Semiconductor (CMOS) based image sensor technology, due to the potential of CMOS imager sensors (CIS) compared to CCD. In this research work, we focus exclusively on CIS. Some key advantages of the CIS technology are listed below:

- **Low power dissipation**
CIS has lower voltage swing, switching frequency and capacitance which allows them to be more suitable for portable applications [2].
- **Integration and miniaturization**
CMOS components such as memory, signal processing circuits, microprocessors can be integrated into the same chip. This reduces complexity in board or System in Package (SiP) design and reduces the cost of the system [3].
- **Cheaper fabrication**
CIS are produced for several years by tweaking the standard digital CMOS processes[4][5]. This supports mass production using existing CMOS fabrication lines, reducing the cost of production. Lately, as the scaling continues these tweaks have become more pronounced and lead today to dedicated production lines to tackle technology scaling and market demand.
- **Reliability**
Due to on-chip integration, the component count for assembly of the overall system is reduced, which improves robustness and reliability. Of course, scaling can tend to offset this advantage since the reliability of the individual circuit elements is reduced.
- **Speed**
On-chip integration of all components lowers interconnect RC time constants between them, and therefore favors increases to the rate of data transfer between the sensor and the processing units. This translates into faster frame rates: CIS with rates of 10,000 frames per second has been reported [6]. Normal commercial sensors work at few hundreds of frames per second.

- **Random access**

With the CIS, because of its two-dimensional structure of the data readout circuit within the imaging sensor, which allows for data readout by selectively addressing X and Y coordinates, it is relatively easy to realize a random-access [7] performance.

Although CIS provides the above advantages it suffers from noise and lower sensitivity compared to CCD technology. Higher fixed pattern noise [8] is observed due to the readout through a chain of buffers and amplifiers. These drawbacks are reduced with technology improvements and the emergence of dedicated CMOS production lines for image sensor fabrication.

1.1.2 CMOS Active Pixel Sensor

The CIS pixel matrix is composed of a 2D array of light-sensitive voltage generators (pixels). In this thesis, we explore the 3T Active Pixel Sensor [9] (APS) (Figure 1.2) structure, one of the simplest and most widely-used structures composed of a photodiode and three transistors. The photodiode is a p-n junction diode operated in reverse bias mode to convert photonic energy into an electrical current via electron-hole generation within the depletion region. The three transistors have specific roles, as a M_{sf} source follower transistor, a M_{sel} - select transistor and a M_{rst} reset transistor. The reset transistor acts as a switch to reset the photodiode. The select transistor allows a single row of pixel matrix to be read by readout electronics. The in-pixel source follower amplifier acts as a buffer and due to its proximity to the photosensitive element, enables a non-destructive read of the information at high speed with high signal to noise ratio.

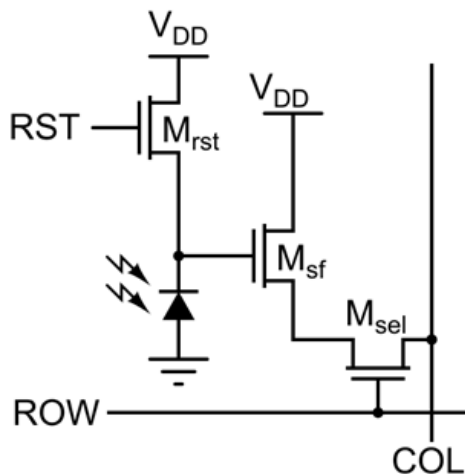


Figure 1.2 APS structure

However, the presence of three transistors in each pixel leads to a low overall pixel fill factor, which persists even though technology scaling reduces transistor sizes. Detailed operation of APS architecture is described in the following chapters.

1.1.3 CMOS image sensor performance metrics

The performance of an APS structure is measured with a number of criteria: Few of them are described in the following paragraphs:

Dynamic range: the range between the minimum and maximum detectable illumination levels, measured in dB. The dynamic range can also be represented as the number of illumination levels that can be encoded. When the incident illumination is high, the photocurrent is large, causing the photodiode to discharge quickly. Therefore, it is necessary to reduce the integration time in order to prevent the pixel from discharging completely. However, in low illumination, the photocurrent is small, causing the photodiode to discharge slowly. In this case, it would be necessary to increase the integration time in order to allow the photodiode to discharge enough to provide a detectable signal at the output.

$$D.R = 20\log_{10} \frac{I_{max}}{I_{min}} = 20\log_{10} \frac{\frac{qQ_{max}}{T_{integration}} - I_{dark}}{\frac{q}{T_{integration}} \sqrt{\frac{1}{q} * I_{dark} * T_{integration} + \sigma_r^2}} \text{dB} \quad --(1.1)$$

where Q_{max} is full well capacity, I_{dark} is the dark current, $T_{integration}$ is integration time and σ_r is read out noise.

The dynamic range of a 3T-APS is determined by the voltage swing between the power supply voltage (V_{DD}) and the ground voltage. However, the threshold voltage drop across the source follower diminishes the voltage detection range at the output. Also, technology scaling reduces the supply voltage (and to a lesser extent the threshold voltage), which affects the dynamic range.

Frame rate: is used to describe the imaging speed of the sensor. Normally it refers to the number of images that can be taken within a second.

Sensitivity describes the output response of the photo sensor as a function of light intensity at specific wavelength. Sensitivity is the ratio of collected charges to the number of incident photons.

Conversion gain: After the photons are converted and collected at pixel floating diffusion (FD) nodes, collected electrons cause a proportional change in voltage depending on the FD node capacitance. This is called charge to voltage conversion gain.

Signal to noise ratio: the ratio of signal power to noise power, measured in dB. SNR can be improved by improving the signal, which provides a better signal dynamic.

$$\text{SNR}(I_{\text{ph}}) = 10 \log_{10} \frac{I_{\text{ph}}^2}{\frac{q^2}{T_{\text{integration}}^2} \left(\frac{1}{q} (I_{\text{ph}} + I_{\text{dark}}) T_{\text{integration}} + \sigma_r^2 \right)} \text{dB} \quad \text{--(1.2)}$$

where I_{ph} is photocurrent signal, I_{dark} is the dark current, $T_{\text{integration}}$ is integration time and σ_r is read out noise. The following section describes in detail the sources of noise in CMOS APS structure.

1.1.4 CMOS image sensor noise

Like any other electronic circuit, CMOS image sensor also suffers from noise. There are two primary sources of noise [10][11][48] in CMOS APS. They are

- Temporal noise
- Fixed pattern noise (FPN)

Temporal noise

Temporal noise is temporally random and not constant from frame to frame. It is described by statistical distributions and can be reduced by averaging successive frames or by using correlated double sampling techniques. In general temporal noise can be divided into three categories: shot noise, 1/f noise and reset noise

Photon shot noise: Photon shot noise describes the fundamental statistical uncertainty on the amount of photoelectrons that are generated by light falling on the photodiode. It depends on fundamental physical laws, little impact from the design decisions.

1/f noise: originates from fluctuation in the conductivity. In CMOS APS different components contribute to total 1/f noise at different operation phases. For example during integration time, this noise is produced by photodiode dark current fluctuation. During readout phase, the column source follower and access transistor generate 1/f noise. In system level, reducing the system temperature helps in improving 1/f noise.

Reset noise: The photo-generated electrons start to accumulate on the junction capacitor after the reset operation. Reset noise is a function of sensor temperature and capacitance. It causes variance in the voltage to which the photodiode is charged.

$$\text{Reset noise} = \sqrt{\frac{kTC}{q}} \quad \text{--(1.3)}$$

where K is the Boltzmann constant, T is the temperature (Kelvins).

Fixed pattern noise

Fixed pattern noise (FPN)[8] is a spatial noise. It is the variation of output from different pixels under the same illumination conditions. It produces variations from pixel to pixel or column to column in the sensor array. The FPN could be due to non-uniformity of the micro-lens, non-uniformity in effective pixel fill factor (variability in pixel circuit dimensions) or non-uniformity in conversion gain (variability in transistor characteristics). FPN can be categorized principally by the signal dependence. Signal independent one is the Dark Signal Non-Uniformity (DSNU) and signal dependent one is Photo Response Non-Uniformity (PRNU).

Dark Signal Non-Uniformity (DSNU): Pixel to pixel dark current variation is one of the sources of FPN. This variation is not signal dependent. It is due to non-uniform spatial patterns of impurity concentrations in the wafer. Additionally, this non-uniformity depends on temperature distribution on the pixel array.

Photo Response Non Uniformity (PRNU): This is signal dependent component of FPN. Local variation in different layer thickness and doping impurities cause variations in photo generated carrier lifetime. These are caused by mask misalignment. They result in modifications of quantum efficiency, source follower gain or pixel capacitance across the pixel array. PRNU depends on process technology, light spectrum, pixel design and timing.

Existing conventional 2D image sensor suffers from many limitations. The main drawback is the limited area available to accommodate the pixel array and other blocks (ADC, ISP etc.) together. Due to this reason fill factor of pixel is reduced. 2D image sensor blocks are connected by long wires increasing the RC delay and reducing the bandwidth. The entire chip is fabricated using single technology. These drawbacks are overcome by the 3D imagers. The main drivers for 3D technology are imagers and memories [13][14]. 3D imager has shorter wirelength and so increased bandwidth. Long term goal of 3D imager is the possibility of increasing the fill factor and increasing the local image processing by stacking pixels above transistors (APS transistors underneath photodiode). But the intermediate term and high granularity approach is to have an image processing block below pixel matrix. This is very attractive due to the technology heterogeneity (using different technology node for each layer and dedicated CMOS imager process lines). 3D stacking would free CMOS imager processes completely from standard digital.

During this research work we will focus on how we can model and design an imager using the 3D technology. Due importance is given to analyzing the problems when moving to 3D and proposed solutions to overcome the associated (mainly thermal) issues.

1.2 3D technology

1.2.1 Trend

In 1965, Gordon Moore postulated his famous and eponymous law, which formalized for the first time scaling trends in the semiconductor industry, trends which continue to this day. However, at the end of the 20th century, the semiconductor industry started slowing from the

trend proposed by the law, and costly technological solutions (e.g. copper interconnect, high-k dielectrics) became increasingly necessary to continue to achieve the levels of performance predicted by Moore's Law. Recently, the concept of 3D integration and use of the vertical dimension as a vector to pursue performance began to gather support in both academic and industrial communities [15][16]. The idea was in fact originated in 1985 by the Nobel laureate Richard Feynman, who expressed the idea of stacking in his address on “Computing machines in the future”. Today, it is widely accepted that 3D integration is well on its way to becoming a future mainstay of the semiconductor industry, with its own specific roadmap for development as proposed by the Advanced Semiconductor Engineering group, as shown in Figure 1.3.

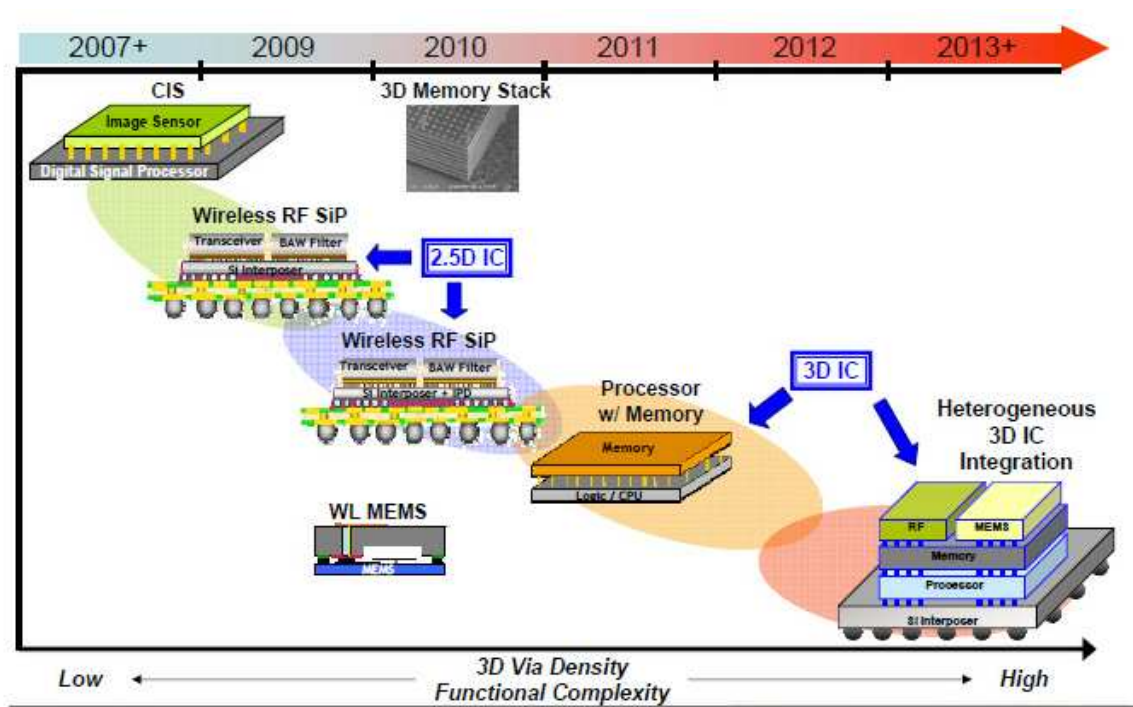


Figure 1.3 3D Roadmap [16]

1.2.2 Opportunities

3D technology has many advantages compared to the 2D counterpart. The main driving factors towards 3D technology are

- **Interconnect delay reduction and circuit speed**

The most important advantage of 3D technology is its capability in reducing the distance between system blocks, leading to a reduction in the length of global wires and consequently

lower global interconnect delay and power. Global interconnect delay (Figure 1.4) is a serious issue in planar (2D) systems, where interconnect delay dominates the gate delay above a length of just a few gate pitches. In 3D technology, the interconnect issue [17] can be strongly mitigated, since while in a given area A (for which the maximum wirelength is $2\sqrt{A}$), the same area split into n layers reduces the maximum wirelength to $2\sqrt{\frac{A}{n}}$. The maximum wirelength (Figure 1.5) exhibits therefore a reduction proportional to \sqrt{n} [17].

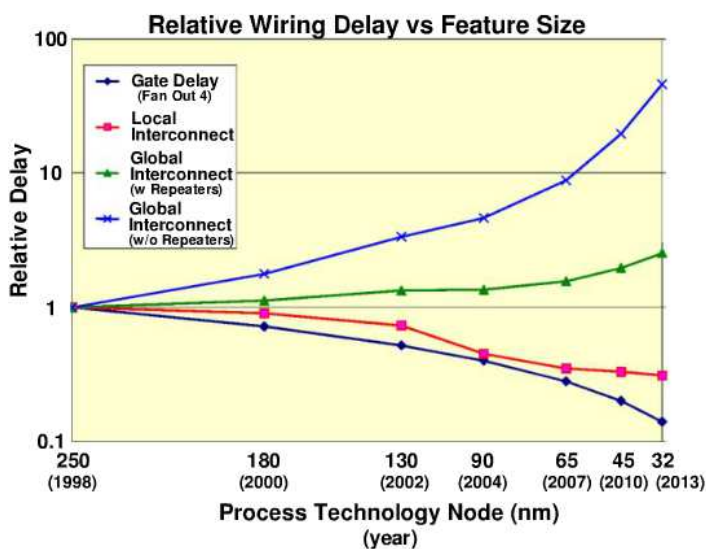


Figure 1.4 Inteconnect delay [18]

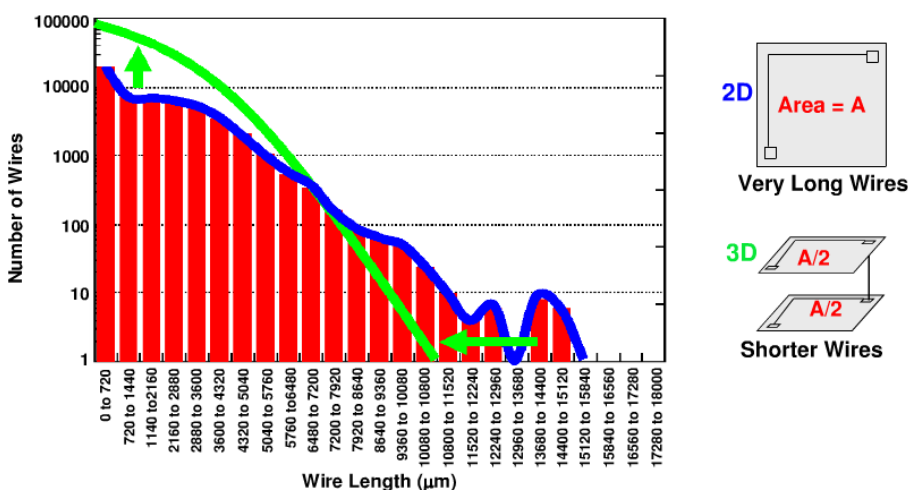


Figure 1.5 2D vs 3D wirelength distribution [18]

A Through Silicon Vias (TSVs) is formed by aligning, defining, and etching a cavity between two tiers to expose an electrode in the lower tier; lining the sidewalls of the cavity with an insulator; and filling the cavity with metal or doped polysilicon to complete the connection. All 3D IC fabrication process (Figure 1.6) comprise three basic steps, namely wafer thinning, TSV etching and filling, and tier bonding. Depending on the sequence of these steps we can distinguish between different approaches. A process is described as “TSV first” or “TSV last” if the TSVs are fabricated before or after tier bonding, respectively, and the order in which TSVs are fabricated within a 3D IC process is an important process decision to be made before developing a 3D IC technology. The length of the vertical connection, in TSVs, is more or less negligible since each layer is less than 100 μm thick. In order to minimize the TSV pitch, we have to maximize the aspect ratio of the TSV cavity defined as the ratio of the depth to the width of the cavity. TSV aspect ratios do not exceed 10 due to fabrication issues. The key projections given by International Technology Roadmap for Semiconductors (ITRS) relevant to TSV are given in Table 1-1. Current technology advancement helps in thinning of the individual chips to reduce the height of the final chip stack

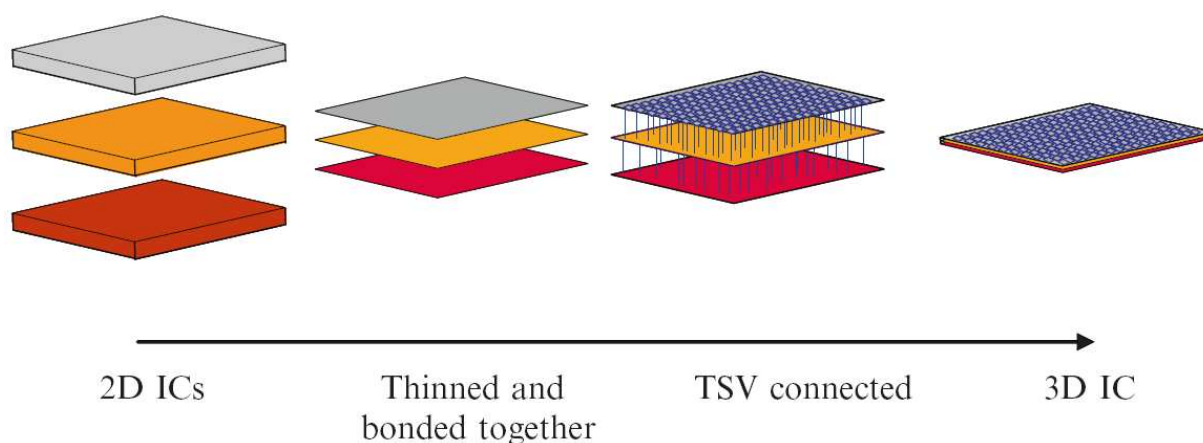


Figure 1.6 3D IC fabrication process [19]

Table 1-1 TSV parameter projections in 2011 ITRS roadmap[20]

Parameter	2011-2014	2015-2018
Minimum TSV diameter	4-8 μm	2-4 μm
Minimum TSV pitch	8-16 μm	4-8 μm
Minimum TSV depth	20-50 μm	20-50 μm
Minimum TSV aspect ratio	5:1 - 10:1	10:1 - 20:1

Since the time constant of an interconnect line increases with the square of its length, it is clear that long interconnects cannot exist without some form of signal regeneration to guarantee a level of circuit speed. The use of repeaters enable the signal delay to depend linearly (rather than quadratically) on interconnect length [21]. By reducing the maximum wirelength in 3D systems, the number of repeaters required will be reduced, which will be beneficial both for circuit speed and for power consumption. Further, transistor resources used for repeaters in the 2D case (upwards of 25% in high performance processors) will be freed up for other functions, such that transistors are used more efficiently.

▪ **Heterogeneous Integration and System Miniaturization**

A compelling and fundamental driver for 3D technology is the possibility of mixed-technology (e.g. digital, analog, RF, optical etc.) systems, or heterogeneous integration (Figure 1.3). This heterogeneity implies that the constraint of everything in the same process is removed, such that each function can in principle be implemented in the most suitable technology. This is a profound change to the semiconductor industry. This selection of different technology will lead to cost optimization (e.g. aggressive and costly digital stacked with mature and cheap analog), then performance optimization as processes become more specialized and the organization more stratified, and finally full system miniaturization with the emergence of many specialized suppliers both at the process and at the IP / system integration level.

To our knowledge the main application explored to date has been imager. The advantage of using 3-D in imager is that no area has to be sacrificed on the imaging layer for additional circuitry such as Correlated Double Sampling (CDS), Image Signal Processor (ISP), Decoder, Analog to Digital Converter (ADC) can be realized in different layers according to the cost, interconnect possibility, thermal impact etc.

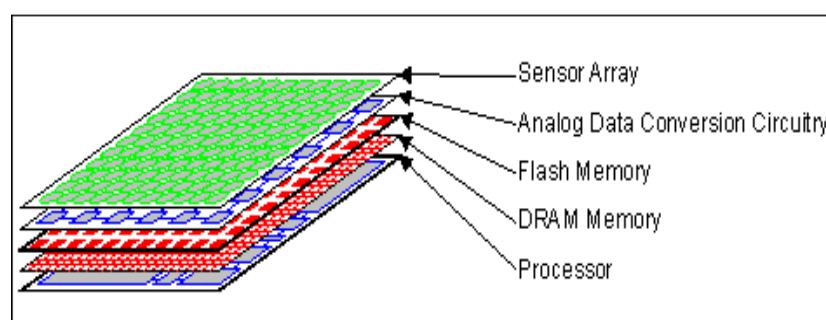


Figure 1.7 Heterogeneous integration [22]

3D integration is not limited to the above but they also have other advantages such as parallel processors, new functionalities, new applications etc.

Although 3D technology possesses many potential advantages, it also imposes many challenges compared to the mature 2D technology. To realize a 3D system, some important issues must be addressed in the design stage, as explained in the following section.

1.2.3 Issues

As described above, 3D technology has the great potential to overcome issues in planar 2D technology to pursue the performance levels predicted by Moore's Law and required by application. However, the technology also has many obstacles to achieve mainstream production capability, impacting the feasibility and reliability of systems implemented with this approach. The main obstacles are described in detail below:

- **Thinning and mechanical stability**

Power consumption[23] creates heat and if it is not dissipated fast enough the temperature of die increases leading to problems such as increased leakage currents in transistor and reliability degradation. Moreover the die is thinned before bonding. This adds complication to the heat dissipation problem: thicker die can spread heat much better than thinner ones along the horizontal plane.

Apart from heat dissipation problem in the thin die, the 3D stacks will comprise a number of die of different sizes thinned to a few micrometers, made of materials stacked and bonded on top of each other so as to retain electrical connections. This system creates lot of problem in terms of mechanical stability when temperature changes. Different materials have different thermal expansion coefficients and are affected in different manner by thermal gradients. This might lead to stack de-bonding leading to electrical failure. Mechanical stress [24] due to thermal expansion can interfere with the stress carefully engineered in transistor channel to destroy the on-currents of transistors. Another major source of problem is handling of the thinned wafers. The thinned wafers are flexible and so extreme care is taken when they are transferred from one process step to other. So carrier wafers to solve this problem, but still bonding and de-bonding to carrier wafer may create mechanical issues.

- **Electromagnetic interference**

The increased power consumption per unit area must be considered in a 3D stacked chip Power Distribution Network (PDN) because total power consumption is proportional to increased current magnitudes through TSVs and EMI (electromagnetic interference) is increased by high current switching and high PDN impedances. Although, TSV shows very small inductance, which is very helpful to 3D IC by giving lower PDN impedance[25]. However, when it combined with the large capacitance of a chip PDN, it can induce high PDN impedances, which are called as TSV effects or TSV inductance effects and can be an EMI source in the GHz range as shown in [26]

- **Thermal issues**

One of the main challenges facing 3D integration is heat dissipation. In a conventional 2D planar approach, a heat sink is attached to the surface of the chip package such that heat flows straight from the chip to the heat sink. Usually, the heat sink uses the whole area of the 2D chip, which results in the lowest (best) achievable power density at the heat sink interface. In this case, there are only two possible approaches: (i) front-cooled, where the heat sink is placed above the chip and heat flows from the transistor level through the interconnect levels to the heat sink, and (ii) back-cooled, where the heat sink is placed below the chip and heat flows from the transistors through the bulk (substrate) to the heat sink. Moving to 3D integration decreases the chip footprint and both increases power density at the heat sink interface, as well as multiplying the number of layers that heat has to pass through to reach the heat sink.

Another problem is that upper layers insulate lower layers from the heat sink. Silicon has a high thermal resistance, so we expect a sharp vertical temperature gradient to develop in the chip. The temperature rise is discussed in [27]

$$\Delta T_n = \frac{P}{A} \left[\frac{R}{2} n^2 + \left(R_1 - \frac{R}{2} \right) n \right] \quad \text{--(1.4)}$$

where P is the identical chip power dissipation in each layer, n is the total number of active layers, A is the total 2D chip surface area, R is the identical thermal resistance between layers, and R₁ is the thermal resistance between the top layer and the heat sink. From (1.4) temperature rise can be expected to rise linearly with power density and the square of number of active layers. If we assume that R₁ >> R, then there is an approximately linear relationship

between n and ΔT_n . This also suggests that for most 3D-ICs with $n \leq 5$, R_1 will dominate the rise of temperature in any layer. For example, when moving to a two layered chip, this relationship indicates that the package thermal resistance has to be halved in order to maintain the same temperature.

Thermal hotspots [27] are created due to non uniformity in power distribution of blocks. The local power distribution varies over time and is not uniform due to many factors such as current flow, transistor size, frequency of operation etc. This condition is exacerbated by: thermal barrier created by the low thermal conductive interface material used to attach two layers (e.g. epoxy), longer heat dissipation path from the die to the heat sink is another factor worsening the local temperature. Thermal hot spots not only increase cooling costs, but also negatively impact reliability and degrade performance. Hot spots accelerate failure mechanisms [28] such as electro-migration, stress migration, dielectric breakdown, device failure and leakage. Leakage is exponentially related to temperature, while the effective carrier mobility (and consequently operating speed) of devices decreases as temperature increases.

- **Design challenges**

The addition of a third dimension would require support from more advanced CAD tools due to the increased complexity [29] of the problem. The 3D system is much larger with many more dimensions in the design space, tradeoffs and design decisions. Moreover it can be heterogeneous. The design decisions of such a complex system has to be at the early architectural exploration.

3D physical design is complex compared to 2D design, each individual design step in 3D has to take the special constraints (e.g Size of the problem, multiple technology database etc.) of 3D integration into account. Hence, physical design of 3D circuits cannot be simply viewed as a stack of multiple 2D physical designs. Normally, during physical design, all circuit components are instantiation with their geometric representations, resulting in a layout representation of the circuit. In other words, geometric images (shape, size, and metal layer) of all macros, cells, gates, transistors, etc., are assigned a location using floorplanning. So this step has to include new, 3D specific characteristics that must be represented in the underlying data structures. For example, high output power modules need comprehensive consideration of

thermal-driven floorplanning [29-31] with vertical dependencies arise in addition to horizontal ones.

3D placement[32] requires optimizing the placement between multiple active layers. Since thermal constraints are crucial for 3D designs. Hence, 3D placement must ensure that thermal considerations are fulfilled. For example, the placement must spread cells such that a reasonable temperature distribution can be expected. Due to increased package density additional techniques are required to tackle the heat dissipation issue in 3D designs. Therefore, vertical metal structures called as thermal vias, play an important role in achieving a thermal solution. 3D placement problem size is increased (placement of blocks in different tiers along with optimized placement of thermal vias [30]).

Next major step is 3D interconnect routing[33][34], caused by the multi-tier position of net terminals that lead to net topologies which span more than one tier. This requires expensive inter-tier vias to be used in addition to regular signal vias which connect metal layers within one tier. Furthermore, 3D routing must take additional constraints into account, such as blockages introduced by thermal and inter-tier vias[30] leading to a more complex heat management is necessary. Finally, the result of physical design is a set of manufacturing specifications that must be subsequently verified.

From the above description, it clear that performing a thermal analysis is essential during the floorplanning at the early stages of design, and this is necessary to avoid very costly redesign later as the cost of redesign increase with each step of design process. Thermal-aware floorplanning is performed to determine if modules need to be rearranged in order to control temperature. The peak temperature and/or the temperature gradient can be reduced by performing a thermal-aware floorplanning of the chip, consisting of finding an optimum floorplan that minimizes area, wire length, and maximum temperature. If a hot (power-hungry) block is placed beside (or, in 3D, above or below) cooler blocks, lateral (and, in 3D, limited vertical through the insulating layers) spreading of heat takes place. As a result, the temperature of the hot block is reduced. Floorplanning process can be also used for adding additional area for thermal vias to reduce temperature. Floorplanning improves the performance, reliability of the chip. Thermal analysis is also necessary at the end of verification. This step will not lead to any major redesign if the first floorplanning step is performed correctly.

1.2.4 3D Imager

Several research groups such as IMEC, CEA-LETI, ST microelectronics, Sony are working on 3D integration for imagers [35-40]. Massachusetts Institute of Technology (MIT) has reported, 1MP 3D imager [37] with first 2 tiers are a 3D imager, and the supporting 5 tiers are a multichip silicon stack. The 3D imager is a 2-tier 1024×1024 pixel image sensor array fabricated with 8μm-pitch, per-pixel 3D vias. The imager is vertically connected to the silicon stack through a gold stud bump array at 500μm pitch. Tier-1 consists of 100% fill factor, deep-depletion photodiodes, thinned to 50μm. In the year 2010, IMEC has reported its work on area 3D integrated imager with detector layer, analog and digital image processor layer using high density bumping and area redistributed TSVs. Recently, IMEC has also announced a project on advanced 3D-Stacked Imager Sensor(3SIS) [41]. CEA-LETI and ST microelectronics has reported their work on 3D integrated imager in [42].

The next section will discuss about the focus of the research work combining the need of the imager technology integrated on 3D technology. The focus of the work has been restricted to few topics which are important from our point of view.

1.3 Research focus

1.3.1 Scalability - Technology

3D integration techniques are proposed as a potential solution to overcome the scaling limit [43]. The challenge lies in developing a design technique to realize a 3D system. The design technique has to take care of scaling, simulation capability needed to handle the complex 3D system and hierarchy to meet all the tradeoffs at early stages of design. When the chip is represented hierarchically, the design process will find solutions for each block in hierarchical description. To realize an efficient and reliable hierarchical methodology, it is necessary to make critical design decisions early on in the design flow, to give a fairly high probability of achieving first-time design (no reliability or functionality issues) and minimize design cost. Therefore some information (e.g system netlist) or estimations (e.g. floorplanning) are required early on in the design process. In the traditional design flow, front-end designers create a Register Transfer Level (RTL) netlist that is transferred to back-end designers. This netlist

mainly covers functionality and interconnectivity, and has low physical information content, which often results in much iteration between the front-end and the back-end designers. These iterations have significantly increased for designers with technology scaling. The lack of early design data during the front end implementation results in initial failure and lead to redesign which is costly. Technology scaling allows the designer to put an increasing amount of functionality on a die, but also with greater uncertainty since device variability and overall system complexity issues are exacerbated.

To overcome the existing problems, models need to be developed at different levels of abstraction in order to analyze the system and for synthesizing the system. The challenge lies in formulating a methodology to analyze a system at very early stages that could be optimized with respect to the intended functionality. Formal abstractions are important to represent an individual model to fit in the hierarchical design flow. Formulating the problem with proper specifications (i.e. design constraints and optimization budget) taking into account technology-related issues confines the problem into acceptable bounds. Constraint propagation between these models at various abstraction levels is carried out to meet all the requirements can lead to a successful synthesis. Also the design flow needs to be generic, not only in analyzing the system but also in integration and testing. The main benefits with this kind of modeling technique are shorter design time (and consequently time to market), adaptability to new technology constraints, reusable models.

As explained earlier, 3D design has to undergo rigorous thermal analysis at floorplanning, placement, routing to have a reliable system. The tool has to be sophisticated to manage the three dimensional problem. During the modeling and design work the lack of thermal information at early stages of design was identified. This information is necessary to analyze the 3D imager system performance. From this understanding deeper focus is given to understand the impact of thermal aspects on imager performance. The next section will focus on imager sensor thermal model and 3D integrated thermal model which could create a detailed analysis into 3D technology.

1.3.2 Simulation scalability– Pixel matrix

In the past few years, the imager industry has evolved to propose imager resolution of 8-12MP (with an extreme case at 41MP [44]) in mobile phone cameras. This trend seems to be growing since the consumer is inclined towards higher resolution for improving image

quality(averaging) and zooms. From a designer's point of view, the simulation of an entire pixel matrix at the system level is important in order to analyze the behavior of the pixel matrix when it interacts with other blocks. Simulating the entire pixel matrix can be useful for

- Early stage exploration of imager
- Analysis of the overall performance
 - Identify critical regions based on
 - Thermal impact
 - Noise
- Improve the algorithms in ISP based on critical regions

Typical analog and multi-domain simulation environments [45] (Spectre or Pspice or modeling languages such as VHDL-AMS [46][47], Verilog-A etc.,) are not suitable for the simulation of high resolution imager matrix structures. It is difficult to make system-level analysis because of the number of inputs and outputs. For example, since a conventional 3T-APS has three inputs ("reset" for initialization, "select" for reading and the light intensity signal itself) as well as two internal nodes (photodiode voltage and amplifier output), and these are replicated for each pixel in a matrix, a 12MP pixel matrix would require the representation of 24M input terminals (reset, select), 12M output terminals (readout) and 24M internal nodes signals. These signals are common for each line, and have to respect precise timings.

In conventional simulation, the light input is often set to be a constant value over the entire pixel matrix (potentially incremental in a parametric simulation). This kind of simulation loses the realism in emulating the imager hardware behavior. One challenge is to fix different values of light for different pixels, where the problem is how to calculate thousands or millions of design variables. The important point to notice with pixel matrix is that there are millions of nominally identical modules (pixel), and that brute force simulation does not exploit the similarity or regularity of the pixel matrix. It is therefore a hugely inefficient approach if we want to simulate the whole pixel array. Moreover it is anyway impossible to simulate with current simulator due to machine limitations. It takes several hours to several days to simulate large matrix. This is the reason typically designers only simulate small matrices to validate the pixel design, and then just check interconnectivity to validate the matrix. Using the existing approach it is not possible to 1. look at the actual functionality of the matrix on a whole image, i.e. carry out a proper validation with realistic application scenarios, and more importantly

2. examine characteristic variations over the pixel matrix and analyse their impact on image quality. There is therefore a need for

Imager models capable of:

- Simulating large pixel matrix size (scalability) in a reasonable time
- Taking into account heterogeneous input variables (light, temperature, integration time) for each pixel

Integrated design flow capable of:

- Integrating a complete 3D imager floorplanner with thermal model
- Simulating the integrated model with realistic temperature and light conditions

1.4 Key research contributions

Several research problems related to CMOS image sensors are addressed in this thesis work.

The following are the key contributions:

- Demonstration of a methodical analysis of imager design to achieve a high level of flexibility and modularity. We developed a modeling approach to enable early design space exploration using a hierarchical approach, and in particular focused on the development of generic models for imager IC in order to explore early design choices.
- Demonstration of a “Thermal-aware imager model” focusing mainly on the thermal impact on imager performance. Existing electrical simulation tools (Spectre or Pspice) help in the design of a single pixel, but scale badly to relevant sizes of pixel matrices since they do not exploit the massive regularity of large pixel matrices and thus lack in speed and face memory issues. The high-level image sensor models developed in this work can simulate any size of imager matrix with a specific focus on thermal impact while overcoming speed and memory issues. Simulation speed-up factors of about 500000x have been achieved using a SystemC model with a relative error of below 4% (average error of about 500 μ V for a quanta of 12.9mV) for a 256*256 pixel matrix.
- Demonstration of a “3D integrated thermal design flow” integrating floorplanner, thermal simulation tool and imager thermal model to visualize the impact of various blocks on the performance of the imager. This flow uses the realistic temperature distribution of each pixel to produce the output.

1.5 Thesis outline

This thesis is organized as follows:

Chapter 2 focuses mainly on the modeling and top-down design approach. The approach is explained with a supporting methodology, consisting of parameter dependency graphs followed by segregation into abstraction levels. Some imager blocks such as the pixel matrix and ADC are chosen to illustrate the methodology. Another methodology based on Pareto fronts is also explained to illustrate the importance of performance tradeoffs.

Chapter 3 focuses mainly on the thermal aspects when moving into 3D technology. Initially, image sensor thermal modeling and requirements are discussed in detail, followed by the description of a methodology to realize the thermal model. The validation of the model is explained by supporting results, and is followed by the implementation of the imager thermal model in SystemC to simulate any pixel matrix size. Finally, the SystemC model is concluded by a validation phase.

Chapter 4 focuses on further development of the imager thermal model discussed in earlier chapters through the establishment of a 3D integrated thermal design flow. This chapter explains in details the need for an integrated thermal design flow including floorplanning, thermal simulations of the imager thermal model with a realistic thermal map and input light generated from an image. Finally the chapter is concluded with results with several test cases.

Chapter 5 This chapter concludes the thesis with final outcome and future perspectives.

Supporting code, and model and tool parameters are attached in the appendices of the thesis.

Bibliography

- [1] El Gamal, H.Eltoukh,. “CMOS Image sensors”. IEEE Circuits and Devices magazine. 21(3), 2005, 6-20.
- [2] S.H.Lim, “Video processing applications of high speed CMOS image sensors”, Stanford university, 2003, Thesis.
- [3] Micron corporation,. CMOS's advantages (technical notes): http://www.micron.com/imaging/Technology/CMOS_Advantages/index.html.
- [4] E.R Fossum, “CMOS image sensors:electronic camera on a chip”, Washington DC, USA : Proceedings of international electron devices, Dec 1995. p.no:17-25.
- [5] H.S.Wong, “Technology and device scaling considerations for CMOS Imagers”, IEEE Transactions on Electron devices, Dec 1996, Vol. 43. 2131-2141.
- [6] Kleinfelder, “A 10,000 frames per second CMOS digital pixel sensor”, IEEE solid state circuits, 2001, Vol. 36. 2049-2059.
- [7] K.Tajima et al, “Development of a high-resolution, high-speed vision system using CMOS image sensor technology enhanced by intelligent pixel selection technique”, Whitepaper, Photron Inc.
- [8] P.Fry, P.Noble, R.Rycroft, “ Fixed pattern noise in photomatrices”, IEEE J. Solid state circuits, 1970, Vol. SC-5. 250-254.
- [9] E.R.Fossum, “CMOS image sensors”, IEEE transactions on electron devices, 1997, Vol. 44. 1689-1698.
- [10] X.Wang, “Noise in submicron CMOS image sensors”, Delft university of technology, 2008, Thesis.
- [11] J.S.Lee, “Photoresponse of CMOS image sensors”, University of waterloo, 2003.
- [12] Suat Utku Ay, “Large format CMOS image sensors performance and design”,VDM Verlag Dr.Muller & co, Published 2008, ISBN: 978-3-8364-7052-0

- [13] U. Kang et al., “8Gb 3D DDR3 DRAM using through-silicon-via technology,” in ISSCC Dig. Tech. Papers, 2009, pp. 130–131
- [14] K. Osada et al., “3D system integration of processor and multi- stacked SRAMs by using inductive coupling links,” in Symp. VLSI Circuits, Dig. Tech. Papers, 2009, pp.256–257.
- [15] J.D.Meindl, “Beyond Moore's law: the interconnect era”, Computing in science and engineering, Jan 2003, Vol. 5. p20-24.
- [16] ASE. <http://www.asejp.aseglobal.com/>.
- [17] Vasilis.F.Pavlidis, Eby G.Friedman, “Three dimensional integrated circuit design”, Elsevier, 2009.
- [18] Craig Keast et al, “ 3D integration for integrated circuits and advanced focal planes”, Fermilab colloquim, Feb 2007.
- [19] A. Papanikolaou et al. (eds.), *Three Dimensional System Integration: IC Stacking 13 Process and Design*, DOI 10.1007/978-1-4419-0962-6_2, Springer Science+Business Media, LLC 2011
- [20] International Technology Roadmap for Semiconductors (ITRS), 2011 <http://www.itrs.net/Links/2011ITRS/2011Chapters/2011Interconnect.pdf>
- [21] T. Sakurai, “Closed-form expressions for interconnect delay, coupling, and crosstalk in VLSIs,” IEEE Trans. Electron Devices, vol. 40, pp.118–124, Jan. 1993
- [22] <http://www.tezzaron.com/technology/FaStack.htm>.
- [23] Yuan Xie et al, “Three dimensional integrated circuit design, EDA, design and microarchitecture”, Springer, Dec 2009
- [24] Antonis Papanikolaou et al, “Three dimensional system integration : IC stacking process and design”, Book, Springer, Dec 2010
- [25] J. S. Pak, C. Ryu, and J. Kim, "Electrical characterization of through silicon via (TSV) depending on structural and material parameters based on 3D full wave simulation," in Proceedings of the 9th International Symposium on Electronic Materials and Packaging, Daejeon, Korea, Nov. 2007.

- [26] J. S. Pak, et al, "Slow wave and dielectric quasi-TEM modes of metal-insulator-semiconductor structure through silicon via in signal propagation and power delivery in 3D chip package," Proc. of the 60th Electronic Components and Technology Conference 2010 (ECTC 2010), Las Vegas, USA, Jun. 2010.
- [27] K.Banerjee, S.J.Souri et al ,“3D ICS: A novel chip design for improving deep-submicrometer interconnect performance and systems-on-chip integration”, Proceedings of the IEEE, May 2001. 89(5): 602-633.
- [28] JEDEC, JEP122C, “Failure mechanisms and models for semiconductor devices”, <http://www.jedec.org>.
- [29] Yuan Xie, Gabriel Loh, Bryan Black, and Kerry Bernstein, "Design Space Exploration for 3D Architecture." ACM Journal of Emerging Technologies for Computer Systems, Vol. 2. No. 2, pp.65-103, April 2006
- [30] B.Goplen, S.S.Saptnekar, “Thermal via placement in 3D ICs”, ISPD, 2005. 167-174.
- [31] P. Zhou et al. 3D-STAF: scalable temperature and leakage aware floorplanning for three-dimensional integrated circuits. In ICCAD, pages 590–597, 2007
- [32] N. Viswanathan and C. C.-N. Chu. FastPlace:Efficient analytical placement using cell shifting, iterative local refinement,and a hybrid net model. IEEE T. Comput. Aid. D., 24(5):722–733, 2005.
- [33] T. Zhang, Y. Zhan, and S. S. Sapatnekar, “Temperature-aware routing in 3D ICs”. In ASPDAC, pages 309–314, 2006.
- [34] J. Cong and Y. Zhang. Thermal-driven multilevel routing for 3D ICs. In ASPDAC, pages 121–126,2005.
- [35] B. Aull, et. al., “Laser Radar Imager Based on 3D Integration of Geiger-Mode Avalanche Photodiodes with Two SOI Timing Circuit layers”, ISSCC 2006, pp 26-27.
- [36] D. Temple, et. al.,“3-D Integration Technology Platform for High Performance Detector Arrays”, public release from RTI International and DRS Technologies.

- [37] V. Suntharalingam, et al., “A 4-side Tileable Back Illuminated 3D-integrated Mpixel CMOS Image Sensor.” Solid-State Circuits Conference -Digest of Technical Papers, 2009. ISSCC 2009.
- [38] V. Suntharalingam et al., “Megapixel cmos image sensor fabricated in three-dimensional integrated circuit technology,” Digest of Technical Papers, IEEE International Solid-State Circuits Conference, pp. 356–357 Vol. 1, Feb. 2005
- [39] Orit Soraka, Dileepan Joseph, “Design and Fabrication of Vertically-Integrated CMOS Image Sensors”, Sensors 2011, vol. 11, pp. 4512-4538;
- [40] M. Motoyoshi, H. Nakamura, M. Bonkohara, and M. Koyanagi, “Current and future 3D-LSI technology for image sensor devices,” Mater. Res. Soc. Symp., Proc., vol. 1112, E01-03.
- [41] Advanced 3D-Stacked Image Sensor (3SIS). <https://projects.imec.be/3sis/>
- [42] Jaffard and Yvon Cazaux, “Image sensors with 3D heterogeneous integration”http://www.cnfm.fr/VersionFrancaise/actualites/GIP_CO09_presentations%20pour%20WEB-CNFM/Atelier3_conception_3D/Jaffard.pdf
- [43] W.R.Davis, J.Wilson et al, “Demistifying 3D ICs: The Pros and Cons of Going Vertical”, IEEE design test of computer, Dec 2005, Vol. 22. pp 498-510.
- [44] <http://www.nokia.com/us-en/products/phone/808/specifications/>
- [45] D.Navarro, Z.Feng, V.Viswanathan, I.O'Connor, “Image toolbox for CMOS Image sensors simulation in Cadence ADE”, Demset, Dec 2011, Florida, USA.
- [46] D.Navarro, D.Ramat, F.Mieyeville, I.O'Connor, F.Gaffiot, L.Carrel , “VHDL & VHDL-AMS modeling and simulation of a CMOS imager IP”, Forum on specification & design languages, Sep 2005, Lausanne, Switzerland.
- [47] F.Dadouche et al, “Modelling of pixel sensors for image systems with VHDL-AMS”, in: International journal of electronics, 95:3(211-225),2008
- [48] S.Feruglio et al., “Exact noise analysis of a CMOS BDI APS”, ISCAS (3) 2005: 2337-2340

Chapter 2

Modeling and Design

2.1 Introduction

Model based design [1][2](MBD) - A model is a simplified representation of a system intended to enhance our ability to understand, predict and possibly control the behavior of the system [3]. Model based design allows flexibility in the early stages of design exploration, improve product time-to-market which helps in minimizing the cost. Models are used for communicating information, help in analyzing a system, thus providing answers to questions about a system and for synthesizing a system. The main focus of this research is based on this approach. We develop flexible models of imager supporting a top-down (TD) design methodology and refine them using bottom-up (BU) approach. In this work models of various blocks (e.g pixel matrix, ADC) are developed at different levels in a TD approach in order to analyze and synthesize the system. Top-down design methodology is essential when designing large complex systems such as imagers. It relies on a hierarchical, constraint driven system description [4]. These models will represent the behavior of the system at a specific level to predict and give range at which the system can operate [3]. Formal abstractions are important for representing individual models. The flexibility of the models helps not only in analyzing the system but also in integration into the design flow and for testing. This modeling approach is proposed to overcome the problems which exist in the Bottom-Up (BU) design methodology. Typically designers resort to a BU approach due to the expertise in making primitive blocks using certain first level simulation with the available specification. Major problem with this design technique is that if the final blocks do not meet the specifications of the system, the entire circuit has to be rebuilt. This is very time consuming, costly and also depends on the expertise of the designer. The proposed modeling technique alleviates the problem incurred in the BU approach. We also propose another methodology to analyze the imager performance using pareto-front methodology to explore the system at system level being aware lower level limitations.

In this chapter, firstly system description is detailed in section 2.2 followed by the methodology used for TD approach in section 2.3 along with the description of parameter dependency graph in section 2.4. Section 2.5 elaborates on segregation of abstraction levels supported by results for pixel block in section 2.6 followed by ADC description in section 2.6.2. Pareto front methodology is explained in section 2.7. Finally the chapter is concluded in section 2.8.

2.2 System description

2.2.1 Pixel matrix

As explained earlier in the introduction, imager is an array of photosensitive devices that convert optical information into electronic signals. An imager IC is generally composed of analog (pixel matrix, correlated double sampling or CDS, analog-digital converter or ADC) and digital (decoder, controller, image signal processor) blocks [6] as shown in Figure 2.1. In this work, we consider the use of a conventional Active Pixel Sensor [7] (also known as a 3T-pixel) within a 1Megapixel array.

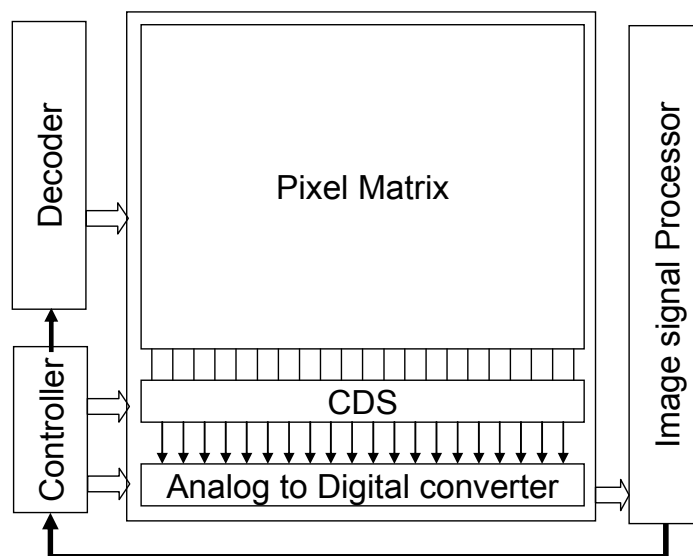


Figure 2.1 Imager blocks

3T-APS (Figure 2.2) consists of three NMOS transistors and a photodiode. Reset (M_{rst}), Follower (M_{sf}) and select transistor (M_{sel}). The signal readout procedure is divided into three phases, such as reset, integration and readout. During the reset operation, the inner photodiode capacitor is reset to source voltage (V_{DD}). When photons hit the photodiode, charges are collected in the form of photocurrent and converted into a voltage signal (discharge) directly by the photodiode junction and parasitic capacitance. Photocurrent is proportional to the light intensity during the integration time. A follower transistor (M_{sf}) is used to amplify the signal. During integration time, the photodiode node capacitance discharge provides a time-dependent signal slope proportional to the intensity of the incident light. At the end of the integration time the signal level is read out through a row select transistor (M_{sel}).

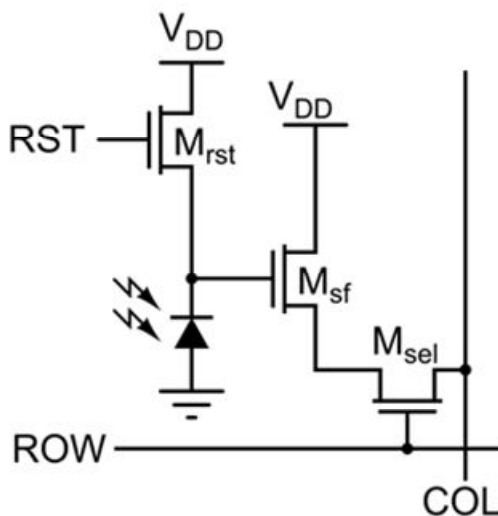


Figure 2.2 3T APS structure

Correlated double sampling circuit is located at the column output as indicated in Figure 2.1. CDS block takes into account two signals which are closely spaced in time. These signals are sampled using sample and hold circuit (SHR, SHS) in the CDS block. The first signal which is the reset signal is subtracted from the second signal namely the readout signal. This subtraction removes the Fixed pattern noise (FPN), low frequency noise, DC offset from the signal[6].

2.2.2 ADC

We have considered 8-bit SAR ADC architecture in this work. The SAR (Successive Approximation Register) ADC is chosen based on the simplicity in its architecture and to prove the methodology respecting our requirements. For example, SAR ADC block has to respect the sampling frequency constraint imposed by the pixel matrix size.

SAR ADC has the lowest-power consumption compared to other ADC architectures. This architecture has the advantage to be very simple; it implements the binary search algorithm. Power dissipation scales with the sample rate, unlike flash ADCs that usually have constant power dissipation versus sample rate. This is especially useful in low-power applications. Moreover SAR ADC does not contain an operational amplifier; that are generally power-hungry, it needs just one comparator that consume much less power than operational amplifiers.

SAR ADC has four mains building blocks (Figure 2.3):

- Sample-and-Hold Stage (S/H)
- Digital-to-Analog Converter (DAC)
- Comparator
- Successive Approximation Register (SAR)

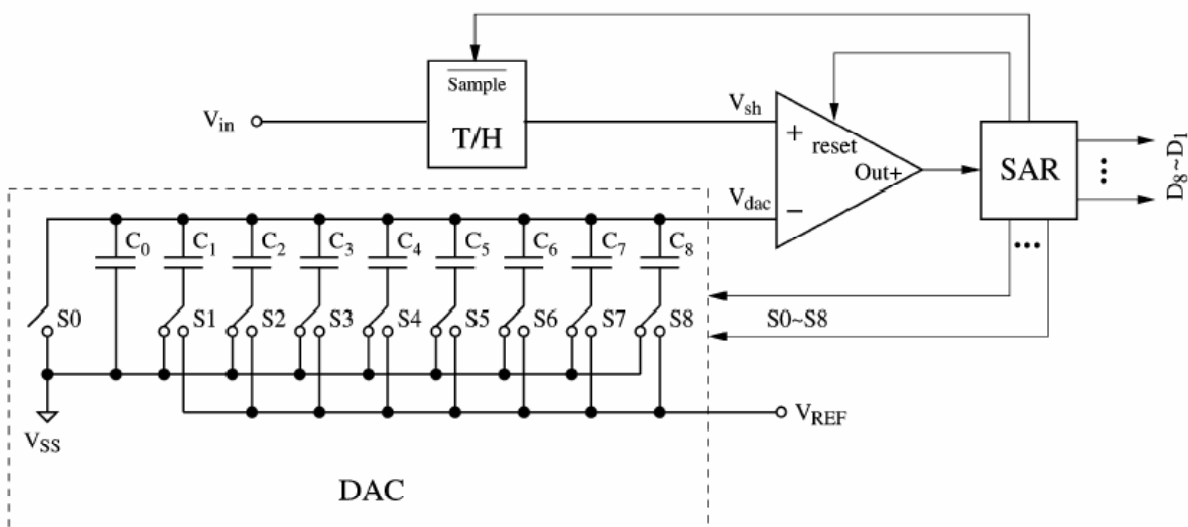


Figure 2.3 SAR architecture[6]

The ADC functionality [6] is as follows. The analog input voltage V_{IN} is sampled by the Track & Hold block. To implement the binary search algorithm, the N-bit register is first set to midscale setting the MSB to '1' and all other bits to '0'. This forces the DAC output, V_{DAC} , to be half of the reference voltage, $V_{REF}/2$. V_{IN} is then compared with V_{DAC} , if V_{IN} is greater than V_{DAC} , the comparator output is logic 1 and the MSB of the N-bit register remains at 1. Conversely, if V_{IN} is less than V_{DAC} , the comparator output is logic 0 and the MSB register of the register is cleared to 0. The SAR control logic then moves down to the next bit down, forces that bit high, and does the other comparison. The sequence continues all the way down to LSB. Once this is done, the conversion is complete and the digital word is available at the output.

Finally, image corrections such as gamma corrections, FPN corrections and color interpolations are made in the digital output of ADC block using the ISP to obtain the final image. This block also holds the memory to store the data output.

In this research work we mainly concentrate on pixel matrix block and the ADC to prove the novel TD hierarchical modeling methodology and switch to the BU refinement approach to fully explain this modeling approach and its capability. This is explained in detail in the next section.

2.3 Methodology

2.3.1 Modeling

The proposed methodology relies on hierarchical abstraction modeling [4][5] and TD constraint driven design. The modeling task will consist in producing models linking each abstraction level in two ways (Figure 2.4a). Firstly, higher abstraction level providing information and guiding design in the lower levels. This is achieved by identifying relationship between system level specifications and each sub blocks (lower level) ones. Thus, parameters of a given abstraction level are used as specifications of the next level (Figure 2.4b). Secondly, lower abstraction level models are used to refine (Figure 2.4a) higher level ones in order to improve the accuracy.

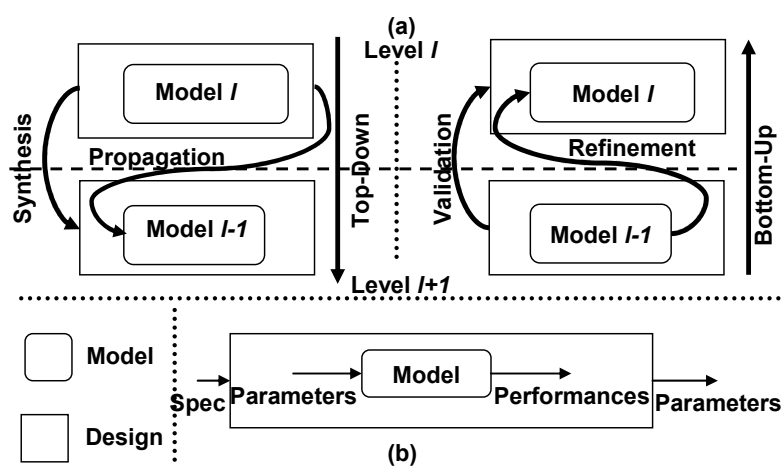


Figure 2.4 Design and Modeling

This work conserves both design and modeling approaches. The BU refinement approach is carried out only in the modeling phase to improve the models to fit into the design flow for synthesis. Moreover, refinement approach is not only carried out for improving the accuracy of the model but it subsequently enables predictive synthesis on other blocks (impacted by the refined models) interacting with block under synthesis within the system. There are certain instances in which we needed information from lower level (e.g temperature impact on circuit behavior). These issues are important in realizing a 3D imager. During the TD approach we use ambient (300K) temperature due to the lack of sufficient information of circuit behavior based on temperature. So in the later part of the work, we use the electrical circuit to extract information and feed back to the models in system level. This is called as refinement. The bottom-up refinement and the model development is explained in Chapter 3.

The design task is performed using optimization based on mathematical formulation at each abstraction levels. The aim is to characterize the solution space achievable respecting constraints inherited from a higher abstraction level. Other constraints like the bounds on the parameters or constant parameters will limit the design space which leads to reduction in solution space (Figure 2.5). Now we will look into several terminologies which we will be dealing during the modeling process. Each model has several its own characteristics (input/output) communication characteristics (propagation/refinement). These are detailed below.

Parameters: As indicated in the Figure 2.4 parameters are the input of the model. This involves selecting the dependent/independent parameters which are needed for the model to meet the performances. Parameters are the design variables. The final set of parameter values which meets the required performances are taken as input for the next lower level model in the synthesis flow.

As indicated in the Figure 2.5 problem is subject to constraints such as the lower and upper bounds for the parameters. Objectives are set to minimize or maximize values of performances or parameters. In the case above (Figure 2.5) the bounds on the parameters and objective limits the design space which leads to reduction in solution space.

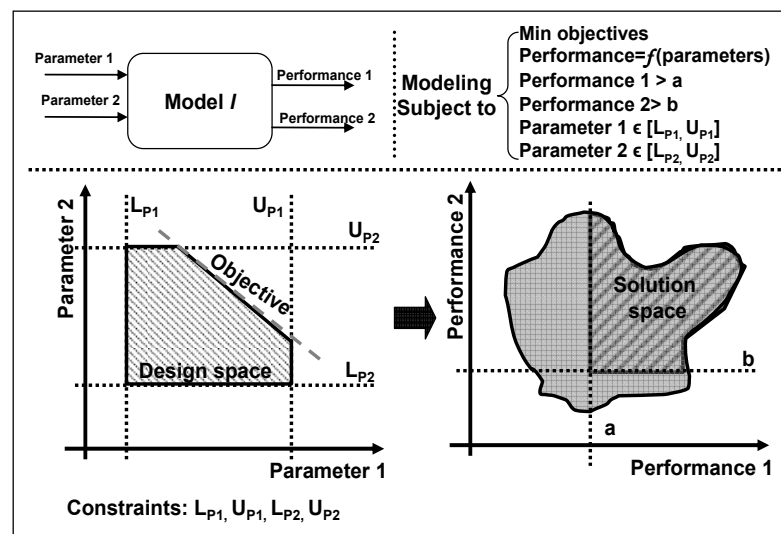


Figure 2.5 Problem formulation

Performances: Performances characterizes the model. Performances are the output of a model. If performances are met, it means the specification at the design flow is also met. As in Figure 2.5 performance should be above 'a' and 'b'. Several iterations with varied parameter selection from the design space which respects the constraints and objective will help in identifying the suitable performance output.

Propagation: Passing the parameters from a model in one level of abstraction to the next lower level model is called propagation. Propagation is referred to directed arrow in Figure

2.4. All the models which are developed for each level are connected through performance/parameter pairs.

Refinement: Refinement is a process of adding accuracy to the higher level model with selected information from the model $l-1$ performances as input parameter to the model l . Refinement is performed only during the modeling phase. It cannot happen in the design phase or during synthesis.

Specification: Specifications are the acceptance criteria on system performance. Specifications are the input at each design level. The *value of the parameter* which has met the performance requirement in the model propagates to the next level as specification in the synthesis flow. The global specification for the application to be designed is obtained from the user. Specification is composed of constraints such as performance constraints, environment constraints (e.g: technology, supply voltage, temperature etc).

Design: In the TD constraint driven approach the system is broken into blocks, sub blocks and so on. Each of these blocks is broken down (structural decomposition) from the system level specification which is imposed by the designer.

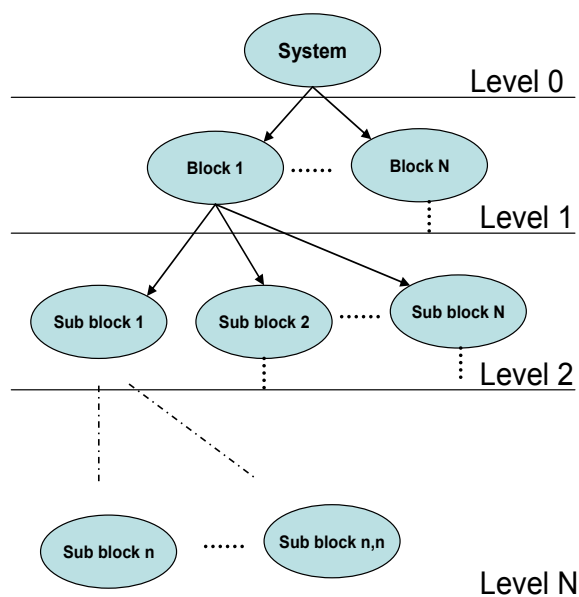


Figure 2.6 Design hierarchy

In the BU approach designers perform certain first level simulation with specification relevant to individual blocks and synthesize the blocks. Each of these blocks are connected together to make the system. Major problem with this design technique is that, if the final blocks do not meet the system specifications, the entire circuit has to be rebuilt. To overcome the long design time in BU approach and to avoid the rebuilding of the entire system if the system specification is not met, we choose the TD constraint driven approach evaluate at system level and build our system.

A Design can be broken into different abstraction levels. Here Level 0 represents the system level and Level N represents the layout level. These levels increases in computational complexity when we go down (level 0→level N) and decomposes each component into sub components (Figure 2.6). Lowest level component will be the primitive components (transistor, diode etc.). In the BU, we design from primitive components to high level block (level N→level 0). The flow (directed arrows) is followed until all the sub blocks in the design space are synthesized. Now that we know what is a model, their input/outputs. To communicate between each model we need a methodology. This is explained in the next section.

2.4 Parameter dependency graph

2.4.1 Formulation

We know the design variables, input and output of a model. But there is a lack of methodology to identify interdependencies between design variable and communicating between different variables. So we propose the parameter dependency graph to overcome this problem. Dependency graph is a directed graph representing inter-dependencies of several parameters. Order of dependency identified in such graphs support in characterizing each of the models at different level. This characterization also supports the propagation from one level to the other. Nevertheless, dependencies are also possible between parameters in the same level which leads to encapsulation of dependent parameters in an abstraction level.

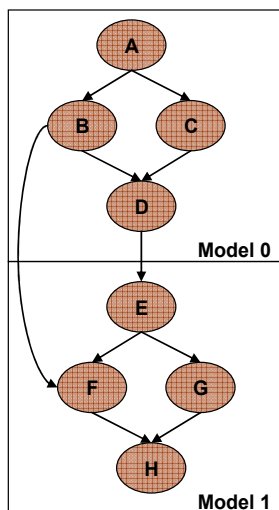


Figure 2.7 Parameter dependency graph

Figure 2.7 represents a simple dependency graph with several nodes and their dependency to other nodes represented with arcs. A-H are the parameters of the system. Two aspects have to be clearly defined: first the boundary between abstraction levels, and second the relationship between parameters at each level and through the levels. For example, it is possible to encapsulate the parameters as model 0 and model 1 or both of them together. For example: 'B' depends on both 'D' and 'F'. Two different models modeling their dependency are possible or modeling them as a single model taking all the dependencies in a single step. These possibilities are chosen by the designer based on known constraints (e.g. complexity, simulation time, tools etc). To illustrate the above methodology image sensor application is taken into account.

The system is characterized by the following performance metrics: maximum frames per second (FPS), dynamic range (DR), signal-to-noise ratio (SNR), quantum efficiency, conversion gain, well capacity, noise, power consumption etc. We have limited the description at the system level to three main characteristics such as FPS, DR, SNR to demonstrate the approach. Each of these metrics give rise to individual dependency graphs. However, there are also cases where some parameters are inter-dependent for one or more performances to be achieved (e.g. Integration time ($T_{\text{integration}}$)) which is detailed in the next section.

2.4.2 Frames per second (FPS) dependency graph

The first step in identifying the parameter dependency is to decompose the system into sub-blocks. Later, all the parameters which are related to FPS of each sub-block are identified with their relationship. The parameters which are considered to achieve the required FPS (performance) are individual timing parameters illustrated in Figure 2.8. The critical timing of the system is set by the timing of the pixel matrix size. The pixel matrix timing depends on parameters such as individual matrix row T_{reset} , T_{select} and $T_{\text{integration}}$ time where T_{reset} , T_{select} are the reset and select windows for resetting a pixel to the supply voltage and selecting the available output voltage from the discharge curve. $T_{\text{integration}}$ is the time available between the reset and select timing.

Along with the main timing parameters, there are other considerations such as column delay ($T_{\text{col delay}}$), which depends on the area of the 1 Mega pixel array to route the readout wire to the output pin of the pixel matrix. $T_{\text{row delay}}$ will take care of the delay which is maintained between each row to initiate the reset and select signal. All these parameters are related to the sensor block. Other timing parameters which must be considered for other blocks such as T_{adc} , T_{cds} can also be identified with their own parameter dependency graph in the same manner. The current work concentrates on the pixel matrix.

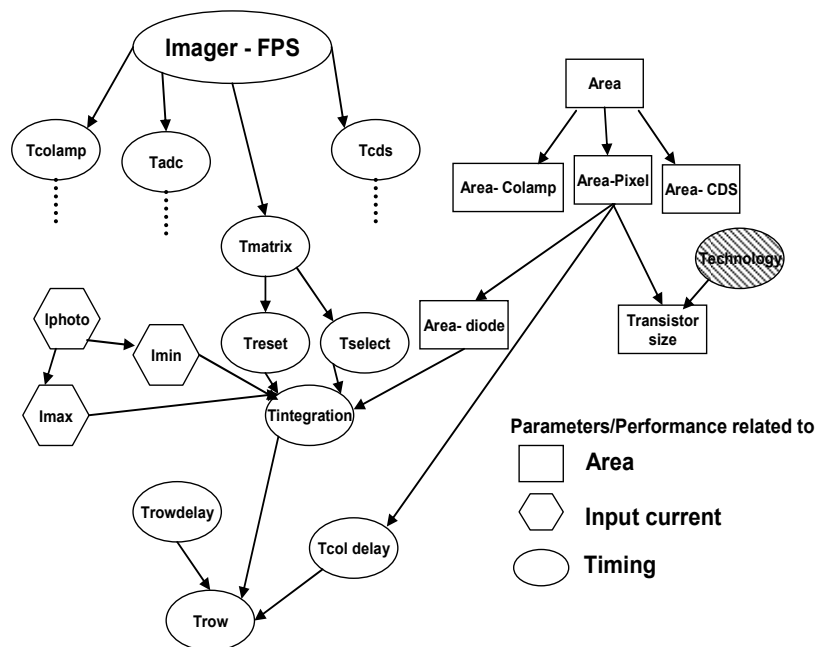


Figure 2.8 FPS dependency graph

Parameters which are related to area are indicated in rectangular box which is an environment related parameter (e.g area depends on technology). Hexagonal box represents the photocurrent available from the input light. Timing related performance (FPS) and dependent parameters are in circular box.

2.4.3 Dynamic Range (D.R) dependency graph

The main parameters which are considered to play a role in achieving the required dynamic range are the maximum photocurrent (I_{\max}) and minimum photocurrent (I_{\min}) of the pixel photodiode. Indeed, the dynamic range is given by [8]

$$\text{D.R} = 20\log_{10} \frac{I_{\max}}{I_{\min}} = 20\log_{10} \frac{\frac{qQ_{\max}}{T_{\text{integration}}} - I_{\text{dark}}}{\frac{q}{T_{\text{integration}}} \sqrt{\frac{1}{q} * I_{\text{dark}} * T_{\text{integration}} + \sigma_r^2}}} \text{dB} \quad \text{-- (2.1)}$$

Where Q_{\max} is the maximum well capacity, I_{dark} is the dark current, and σ_r^2 is the read noise power.

D.R depends on integration time parameter. FPS also depends on integration time. So this parameter has to take a value which will satisfy both FPS and D.R performances. Dark current depends on the area of the pixel and the temperature of the chip. These parameter dependencies are shown in Figure 2.9.

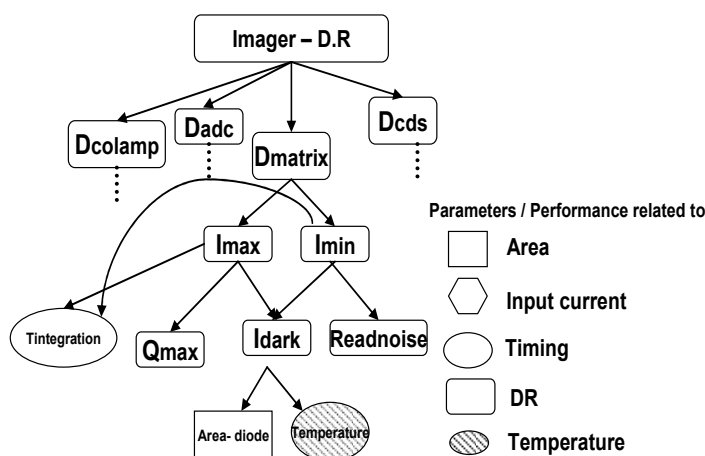


Figure 2.9 Dynamic range dependency graph

2.4.4 Signal to Noise Ratio (SNR) dependency graph

SNR dependency graph is depicted in Fig.7. SNR is given by[5]

$$\text{SNR}(I_{\text{ph}}) = 10 \log_{10} \frac{I_{\text{ph}}^2}{\frac{q^2}{T_{\text{integration}}^2} \left(\frac{1}{q} (I_{\text{ph}} + I_{\text{dark}}) T_{\text{integration}} + \sigma_r^2 \right)} \text{dB} \quad \text{-- (2.2)}$$

where I_{ph} is the signal available from the input picture. I_{dark} the dark current and σ_r^2 is the read noise power.

SNR depends on various other blocks (e.g. ADC) other than pixel matrix. SNR performance for the pixel matrix defines the required output voltage and the possible noise which the block could have due to readout noise, temperature. The required voltage due to the SNR specification imposes a constraint for the range of $T_{\text{integration}}$ possible due to the FPS performance.

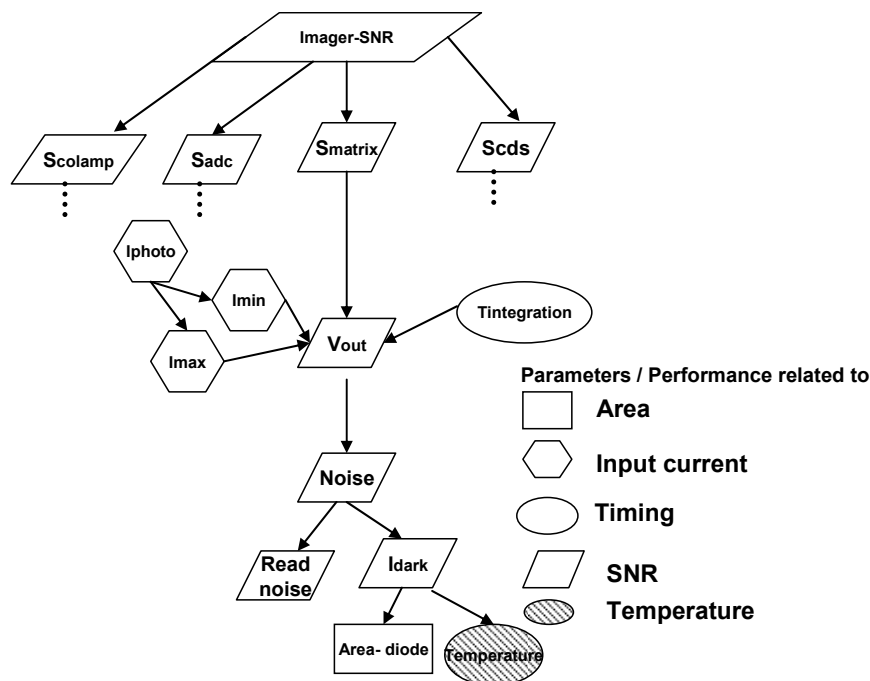


Figure 2.10 SNR dependency graph

Now having formulated the dependencies of all the considered performance metrics, it is important to segregate them into abstraction levels to build model for each of them.

2.5 Abstraction

2.5.1 Segregation of abstractions

From the parameter dependency graph, the identification of parameters and their inter-relationships enables their encapsulation as models. These models are placed at relevant abstraction levels and their hierarchical relationships are formulated. Each abstraction level is modeled individually and optimized to reach the desired performance metrics. The models are developed ensuring constraint propagation through the different levels using information obtained from the parameter dependencies. We have segregated the system into four abstraction levels namely system level, behavioral level, accurate behavioral level and physical level.

System level abstraction (Figure 2.11) consists of the various blocks (e.g. pixel matrix, ADC) which will be performing different functionalities in the system. This level defines the performances to be achieved by different blocks in the system. This level also helps in understanding the interrelationships between different blocks in the system.

The aim of the behavioral abstraction level is to define the behavior of each block (e.g. pixel matrix). In the example specific to the pixel matrix, the capacitance defines the behavior of the pixel due to the current produced by light falling on the diode. So the behavior of pixel can be defined by the available maximum and minimum current.

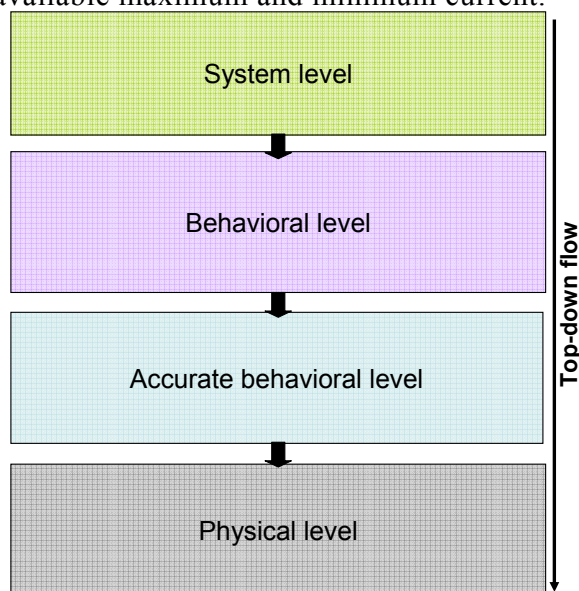


Figure 2.11 Abstraction levels

This maximum current helps to restrict the maximum possible select window timing of a row of pixels. This select window timing will be reflected as T_{reset} , T_{select} and $T_{\text{integration}}$ timing in accurate behavioral abstraction. Behavioral level gives only an idea/behavior of the system and timing possibility. With respect to ADC, we have restricted our methodology till behavioral level, since it meets all important requirements imposed by the pixel matrix. This is detailed later in the results section.

Accurate behavioral level adds additional information to the pixel matrix block from network of connections connecting the individual modules (pixels). The behavior of the pixel matrix module is defined by the network connections between the individual pixel modules. Accurate behavioral level is derived especially for the pixel matrix which is the important in the imager. At this level the pixel matrix is decomposed structurally into row pixels which have individual pixels connected between them using same reset, select lines (Figure 2.12).

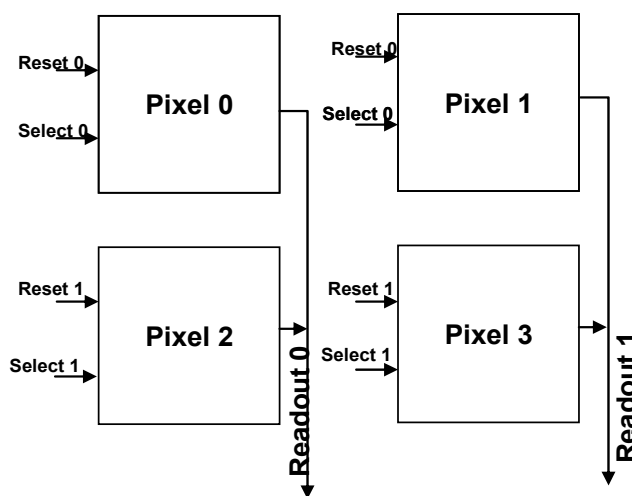


Figure 2.12 Pixel matrix structure.

Also at the accurate behavioral level, the column delay is predicted according to the predicted area of the pixel. The area is predicted based on the requirement of the output signal possible from the SNR specification and the photodiode area which allows us to have the required signal. This level also considers the timing delay, which has to be guaranteed between initializations of each row of the pixel matrix, to make sure that other blocks (e.g. ADC) work at the same pace.

Physical level represents the lowest level of abstraction. Physical level model is developed based on the firm-IP (pixel) designed at schematic. We utilize the electrical level simulation for our work in bottom up refinement.

2.5.2 Formulation

As explained earlier, using parameter dependency graph identification of parameters along with their relationship supports in encapsulating them at different abstraction levels and defining their hierarchical relationships. Each abstraction level is modeled individually and optimized to reach the desired performances metrics. The models are developed ensuring constraint propagation through the different levels using information obtained from the parameter dependencies. The abstraction levels which are identified with their input and output parameters are indicated in

Figure 2.13.

Starting from system level, we consider DR, FPS, SNR of the imager. We formulate the optimization problem to find the best set of parameters that respect the system specification. We followed the `fmincon`, to find the minimum of constrained nonlinear based optimization. This optimization minimized the cost function at each level to achieve the desired performance. In this optimization problem, blooming effect, effect of lens are not considered. All the optimizations were performed using Matlab run on Intel (2GB RAM, 2GHz) machine. As shown in

Figure 2.13, the performance model is built at each level in order to use the set of output parameters in other abstraction levels.

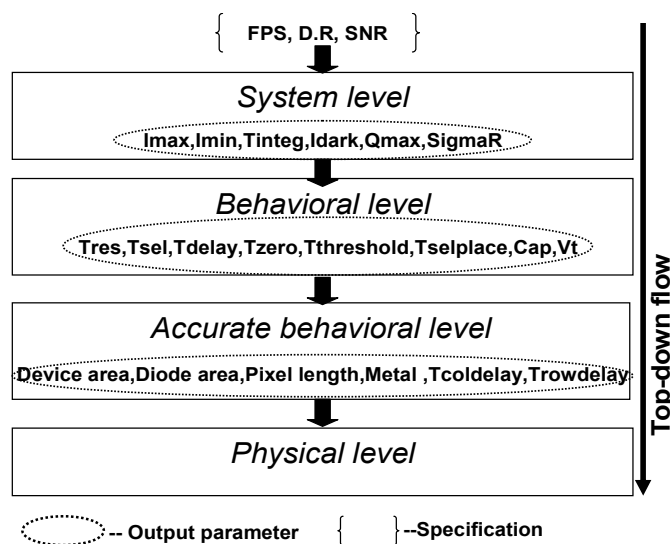


Figure 2.13 Abstraction level input/outputs

2.6 Results

2.6.1 Pixel matrix

Pixel matrix block is segregated into three abstraction levels namely 1. System level 2. Behavioral level 3. Accurate behavioral level. Their results are discussed in different sections.

2.6.1.1 System level

At the system level (2.1) and (2.2) are considered. The parameters such as Q_{\max} , $T_{\text{integration}}$, I_{dark} and readout noise values are optimized to achieve the D.R, FPS and SNR performances. Table 2-1 represents the parameters which were obtained at the end of 36 iterations achieving the required performances. The cost function (2.3) takes into account all performance tradeoffs using the weighted sum method. The cost function optimization graph is indicated in Figure 2.14. Values obtained for parameters (ex. Q_{\max}) will then be used as specification to characterize the pixel matrix in lower levels. The cost function for system level is

$$\text{Cost} = \alpha.FPS + \beta.DR + \gamma.SNR \quad \text{--(2.3)}$$

Where α, β and γ are weighting parameters.

The problem formulation is as follows: For e.g dynamic range (performance) (2.1) is a function of maximum (I_{\max}), minimum current (I_{\min}), readnoise, integration time(T_{integ}) and full well capacity (Q_{\max}). We optimize these design variables to achieve the desired performance metrics. These design variables are constrained by bounds as indicated in Table 2-1(A).

Table 2-1 System level input and outputs

(A) OPTIMISED PARAMETER INPUT			(B) PERFORMANCE RESULT		
Parameters	Constraint	Values	Performance	Spec	Result
Tinteg	<29us	28.2899us	Dynamic range	>60dB	64.9386dB
Idark	<10fA	1.03628E-16A	Signal to noise r	40-50dB	42.4452dB
Read noise	<10e-	10e-	FPS	25	25
Qmax	<50000	17659.1e-			
I _{max}		0.999998nA			
I _{min}		56.6332fA			

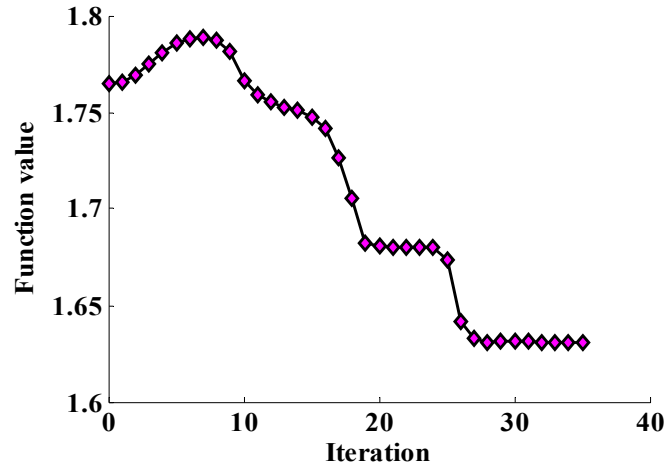


Figure 2.14 System level cost function optimization graph

2.6.1.2 Behavioral level

Behavioral level defines the behavior of each block which was decomposed in system level. Q_{\max} from system level is the performance which is to be achieved using the capacitance (as a parameter) of the photodiode by (2.4)

$$Capacitance = \frac{q * Q_{max}}{V} \text{ farads} \quad --(2.4)$$

This capacitance value defines the discharge behavior of the pixel matrix block based on the current produced due to the light falling on the diode. Technology (AMS 0.35 μ m) used fixes the voltage value. From the available photocurrent of each pixel, the time at which the discharge curve reaches zero is calculated using (2.5). Table 2-2 represents the best set of values which were obtained at the end of the optimization. Result is obtained within 4 iterations since the performance required is very well within the solution space. The cost function optimization graph is indicated in Figure 2.15.

$$T_{zero} = T_{reset} + T_{delay} + Mintime + a \quad --(2.5)$$

$$a = (CapBehavior * Dischargevoltstart * (\frac{1}{Photocurrent} - \frac{1}{Maxcurrent}))$$

Where T_{zero} is the time for the discharge to reach zero volt, T_{reset} the reset timing, $Mintime$ is the time needed for the maximum current that the image sensor handles and reaches zero volt,

CapBehavior is the capacitance value obtained, Dischargevoltstart is the voltage at which the capacitance starts to discharge, Photocurrent is the value of current which is input to the model to decide the time at which the voltage reaches zero and Maxcurrent is the maximum current upto which image sensor operates. Cost function for this level is in (2.6)

$$Cost = \alpha.Tmat + \beta.Qmax + \gamma.Imax + \delta.Imin \quad \text{--(2.6)}$$

Table 2-2 Behavior level input and output

(A) OPTIMISED PARAMETER INPUT			(B) PERFORMANCE RESULT		
Parameters	Constraint	Values	Performance	Spec	Result
Tres	<0.5us	0.2423us	Tmat	<30us	28.889us
Tsel	<0.5us	0.338us	Qmax		17659.1e-
Tinteg		28.3us	Imax		0.999998nA
Tdelay	<0.01us	9.98ns	Imin		56.6332fA
Tzero	<30us	26.35us			
Tthreshold	<Tzero	22.1461us			
Tselplace	<Tthreshold	21.7975us			
Cap	<0.9E-15	8.5726E-16F			
Vt	<0.5V	0.4921V			

The problem formulation is as follows: For e.g Q_{max} (performance) (2.4)(2.5) is a function of capacitance (Cap), Voltage (V). We optimize these two design variables also taking into account of other design variables (Capbehavior) relevant to other performance metrics to achieve the desired performance metrics. These design variables are constrained by bounds as indicated in Table 2-2

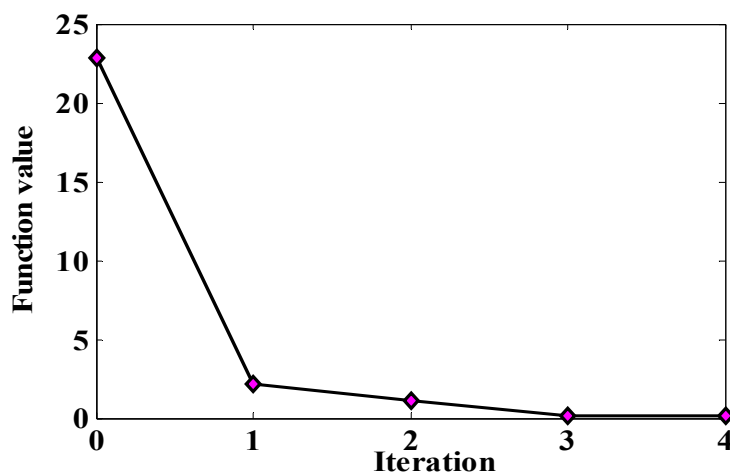


Figure 2.15 Behavior level cost function optimization graph

2.6.1.3 Accurate behavioral level

As described earlier at the accurate behavioral level the pixel matrix is decomposed structurally into row pixels which have individual pixels connected between them. The behavior is described as mathematical equation and it is optimized using Matlab. At this level the area of photodiode (parameter) is determined to achieve the capacitance (performance) using (2.7)

$$Area_{diode} = \frac{Capacitance \cdot W}{\epsilon} \mu m^2 \quad --(2.7)$$

Where W is the width of space charge region and ϵ is the material permittivity.

$$Fillfactor = \frac{Area_{diode}}{Area_{diode} + Area_{device}} \% \quad --(2.8)$$

$$Delay = 3.56 \cdot K_{ox} \cdot \epsilon \cdot \rho \cdot \frac{L^2}{\lambda^2} \quad --(2.9)$$

$$Cost = \alpha \cdot Fillfactor + \beta \cdot Cap + \gamma \cdot Tdelay + \delta \cdot Tmat \quad --(2.10)$$

Where K_{ox} is dielectric constant of oxide, ρ is the resistivity of the metal and λ is the technology. α, β, δ and γ are weighting parameters

From (2.7) and (2.8) area of the pixel is obtained. Assuming a square pixel, length of the pixel is also calculated. Using the length of the pixel the column delay [9] is calculated using (2.9). Five metal layers from 0.35um CMOS technology have been taken into account to calculate the appropriate delay incurred. These delay values are for the voltage of row 1 to reach the output of pixel matrix. Fill factor is optimized using the calculated area of diode, area of device parameters at the end of 11 iteration is indicated in Table 2-3 along with the cost function optimization graph in Figure 2.16.

The problem formulation is as follows: For e.g Capacitance (performance) (2.7) is a function of area of diode, width of depletion region (W). We optimize these two design variables also taking into account of other design variables (area of device) relevant to other

performance (Fillfactor) to achieve the desired capacitance performance. These design variables are constrained by bounds as indicated in Table 2-3

Table 2-3 Accurate behavioral level input and output

(A) OPTIMISED PARAMETER INPUT			(B) PERFORMANCE RESULT		
Parameters	Constraint	Values	Performance	Spec	Result
Area_device		19um ²	Cap		8.57E-16F
Area_diode		28.4837um ²	Tmat		27.9us
Pixelarea		47.4729um ²	fillfactor	<0.6	0.5999.
Length_pixel		6.8901um	Tdelay		9.98ns
Tcoldelay1		2.2703E-21s			
Tcoldelay2		2.185E-21s			
Tcoldelay3		1.8045E-21s			

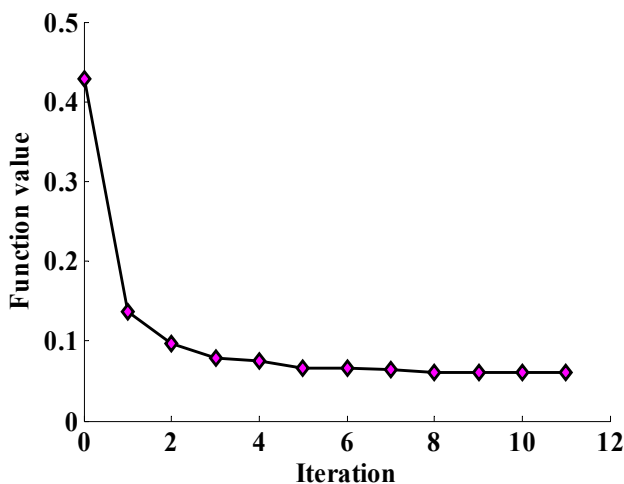


Figure 2.16 Accurate behavior level cost function optimization graph

2.6.2 ADC - Results

In this part we will discuss the ADC modeling results. ADC is segregated into system level and behavioral abstraction levels. At the behavioral level we divide the ADC into two sub-blocks namely DAC and comparator. These abstraction levels and their relevant results are explained below.

2.6.2.1 System level

Overall ADC system performance is based on few performances such as the signal to noise performance, sampling rate etc., But ADC is not limited only by these performances. Sampling rate of the ADC is imposed by the pixel matrix frames per second requirement. This is taken at this level of ADC.

The Signal to Noise Ratio is the ratio between the power of the signal and the total noise produced by quantization and the noise of the circuit. The SNR accounts for the noise in the entire Nyquist interval. It may depend on the frequency of the input signal but normally it is constant in the Nyquist zone and it decreases proportional to the input amplitude, resolution and sampling frequency. At the system level the SNR can be calculated by (2.11) [12]:

$$SNR = 20 \log \left(\frac{2^N}{\text{Noise ratio} * 2\sqrt{2}} \right) dB \quad --(2.11)$$

Where

$$\text{Noise ratio} = \sqrt{\text{Sampling noise}^2 + \text{Comparator noise}^2 + \text{Quantization noise}^2} \quad --(2.12)$$

Following are the different noise sources possible in ADC [12][13]: Sampling noise is dependent on temperature and the capacitance C_0 . It is given by (2.13)

$$\text{Sampling noise} = \sqrt{2 \cdot K \cdot T} / C_0 \quad --(2.13)$$

Followed by (2.14)

$$\text{Comparator noise} = \sqrt{2} \cdot \text{noise density} \cdot f_{3dB} \quad --(2.14)$$

Where

$$f_{3dB} = \frac{0.69 \cdot (N_{\text{resolution}} + 1)}{(2 \cdot \pi \cdot 0.5 \cdot t_{\text{clk}})} \quad --(2.15)$$

Amplitude quantization is the change of a sampled data signal from continuous level to discrete level. The dynamic range of the ideal quantizer is divided into a number of equal quantization intervals, each of which is represented by a given analog amplitude. An input amplitude that resides within a certain quantization interval is converted to the analog amplitude representing this interval. Often the value representing a quantization interval is the mid-point of the interval.

$$\text{Quantization noise} = \frac{V_{lsb}}{\sqrt{12}} \quad \text{--(2.16)}$$

The following relation is the maximum achievable (2.17) SNR in relation to the number of bits of the quantizer for a sinusoidal input.

$$\text{Theoretical SNR} = 6.02 \cdot N_{\text{resolution}} + 1.78 \quad \text{--(2.17)}$$

Normally the practically available SNR in the system is lower than the theoretical SNR obtained. This can be used to ensure that the practical SNR obtained during optimization is correct.

The maximum achievable SNR is also called signal-to-quantization noise ratio. The equation below reveals that every added bit of resolution increases the SNR by 6 dB. Accordingly, the power of quantization error decreases by a factor of 4. But since this equation accounts only for quantization noise, a more general form is used to consider all possible noise sources defining the equivalent or the effective number of bits (ENOB) of the ADC and is given by (2.18)

$$\text{ENOB} = \frac{\text{SNR} - 1.78}{6.02} \quad \text{--(2.18)}$$

Another performance which is important for ADC is the bandwidth. Bandwidth depends mainly on the resolutions and sampling rate. It is given by (2.19)

$$\text{Bandwidth} = \frac{1}{t_{\text{clk}}} \text{ Hz} \quad \text{--(2.19)}$$

Where

$$t_{\text{clk}} = \frac{1}{\text{Sampling rate} \cdot (N_{\text{resolution}} + 1)} \quad \text{--(2.20)}$$

These above equations give the basic performance metrics of the ADC operation at system level. Overall ADC system performance and its results are presented here. The optimizations is performed in Matlab. The system level cost function is formulated as the weighted sum of the performance requirement as in (2.21)

$$Cost = \alpha.SNR + \beta.Bandwidth \quad --(2.21)$$

System level model input and output is tabulated in Table 2-4. The cost function optimization curve is indicated in Figure 2.17.

Table 2-4 ADC System level input and output

(a) Performance result			(b) Parameter input		
Performance	Spec	Value	Parameter	Constraint	Value
SNR	>45dB	47.88dB	N- resolution	<16	8.0
Bandwidth	<350MHz	270MHz	Noise ratio	<0.5	0.364
			Sampling rate	>25MSPS	30MSPS

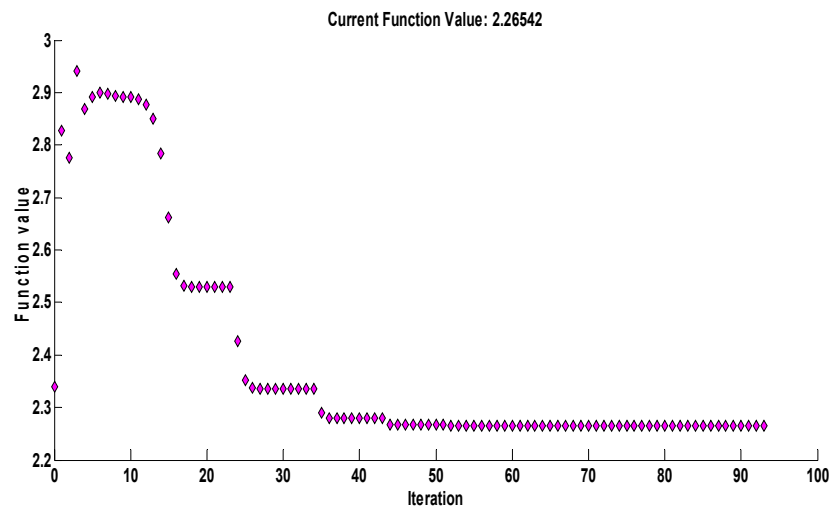


Figure 2.17 ADC system level cost function optimization graph

Furthermore detailed analysis of each sub-block at the behavioral level and their performance metrics are explained in the following sections.

2.6.2.2 Behavioral level – DAC

This DAC [10] is an array of binary weighted capacitors plus one additional capacitor of weight corresponding to the last significant bit (LSB), and switches that connect the capacitor bottom plates to three different voltages: VDD, Vref and ground. For a n -bit DAC, the value of the capacitors are as per (2.22)

$$C_i = 2^{i-1} \cdot C_0, i \in \{1 \dots n\} \quad \text{--(2.22)}$$

The capacitor banks will be used as track and hold block as well. The capacitor array is used to acquire the analog signal during the sampling phase. Such a usage reduces power consumption due to a switch and a capacitor [11]. In order to use directly the DAC capacitors, the sampling frequency is set as a performance to be achieved to have a relative high impedance. The time constant required for charging the capacitor array is given by (2.23)

$$\tau = R \cdot C_{total} \quad \text{--(2.23)}$$

Where

$$C_{total} = C_0 \cdot 2^N \quad \text{--(2.24)}$$

Where, N is resolution of ADC. From the above expression we could calculate the minimum period is expressed as (2.25)

$$T_{min} = \tau \cdot \ln \frac{1}{\varepsilon} \quad \text{--(2.25)}$$

Where ε is the error. The maximum error that we can tolerate is half of the LSB.

$$V_{LSB} = \frac{V_{in}}{2^N} \quad \text{--(2.26)}$$

From the above calculations it is possible to obtain the sampling rate which is the required performance given in (2.27)

$$Sampling\ rate = \frac{1}{9 \cdot T_{min}} \quad \text{--(2.27)}$$

The energy consumed by the DAC is calculated (2.28) based on the sampling rate followed by power calculation (2.29)

$$Energy_{DAC} = \frac{1}{2} \cdot C_{total} \cdot V_{in}^2 \quad \text{--(2.28)}$$

$$Power_{DAC} = \frac{\eta \cdot Energy \cdot Sampling\ rate}{N} \quad --(2.29)$$

Where η is the factor modeling [10] dependence of total energy drawn from the supply V_{in} .

2.6.2.3 Behavioral level - Comparator

Due to the tight constraint imposed by the pixel matrix size to achieve the high speed operation, selection of the comparator which will work hand in hand with the DAC is necessary. The comparator settling time should be less than the rise time of DAC to achieve the sampling rate performance. Source-Coupled Logic [12] [13] is one such architecture which allows reducing the sensitivity of the circuit to the supply voltage variation. Hence the speed of operation of this logic is independent from the supply voltage while it can be controlled by acting on the tail bias current. The voltage output swing maintenance depends on the comparator block. These following equations (2.29)-(2.31) give the basic performance metrics of the comparator operation.

$$V_{swing} = R_{load} \cdot I_{ss} \quad --(2.29)$$

Where R_{load} is load resistance and I_{ss} is the bias current of the PMOS load device. Where

$$I_{ss} = 2 \cdot n \cdot \mu \cdot C_{ox} \cdot U_T^2 \cdot \frac{W}{L} \quad --(2.30)$$

Where n is the subthreshold slope factor [14] which is 1.2, μ is the mobility of charge carrier, C_{ox} is the oxide capacitance, U_T is thermal voltage, W is width of transistor and L is length of transistor.

With the above equation the settling time of comparator can be calculated using (2.31)

$$T_{settling} = \tau \cdot \log \frac{V_{in}}{\left(\frac{V_{lsb}}{2}\right)} \quad --(2.31)$$

The cost formulation at the behavioral level for DAC and comparator is indicated in (2.32)

$$Cost = \alpha.Sampling\ rate + \beta.DAC\ Power + \gamma.Setting\ time + \lambda.Comparator\ gain \quad --(2.32)$$

For the sake of clarity DAC and comparator performance input and output are indicated in Table 2-5 and Table 2-6 and their cost function optimization graph is indicated in Figure 2.18.

Table 2-5 DAC output and inputs

(a) Performance result

Performance	Spec	Value
Sampling rate	>25MSPS	30 MSPS
Power _{DAC}	<25uW	3.659μW

(b) Parameter input

Parameter	Constraint	Value
N– resolution	<16	8.03
C ₀	<2fF	1fF
R	<1MΩ	2.032MΩ
TminDAC	<10ns	3.703ns

The important point to note from the results of DAC is the sampling rate. The problem is constrained by requirement of more than 25MSPS to handle the output from 1MP pixel matrix array at 25FPS. Table 2-5 (b) shows the parameters which were achieved during the optimization.

The comparator is obliged to have a settling time lower than the rise time of the DAC to achieve the required sampling rate performance. The Table 2-6 tabulates the details on this performance.

Table 2-6 Comparator input and outputs

(a) Performance result

Performance	Spec	Value
Tsettling	<TminDAC	6.35ps
Vgain	>30	35.24

(b) Parameter input

Parameter	Constraint	Value
N– resolution	<16	8.03
W	<20uM	4.7uM
L	<20uM	13.99uM
Rload	>1MΩ	2.03MΩ

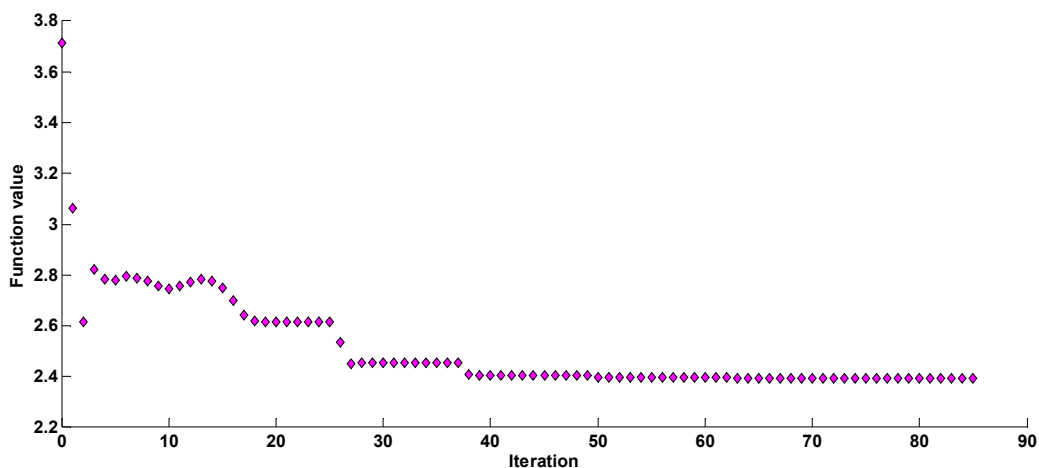


Figure 2.18 ADC- Behavioral level cost function optimization curve

Thus the hierarchical modeling is performed with ADC block to meet the requirements of the Imager system. The optimization converged to a solution in about 80 iterations taking few ms time for the simulation.

In the TD approach the feasibility of the obtained parameters values are not checked. Sometimes due to the weak or infeasible constraints for various blocks, the results obtained might be unachievable. The optimization problem formulated used a weighted sum approach and consequently can lead to unfeasible solutions. A way to bypass this limitation is to use pareto-front approach. In this methodology the problem formulation allows to build a feasible design space representing tradeoff between several performance metrics. This work has been done only with the pixel matrix and other block developments are still ongoing. The next section explains in detail about the pareto-front methodology.

2.7 Pareto-front methodology

Hierarchical design can be efficiently done in a top-down manner as explained in section 2.4: at each level in the hierarchy, the corresponding model is optimized and the result used to derive performance requirements for the next lower-level [17]. A known drawback of this approach is that the derived requirements may be non feasible by technology available or it might be overambitious, lying out of the feasible performance region of the lower-level blocks. To overcome this limitation, recent work on analog synthesis proposes techniques to explicitly

compute the feasible performance regions of circuits and use them to constrain the hierarchical optimization process [18]–[20]. Among the proposed techniques, we highlight those that make use of Pareto-fronts, which are sufficient for hierarchical design. The Pareto-front is the part of the boundary of the feasible performance region that designers are most interested in, as it captures the optimal trade-off between competing performances. Furthermore [21] utilizes the Multi-objective Bottom-Up (MUBU) to describe the method where Pareto-fronts computed for low level components are combined to generate the tradeoff surface for the full system. This method has the benefit that all generated points correspond to fully sized solutions, and no further optimization is needed. In this work the MUBU approach is extended [22] by approximating the Pareto-fronts using interpolation and present a hierarchical synthesis framework that handles multiple levels of abstraction.

In the Pareto-front methodology the following are performed

- 1.Exploration of feasible solution at system level
- 2.Exploration being aware of limitation at lower levels

2.7.1 Methodology

All practical design problems involve the simultaneous optimization of multiple competing performance metrics. This multi-objective (MO) problem is generally formulated [19] in (2.33):

$$\min f = f(x) = \begin{bmatrix} f_1(x) \\ \vdots \\ f_n(x) \end{bmatrix} \text{ subject to: } \begin{cases} C_{eq}(X) = 0 \\ C_{ineq}(X) \leq 0 \end{cases} \quad \text{--(2.33)}$$

Where f is the vector of performance, x is the vector of design parameters, $f(x)$ is the simulation model linking the parameter space X ($x \in X$) to the performance space F and C_{eq} , C_{ineq} are equality and inequality constraints to be satisfied.

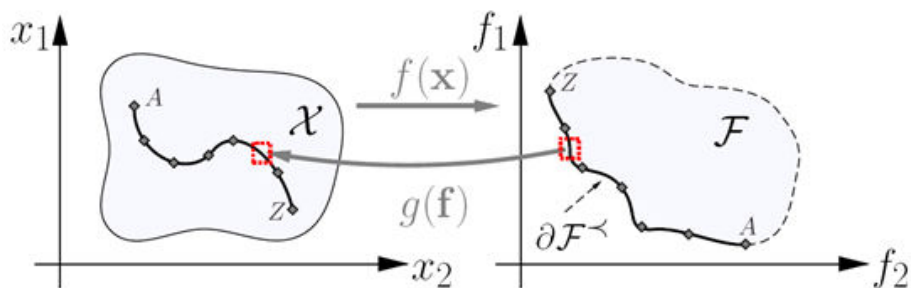


Figure 2.19 Parameter space (left) and performance space (right)[19]

Solving the above equation leads to Pareto-optimal designs. Always improving one performance comes at the cost of other. The outcome of all these optimal designs is the so called Pareto-frontier. The approach presented next consists of characterizing the Pareto-front of a block by computing a few optimal designs and then generating interpolation functions $g(f)$ to predict the optimal design for different performance requirements (Figure 2.19).

The simulation of a model can give access to multiple performance metrics (e.g: FPS, DR, SNR, Area etc). Sometimes not all the performances are competing or of main interest for the design process. Using this knowledge on the architecture at hand, the designer decides which metrics can be excluded from the analysis, ending up with a subset that we will call the trade-off performances.

To visualize the performance evolution several constraints were applied in the optimization. Constraints are used with two goals: ensure the proper operation of the component and confine the trade-off analysis to a region of interest. After identifying the performances to be solved and applying the appropriate constraints we were able to compute the pareto optimal design. This is explained in the next section along with supporting results.

2.7.2 Pixel pareto-front - Results

To produce the pixel pareto-front, Dynamic range (DR), Signal to noise ratio (SNR) and Area performances are taken into account to prove the pareto-front methodology in the design flow. Additional performances could be added easily following the same procedure.

DR is expressed using (2.34)

$$D.R = 20\log_{10} \frac{I_{max}}{I_{min}} = 20\log_{10} \frac{\frac{qQ_{max}}{T_{integration}} - I_{dark}}{\frac{q}{T_{integration}} \sqrt{\frac{1}{q} * I_{dark} * T_{integration} + \sigma_r^2}} \text{ dB} \quad --(2.34)$$

where q is the charge of electrons, Q_{max} is the full well capacity expressed in electrons, $T_{integration}$ is the integration time in seconds, I_{dark} is the dark current in Amperes, σ_r is the read noise in electrons. Assuming I_{dark} equal to 1fA and read noise as $10e^-$ the following output curves is obtained as in Figure 2.20. This curve is an illustration of DR (performance) evolution as a function of $T_{integration}$ and Full well capacity (parameters).

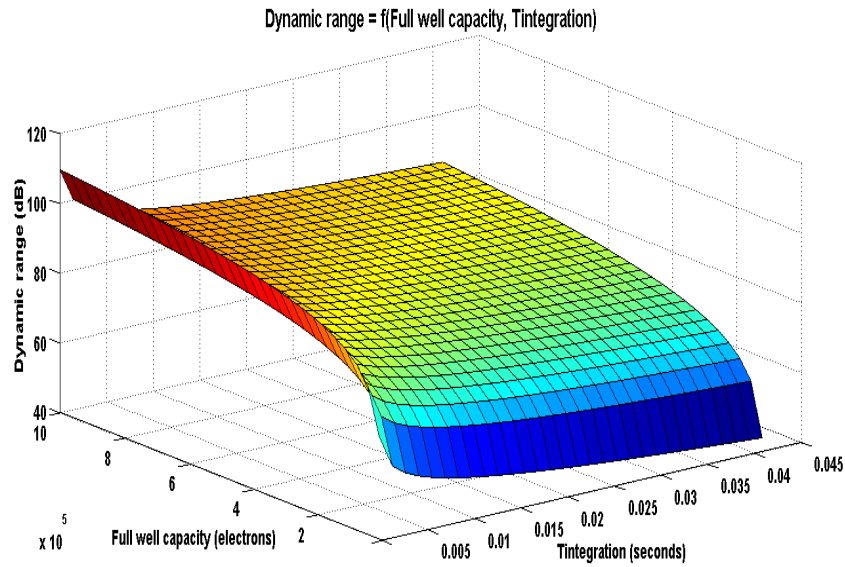


Figure 2.20 Dynamic range evolution

The same way SNR could be expressed in terms of full well capacity and Tintegration from the following equation (2.35)

$$\text{SNR}(I_{\text{ph}}) = 10 \log_{10} \frac{I_{\text{ph}}^2}{\frac{q^2}{T_{\text{integration}}^2} \left(\frac{1}{q} (I_{\text{ph}} + I_{\text{dark}}) T_{\text{integration}} + \sigma_r^2 \right)} \text{dB} \quad \text{--(2.35)}$$

Assuming the same values for the dark current and read noise the evolution of SNR (performance) is indicated as in Figure 2.21.

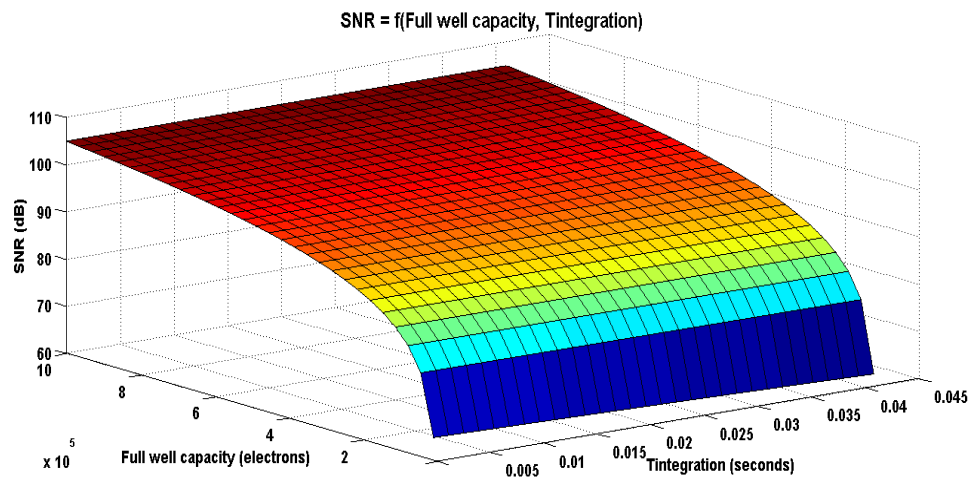


Figure 2.21 SNR evolution

In the same way evolution of pixel area could be formulated using (2.36) & (2.37)

$$\text{Area} = \frac{\text{Capacitance} * \text{Width of depletion region}}{\epsilon_0 * \epsilon_r} \quad \text{--(2.36)}$$

$$\text{where Capacitance} = \frac{q * Q_{\max}}{\text{Voltage}} \quad \text{--(2.37)}$$

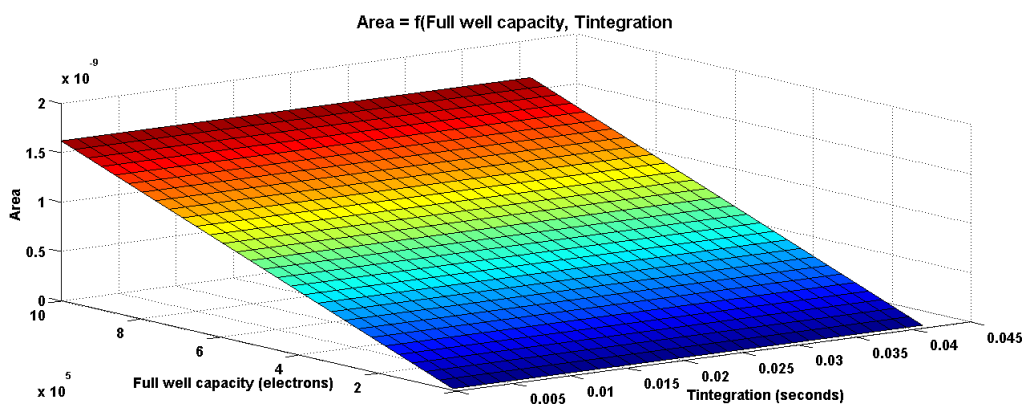


Figure 2.22 Area evolution

Thus from the above Figure 2.20, Figure 2.21 and Figure 2.22 it is possible to see the evolution of various performances as a function of their parameters.

The goal of the pixel pareto-front methodology is to see the performance tradeoff and their feasible regions. This is depicted in the Figure 2.23.

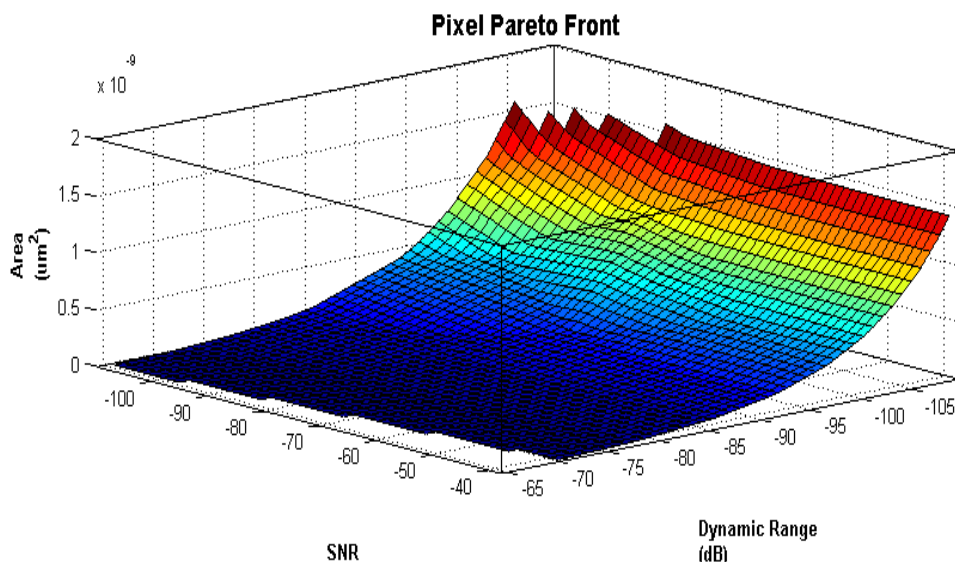


Figure 2.23 Pixel pareto-front

The above figure clearly shows the entire region of operational feasibility for the pixel respecting all the constraints imposed during the optimization. It also provides an alternate methodology to understand the tradeoff between competing performances and selection. This methodology gives much more realistic behavior of the system compared to the top-down approach.

2.8 Conclusion

The modeling approach followed during this research work accomplished the following:

Top-down design methodology

Hierarchical approach realized using

- Parameter dependency graphs
- Pixel performances studied extensively
- Segregated into various abstraction levels
- Achieved the required performances along with cost function

Hierarchical top-down approach in ADC

- Achieved the necessary performance imposed by pixel matrix

Pareto-front methodology

- Pixel matrix block utilized to prove the methodology
- Tradeoff between various performances has been evaluated
- Ongoing work with other blocks

The above modeling work has extensively studied the details of top-down to synthesize various blocks. During the TD approach, the temperature used is ambient condition (300K) due to the lack of information on discharge behavior based on temperature. Firstly, in a realistic situation imager operates at temperature higher than ambient condition. Secondly, moving to 3D architecture creates hotspots. So the problem of inter-pixel variability gets aggravated. There are no scalable high level models to simulate pixel matrix giving importance to inter-pixel variability. To have an accurate model at system level we follow the bottom-up refinement approach to collect data from electrical level and feed back at system level. This improves the accuracy of system level model with respect to temperature. in the research arena

on a model looking at thermal aspects in 3D architecture specialized in imager. Next chapters will mainly focus on

- Modeling:
 - Modeling of pixel matrix to analyze thermal impact (Bottom-up)
 - Novel (scalable) model capable of simulating huge matrix (For ex. 0.5 MP or more)
 - High speed simulation capability
- 3D Integrated design flow
 - Floorplanning
 - Thermal simulation
 - High speed simulation of pixel matrix with thermal model

The next chapters will be focusing on the above aspects and will give deeper insights into the 3D-Imager especially in thermal aspect based floorplanning and in finding solution which might deteriorate the performance of the imager.

Bibliography

- [1] M.Torngren et al, « Component-based and Model based development: A comparison in the context of embedded systems” Proceeding of EUROMICRO’05 pp:432-441
- [2] R Stevens, P Brook, K Jackson & S Arnold. Systems Engineering - coping with complexity. Pearson Education 1998. ISBN 0-13-095085-8
- [3] F Neelamkavil. Computer simulation and modelling. John Wiley & Sons Inc, 1987
- [4] V.Viswanathan, L.Labrak,F.Frantz, D.Navarro and I.O’Connor, “Model based design of Imager using abstraction segregated parameter dependency graphs”, Newcas 2011, June 26-29, Bordeaux, France
- [5] L.Labrak, I.O’Connor, “Heterogeneous System Design Platform and Perspectives for 3D integration”, 21th IEEE International Conference on Microelectronics ICM’09, Marrakech, Morocco, 2009
- [6] M.Bigas et al, “Review of CMOS image Sensors” Microelectronic Journal,2006,37,433-451
- [7] E.R. Fossum, “Active Pixel Sensors(APS)- Are CCDs Dinosaurs?” Proc.SPIE vol.1900,pp.2-14, 1992
- [8] A.El Gamal “High dynamic range image sensors” lectures and classnotes, Stanford university
- [9] http://www.maxim-ic.com/appnotes.cfm/an_pk/1080/, 21 juin 2009.
- [10] B. P. Ginsburg and A. Chandrakasan, “An energy-efficient charge recycling approach for a SAR converter with capacitive DAC,” in IEEE ISCAS Int.Symp. Circuits and Systems, 2005, pp. 184-187.
- [11] G.Beanato, “Design of very low power SAR analog to digital converter”, thesis, 14 August 2009
- [12] A. Tajalli, E. J. Brauer, Y.Leblebici “Ultra-low power 32-bit pipelined adder using subthreshold source-coupled logic with 5 fJ/stage PDP” Microelectronics Journal 40 (2009) 973-978.

- [13] A. Tajalli, Elizabeth J. Brauer et al., “Subthreshold Source-Coupled Logic Circuits for Ultra-Low-Power Applications”, IEEE J. Solid-State Circuits, vol. 43, no.7, pp. 1699-1710, July 2008.
- [14] <http://www.iue.tuwien.ac.at/phd/stockinger/node13.html>
- [15] Mootaz, “Systematic design of SAR Analog to digital converter, Thesis, Cairo university, 2008
- [16] http://www.lte.e-technik.uni-rlangen.de/download/ADU/Converter_class4.pdf
- [17] H. Chang, E. Charbon, U. Choudhury, A. Demir, E. Felt, E. Liu, E. Malavasi, A. Sangiovanni-Vincentelli, and I. Vassiliou, A Top-Down, Constraint-Driven Design Methodology for Analog Integrated Circuits. Springer, 1996.
- [18] P. Nuzzo, X. Sun, C.-C. Wu, F. D. Bernardinis, and A. Sangiovanni-Vincentelli, “A platform-based methodology for system-level mixedsignal design,” EURASIP J. Embedded Syst., vol. 2010, pp. 6:4–6:4, January 2010.
- [19] G. Stehr, H. Graeb, and K. Antreich, “Analog performance space exploration by normal-boundary intersection and by fourier motzkin elimination,” computer-Aided Design of Integrated Circuits and Systems, IEEE Transactions on, vol. 26, no. 10, pp. 1733 –1748, oct. 2007.
- [20] T. Eeckelaert, R. Schoofs, G. Gielen, M. Steyaert, and W. Sansen, “An efficient methodology for hierarchical synthesis of mixed-signal systems with fully integrated building block topology selection,” in Proceedings of the conference on Design, automation and test in Europe, ser. DATE’07. San Jose, CA, USA: EDA Consortium, 2007, pp. 81–86.
- [21] G. Gielen, T. McConaghy, and T. Eeckelaert, “Performance spacemodeling for hierarchical synthesis of analog integrated circuits,” in Proceedings of the 42nd annual Design Automation Conference, DAC ’05. New York, NY, USA: ACM, 2005, pp. 881–886.
- [22] Felipe Frantz, Lioua Labrak, Ian O'Connor, Hierarchical Design Flow for Heterogeneous Systems using Pareto Front Interpolation, IEEE Transaction on Computer Aided Design (TCAD), (under review)

Chapter 3

Thermal-aware image sensor model

3.1 Introduction

One of the unavoidable sources of pixel noise in 3D stacked CMOS imagers is thermal - both in terms of absolute temperature for thermal noise, and in terms of imager-wide temperature variation for inter-pixel variability. In the former case the thermal noise is generated by random thermally induced motion of electrons. It exhibits [1] a zero-mean, flat and wide bandwidth Gaussian power spectral density. Several analysis have been published [2][3][4] on the absolute temperature impact on thermal noise. We are interested in proving and proposing solutions for the inter-pixel variability due to the impact of temperature. This is important in system level modeling perspective moving from 2D to 3D stacked chip. Although temperature can be of some impact in 2D imagers, it is exacerbated in 3D imagers due to a higher overall power density. Thermal noise also of course leads to greater performance degradation in 3D chip. In order to minimize the thermal impact on the pixel matrix it is essential to analyze the thermal problem in detail and provide possible solutions.

In this chapter, the thermal aware model generation for analyzing the thermal impact is explained in detail. Firstly, the need for the model and the properties which have to be fulfilled by the new model will be discussed in section 3.2. The model generation takes into account exhaustive data generation from electrical simulations, as discussed in section 3.3. With the obtained data, we describe the methodology used to create the thermal model in section 3.4, followed by a pre-validation phase, discussed in section 3.5. The integration of the pre-validated model into a SystemC-based modeling tool will be discussed in section 3.6. Post-validation of the final model is discussed in section 3.7. In section 3.8, conclusions will be drawn from the analysis made through several test cases.

3.2 Thermal Model

3.2.1 Problems and requirements

Few tools exist to analyze the impact of temperature variation over different regions of the entire pixel matrix on the output. Such analyses could give a clear picture of the impact of temperature during the early stages of design space exploration. This is not feasible with existing tools such as Spectre or PSpice, since these tools are very costly in terms of computation time to simulate large (>1Mpixels) imager pixel matrices. Even more costly are finite element method based tools (such as ANSYS), which require sophisticated meshing methodologies and long simulation times for high-resolution simulation. It is not currently feasible to simulate a complete matrix with this approach – instead, designers simulate individual pixels or groups of pixels to analyze their behavior. Hence, system-level designers face real difficulties in the development of simulation and modeling methods for fast, scalable and accurate pixel matrix evaluation. The focus of research work for simulation and modeling at high abstraction levels strive to overcome these problems. The main factors which are targeted in this work are:

- Short simulation cycles (speed)
- Ability to simulate any pixel matrix size (scalability)
- Low error (a few %) when compared to electrical simulation results (accuracy)

Such a thermal model could offer the designer:

- More accurate verification of design decisions in terms of the pixel matrix output
- Choice of technology parameters (silicon thickness, area, power etc.) based on thermal impact
- Early and thermal aware floorplanning
- Hardware block specifications to apply correction (Correlated Double Sampling (CDS), filters etc.)
- Introduction of thermal Fixed Pattern Noise (FPN) - Software based correction algorithms applied only to regions which have higher thermal impact. This could reduce the workload of ISP

To achieve this, a basic understanding of the thermal model is necessary – we cover this in the next section.

3.2.2 Compact thermal model

Hotspot [5] is a tool enabling the description of simplified models of thermal resistance networks, and subsequent simulation using the thermal-electrical analogy. The temperature difference caused by the heat flowing through a material becomes a voltage difference caused by the current through a resistance. The volume of the stack is meshed in cubes, building up a resistive matrix \mathbf{R}^t and capturing both the silicon stack and the heat-spreader/heatsink as shown in Figure 3.1. For a system with power (heat) sources P , the temperature in each point of the stack, T , is then obtained solving the linear system of equations as in (3.1)

$$\begin{bmatrix} T_1 \\ \vdots \\ T_n \end{bmatrix} = \begin{bmatrix} R_{11} & \dots & R_{1n} \\ \vdots & \ddots & \vdots \\ R_{n1} & \dots & R_{nn} \end{bmatrix} \begin{bmatrix} P_1 \\ \vdots \\ P_n \end{bmatrix} \quad \text{--(3.1)}$$

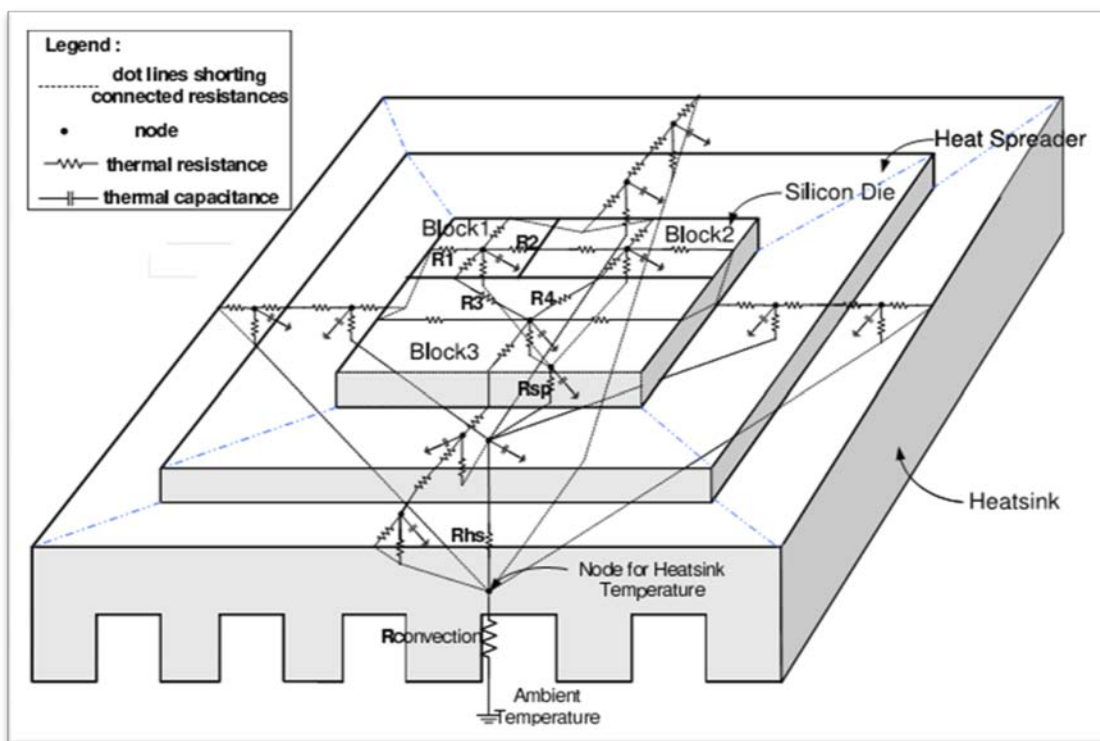


Figure 3.1 HotSpot model [5]

Although this model can aid in visualizing the temperature evolution across the layer, based on the power density of each block and material properties available at each layer, an imager thermal model requires more information to accurately evaluate discharge behavior, which is dependent on:

- Temperature
- Light intensity
- Integration time

In our approach, we implement an imager thermal model with SystemC to include description of discharge behavior based on light intensity and integration time, and couple this to the HotSpot based compact modeling technique to obtain a temperature map, which is fed into the imager thermal model. This integration of imager thermal model along with the compact model is described in detail in Chapter 4. In the next step, we will go through the imager thermal model development steps.

3.2.3 Model development steps

We follow a bottom-up (Figure 3.2) and empirical approach modeling to achieve an accurate (but design-specific) high-level model. We qualify the approach as bottom-up because we extract data from an existing circuit described at the transistor level; it is therefore intended to be used in system validation steps or in system exploration steps (where free exploration parameters are in blocks other than the imager). The approach is also empirical, because we generate mathematical models from the data, without the use of any physical parameters, and further without any preconception of the type of mathematical model to be used. Detailed description on model and its characteristics is made in Chapter 2.

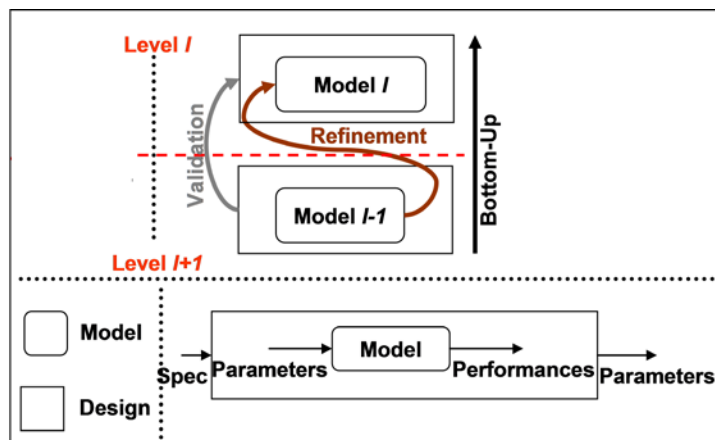


Figure 3.2 Bottom-up approach

The model development process follows a set of steps, as depicted in . This process is generic and can be easily adapted to any pixel design. As explained earlier, Compact modeling technique is used just to analyze the temperature evolution on a chip. The requirement with respect to imager is a model expressing the behavior of pixel as a function of temperature, light and integration time. The following modeling steps can be used to realize imager specific model.

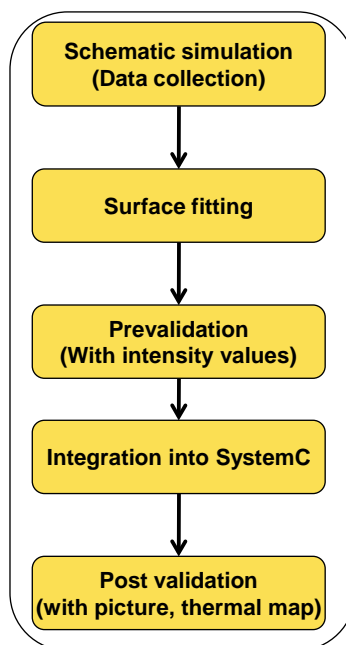


Figure 3.3 Model development process

Two model validation steps are integrated into the development process. First, the pre-validation step is carried out on a single pixel simulation. This step supports in selection of orders of fitting to meet the required accuracy. Second, the post validation step is carried out on a pixel matrix. This step supports in selection of orders of fitting based on simulation time.

3.3 Exhaustive data generation

3.3.1 Pixel behavior

Firstly let us understand the structure and behavior of the pixel operation. The 3T-Active Pixel Sensor (APS) [6] [7] structure uses a photodiode as a photon-sensing node. Figure 3.4(a) shows the pixel schematic with photodiode, while its timing graph is shown in Figure 3.4(b). The pixel consists of three nMOS transistors. The potential of the photodiode is set to V_{DD} through a reset transistor (M_{rst}). When photons hit the photodiode, charges are collected in the form of photocurrent and converted into a voltage signal (discharge) directly by the photodiode junction and parasitic capacitance. A follower transistor (M_{sf}) is used to amplify the signal. During integration time, the photodiode node capacitance discharge provides a time-dependent signal slope proportional to the intensity of the incident light. At the end of the integration time the signal level is read out through a row select transistor (M_{sel}).

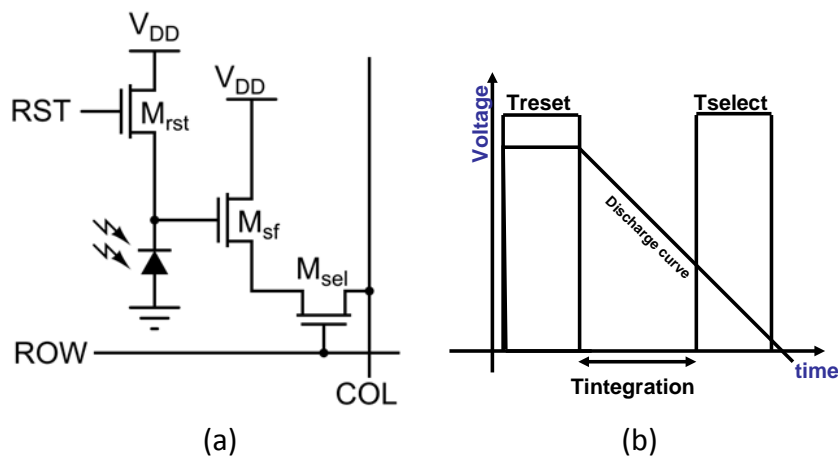


Figure 3.4 (a) 3T-APS structure (b) Timing graph

3.3.2 Imager thermal model

The imager thermal model has to incorporate the previously explained pixel behavior along with the thermal impact on the discharge behavior. To add these details into the model, several electrical simulations were performed to analyze the normal behavior of a pixel in room temperature conditions, as well as for various other temperature conditions.

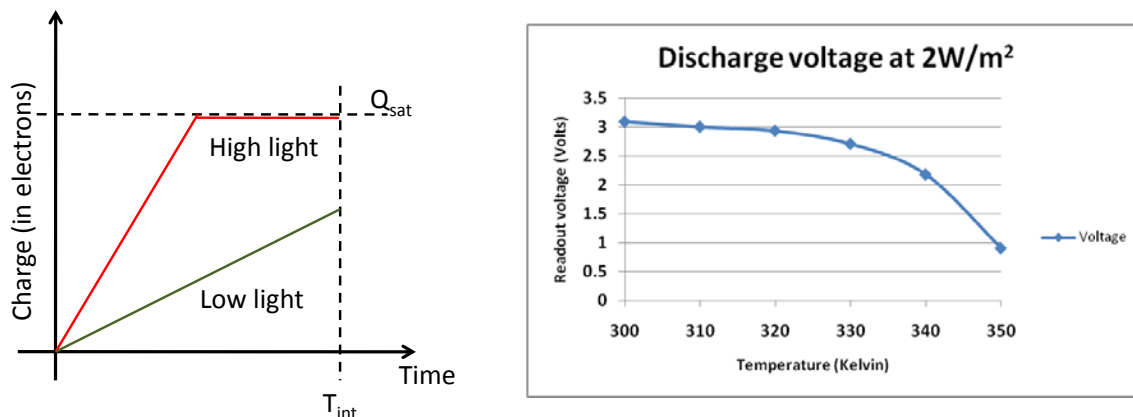


Figure 3.5(a) Charge vs Time (b) Discharge voltage vs Temperature(@10msTintegration)

The ideal charge versus time characteristic for two photocurrent values is illustrated in Figure 3.5(a). In the low light case, the charge at the end of integration is proportional to the light intensity, while in the high light case, the diode saturates, and the output charge is equal to the well capacity Q_{sat} , which is defined as the maximum amount of charge that can be held by the integration capacitance [8].

The discharge curve is also dependent on temperature, which is clearly visible in Figure 3.5(b), resulting from simulations performed at a fixed light intensity of $2W/m^2$ for varying temperature values from 300K to 350K. The light intensity ($2W/m^2$) is low light condition and it does not cause any saturation in the circuit parameters.

The imager thermal model functionality can thus be summarized here using (3.2)

$$Readout\ voltage = f(Temperature, Light\ intensity, Tintegration) \quad --(3.2)$$

Ultimately the aim of this work is to combine the pixel discharge behavior along with the temperature evolution of the entire system. With this model a designer could easily visualize the impact of temperature, light intensity and integration time on the output performance of pixel matrix.

Chapter 3 – Thermal-aware image sensor model

This model does not include parameters such as impact of supply voltage, cross-talk, statistical process parameter variation etc. that can have influence on the performance of pixel matrix.

3.3.3 Electrical simulations

Electrical simulations were performed using the Cadence Spectre simulation tool and with the AMS 0.35um technology design kit. Figure 3.6 shows the circuit schematic [9] that was simulated, of a single pixel with sized parameters for all components. This includes a generic photodiode model [9], developed using Verilog-A, which can take into account various technology parameters, light and temperature related data. The simulation results are already presented in Figure 3.5(b).

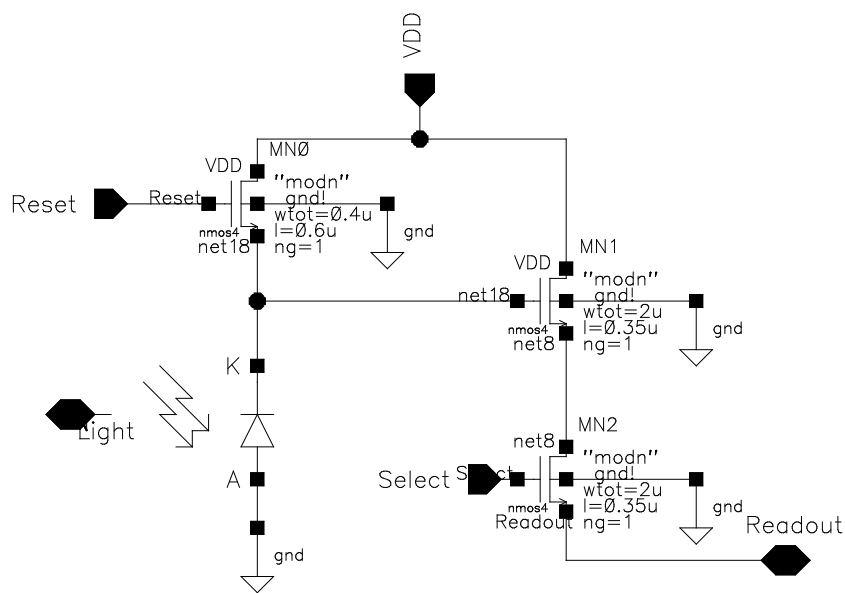


Figure 3.6 Pixel schematic with sized parameters

The circuit schematic is used to perform parametric simulations covering the entire expected range of operation of the imager, as indicated in Table 3-1. Although simulations were performed up to 380K, values above 350K were omitted since the output voltage values were below the threshold voltage of 0.1V. The threshold voltage is decided as 0.1V based on the following reasons: 1. Firstly, the selection of integration time is a tradeoff covering both bright light and low light condition. Simulations performed using the above pixel showed that

Chapter 3 – Thermal-aware image sensor model

integration time between 2ms to 10ms is appropriate to cover maximum region of operation of the pixel. 2. The simulation performed at maximum conditions of temperature, light intensity and integration time (350K, 10ms and 200W/m²), showed that 0.1V is the least possible discharge voltage from the pixel. Any voltage below this threshold voltage is considered not meaningful. Since the discharge of the photodiode is almost linear, the selection of simulation variables was taken at regular (linear) intervals over the entire range of operation of the image sensor. Data from a total of 330 simulations were generated for further model development.

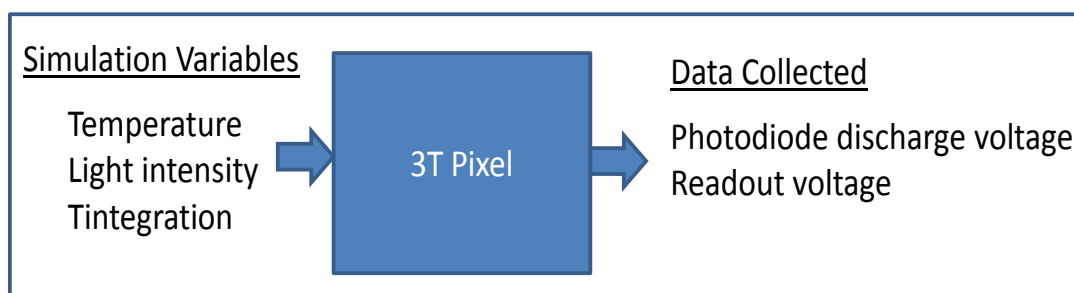


Figure 3.7 Parametric simulation input and output

Table 3-1 Parametric simulation operational range

Variables	Minimum value	Maximum value	Step	No of simulations
Temperature	300K	350K	10K	6
Light intensity	0 W/m ²	200 W/m ²	20W/m ²	11
Integration time	2ms	10ms	2ms	5

A parametric simulation (Figure 3.7), running for the above mentioned range, lasted for one minute for each set of simulation. Dedicated Skill™ function code is written to read all the data points and store. The photodiode discharge voltage and readout voltage were collected in tabular format. The results are ported to the Matlab environment for post-processing and to do fitting.

3.4 Fitting

3.4.1 Types of fitting

Fitting is a process of constructing a curve or mathematical function that fits the series of data points. We have performed various simulations and collected the series of data points which exhibits the behavior of pixel. The aim of the fitting is to find a mathematical function that fits well with the data points. The well known types of fitting are

- Least Squares fitting
- Non linear fitting
- Smoothing fitting

Least Squares is the most popular method of fitting. It is relatively simple in terms of required computing power. Least Squares minimizes the square of the error between the original data and the values predicted by the equation. Least Squares method is sensitivity to outliers in the data. If a data point is widely different from the majority of the data, it can skew the results of the regression. So it is important to examine the data before fitting. The most well known types of Least squares fitting are linear, polynomial, exponential and logarithmic. As the name suggests linear least square fitting uses a function to fit a straight line through the data. Polynomial function fits a curve through the data. Higher order polynomial can be used if the curve needs a complex curvature. Exponential function is used if the data increases or decreases at high rate. Logarithmic is used if the data that spans in decades. Exponential and Logarithmic cannot be used if the data spans through negative or zero values.

The non linear fitting is a method that provides a numerical solution for a problem of minimizing function which are non linear. This method starts with an initial guess of an unknown parameter that calculates a value which represents the sum of squared error between data and the calculated fit.

Smoothing fitting, as the name suggests is used to improve the appearance of plot by drawing a smooth curve through the data. This fitting generally does not generate any equation for the resulting curve. This is because there is no single equation that can be used to represent the curve. Commonly known smooth fitting methodologies are Smooth, Weighted, Cubic Spline and Interpolate. Smooth and Interpolate uses a geometric weight to arrive to a final

curve. Weighted curve uses a weighted least squares error (lowess) method. Cubic spline uses a series of cubic polynomials.

Selection of fitting methodology is mainly based on the behavior of the pixel and the data collected. Electrical simulation suggests: 1. discharge behavior of pixel to be almost linear 2. data collected were free from any abrupt rise or fall in values 3. data did not span through negative values but there are regions with values equal to zero. The model needs the following: 1. need a behavioral equation as a function of all the parameters 2. portable into the SystemC environment for simulating pixel matrix 3. capable to deal with values equal to zero. With the above requirements and behavior of the data points, “Polynomial fitting” is the most suitable, since it satisfies all the requisites.

3.4.2 Surface fitting

The data points can be established as a function of two independent variables (x,y) to implement the surface fitting (polynomial) methodology [10]. The data points are denoted as in (3.3):

$$\mathbf{Output} = \mathbf{f}(x_i, y_i) \text{ for } i = 1, 2 \dots \dots n \quad \text{--(3.3)}$$

This data is used to construct a surface function $\phi(x, y)$ which approximates the given data set as closely as possible. This is measured by the accuracy (i.e. the distance between the approximation function and the collected data points) and to a lesser extent the smoothness of the resulting function, and is achieved by the type of mathematical function and the number of coefficients allowed in the fitting. A higher number of coefficients for a given function approximation will lead to greater accuracy and smoothness but will also require more computational effort, both to find during the fitting process, and also to evaluate during model execution and system simulation. To measure the accuracy, i.e. the distance between the data points and the approximation function $\phi(x, y)$, we use the standard definition of the residual, as denoted in (3.4):

$$\mathit{Residual}_i = f_i - \phi(x, y) \quad \text{--(3.4)}$$

Hence, the selection of type of function approximation is critical since the accuracy per number of coefficients varies according to the suitability of the function approximation to model the set of data points. The selection of order of polynomial fitting can be done by

comparing the number of coefficients and different surface fitted results. When the order is low the fitting will be poor and if the order is high the fitting will be as close as possible. However, we can already indicate that we use polynomial fitting in the current problem because the performance space represented by z does not have any sharp peaks or sudden change in behavior, and we should therefore use a continuous mathematical function. We also consider that the set of data points with which we are dealing extends to the entire range of operation of the system. In other words, the system is not expected to operate (and it is not expected to simulate the model) outside this range, so the fitting range is bounded. The robustness of this methodology will be proved by checking the fitting at number of intermediate points (i.e. points which have been evaluated at electrical but which have not been used in the fitting process).

As a starting point to prove the methodology, we formulated the problem with only two independent variables (temperature, light intensity) as expanded in (3.5)

$$\text{Readoutvoltage}_i = f(\text{Temperature}_i, \text{Lightintensity}_i) \quad \text{--(3.5)}$$

Parametric simulations were performed to collect the photodiode discharge voltage and readout voltage for the above function at a fixed integration time value (10ms). This value is chosen to check the model capability at the end of system operating range (350K, 200W/m² and 10ms). Moreover, this is just an indicative value chosen to prove the surface fitting methodology and proceed with developing a model with all the three variables to cover the

$$\text{Readoutvoltage} = \begin{pmatrix} \text{Coeff}_1 \\ \vdots \\ \text{Coeff}_m \end{pmatrix} * (\text{Temperature} \quad \text{Lightintensity})^{\begin{pmatrix} 0 & 0 \\ \vdots & \vdots \\ 5 & 5 \end{pmatrix}} \quad \text{--(3.6)}$$

entire system range. Figure 3.8 shows the fitting obtained for a fifth order function in terms of temperature and light intensity as indicated in equation (3.6).

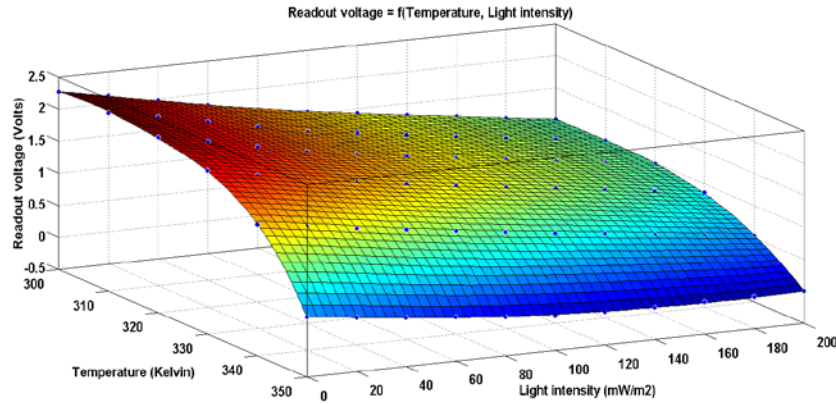


Figure 3.8 Surface fitting with two variables

The complete equation used in solving this problem, coefficient values and goodness of fit values along with the residual plot are given in Appendix I.

Having established the basic methodology for two independent variables, we must now deal with three variables and extend the approach to the entire range of pixel operation.

3.4.3 Volume fitting

In this section we will discuss in detail about including another independent variable in the surface fitting [10] methodology. Integration time is the third independent variable which is dealt along with temperature and light intensity. The photodiode discharge voltage or readout voltage dependence is expressed in (3.7):

$$\text{Readout voltage}_i = f(\text{Temperature}_i, \text{Light intensity}_i, \text{Integration}_i) \quad \text{--(3.7)}$$

We have used readout voltage in most of the work, since we are more interested in the output voltage of the pixel. Nevertheless, the model is capable of providing the photodiode voltage as well as illustrated in Figure 3.9. The model has the capability to use of any order of polynomial to. We have restricted the orders of fitting from third to sixth order for the following reasons: 1. below the third order the fitting error is high in comparison to electrical simulation results 2. At the sixth order the accuracy was as expected in terms of quanta 3. Increasing the order than required will result in simulation time. These points are explained in the following sections.

Formulation of the multivariate polynomial [11][12], to perform the fitting with constant coefficients is given by (3.8). Consider x, y, z as temperature, light intensity and integration time.

$$P(x, y, z) = a_{klm} x^k y^l z^m + \dots + a_{222} x^2 y^2 z^2 + \dots + a_{111} xyz + \dots + a_{100} x + a_{010} y + a_{001} z + a_{000} \quad \text{--(3.8)}$$

To reduce the coefficients, sum of polynomial power is obtained. The coefficients of the term which have power equal to or less than the order of fitting is taken and the rest (mixed term) is omitted. For example with the polynomial $x^k y^l z^m$ we can reduce mixed term using (3.9)

$$(k + l + m) \leq \text{order of fitting} \quad \text{--(3.9)}$$

This is performed when the order is less than or equal to the maximum order of the original two polynomials. This process is used to reduce the mixed terms in the problem. If we keep all the mixed terms the number of coefficients is calculated as M^N where M is the number of variables and N is the order. For instance with our three variables and third order polynomial, normally the number of coefficients is 27 but due to the reduction of mixed terms we obtain 20 as indicated in Table 3-2. In this work we explore the use of third order to sixth order polynomials to analyze the fitting efficiency. The table below also indicates the increasing number of coefficients when the orders of fitting are increased.

Table 3-2 Fitting order

Fitting order	Coefficients
Third	20
Fourth	35
Fifth	56
Sixth	84

After performing the reduction of mixed terms, the coefficients of the polynomial in its power form can be computed by solving a system of simultaneous linear equation as expressed in (3.10)

$$\begin{pmatrix} x_1^{n-1} & x_1^{n-2} & 1 \\ \vdots & \vdots & 1 \\ x_n^{n-1} & x_n^{n-2} & 1 \end{pmatrix} \begin{pmatrix} a_1 \\ \vdots \\ a_n \end{pmatrix} = \begin{pmatrix} R_1 \\ \vdots \\ R_n \end{pmatrix} \quad \text{--(3.10)}$$

a_1 to a_n are the coefficients derived after removing the mixed terms and R_1 to R_n are the output values. The linear system matrix (x values) is known as Vandermonde matrix[14].

The simplified final equation used in calculating the readout voltage using fitting process is (3.11):

$$\text{Readoutvoltage} = \begin{pmatrix} \text{Coeff}_1 \\ \vdots \\ \text{Coeff}_m \end{pmatrix} * (\text{Temperature} \quad \text{Lightintensity} \quad \text{Temperature})^{\begin{pmatrix} 0 & 0 & 0 \\ \vdots & \vdots & \vdots \\ 6 & 6 & 6 \end{pmatrix}} \quad \text{--} \quad (3.11)$$

The above equation is solved with all the variables with Figure 3.9 and Figure 3.10 depicting the fitting of photodiode node voltage and the pixel readout voltage respectively. The impact of the third independent variable (integration time) is clearly seen in the multiple voltage surfaces (five surfaces for discrete values of integration time from 2ms to 10ms). The topmost curve shows the voltage for $T_{\text{integration}}=2\text{ms}$ and the bottom curve is for $T_{\text{integration}}=10\text{ms}$.

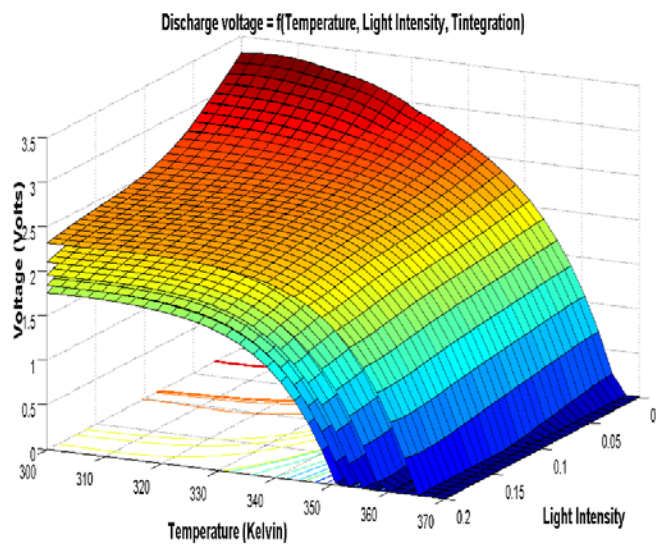


Figure 3.9 Photodiode discharge voltage (Top curve at 2ms and bottom curve at 10ms)

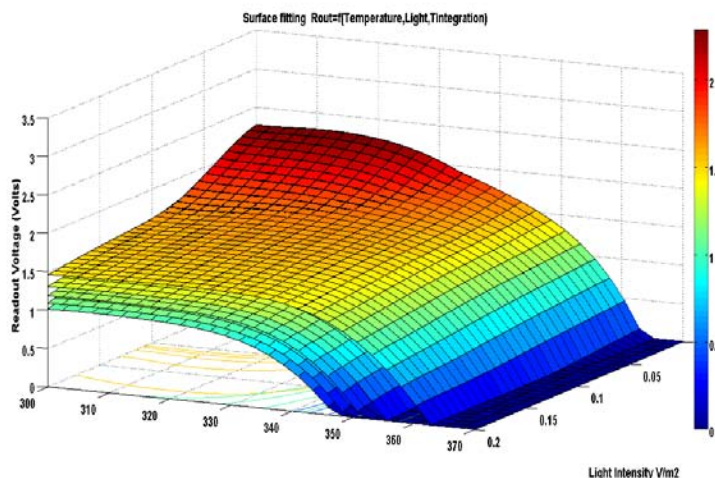


Figure 3.10 Readout voltage
(Top curve at 2ms and bottom curve at 10ms)

The equation, coefficient values and orders of fitting details are attached in Appendix II. The selection of fitting order will be explained in the following section.

3.5 Pre-Validation

3.5.1 Requirement

As mentioned in the previous section the volume fitting is complex and so a pre-validation step is necessary. Firstly, it helps in verifying the model results before integrating them for the simulation of entire pixel matrix. Secondly, this verification also helps to identify the orders of fitting that is accurate with respect to the electrical simulation results. Thirdly, regions of deviation from accuracy could be identified (e.g. bright light or low light condition errors) and improved before integration.

To perform the pre-validation step, the operating range of the system has to be chosen. For instance, we chose the light input ranging from 2W/m^2 (dark current) to maximum system

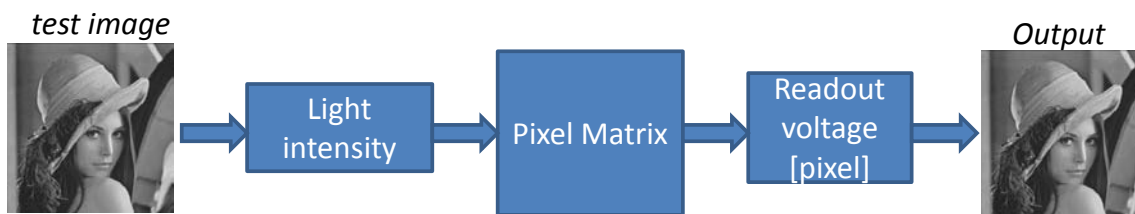


Figure 3.11 Signal path of proposed model

photocurrent 200W/m^2 . These are just indicative example values. We assume 8 bit resolution. This resolution provides 256 grey levels.

To simplify the process of pre-validation, rather than considering the imager as continuous system from the input perspective (light intensity from 0 – 200W/m^2) it is much easier to consider the imager as a discrete system from the output perspective (256 grey levels). Thanks to the integer type grey levels. The input image with various grey levels as illustrated in the Figure 3.11 is converted into linearly relative light intensity value as indicated in Figure 3.12. This light intensity is fed into the pixel matrix to have a realistic light intensity distribution. Pixel generates an output voltage which can be converted into an 8 bit depth grey level image with intensity data ranging from 0 to 255. So we need 256 different output voltage bounds from the highest to the lowest corresponding from intensity 0 to intensity 255 and these voltage stages all relate to a specific light intensity. Since we need 256 different output voltage stages, we segregate the input light intensity into 256 blocks. 256 light intensity values are simulated both in the electrical simulation and using the developed model at different orders of fitting. The output voltage value of both the simulations is compared to evaluate the accuracy.

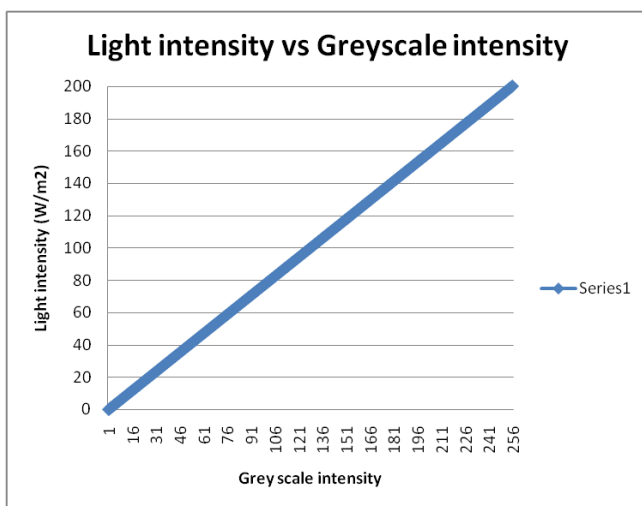


Figure 3.12 Light intensity vs Grey scale intensity

This methodology has the following advantages: In the system point of view, this step helps in simulating the continuous system as discrete system; it allows identifying the range of light intensity (float) that yields specific range of output voltage (float) yielding grey level (integer). In the modeling point of view, it reduces the number of simulations needed to

analyze the accuracy of the model, it helps in correlating the influence of temperature in terms of intensity level.

3.5.2 Preliminary results

Once the input (light intensity, temperature) is set for the pixel, the select window is placed at the required integration time to obtain the readout voltage. This process is also performed in the electrical simulation. Both the model and the electrical simulation readout voltage results are compared against the intensity value. Figure 3.13 represents the readout voltage validation for the third to sixth order of fitting against the electrical simulation readout voltage (in red). Validation step is performed for the entire range of the system operation. Here only few of them are illustrated. First one is the validation step performed at 300K, with 2ms integration time for the entire range of 8-bit grey scale input light intensity values.

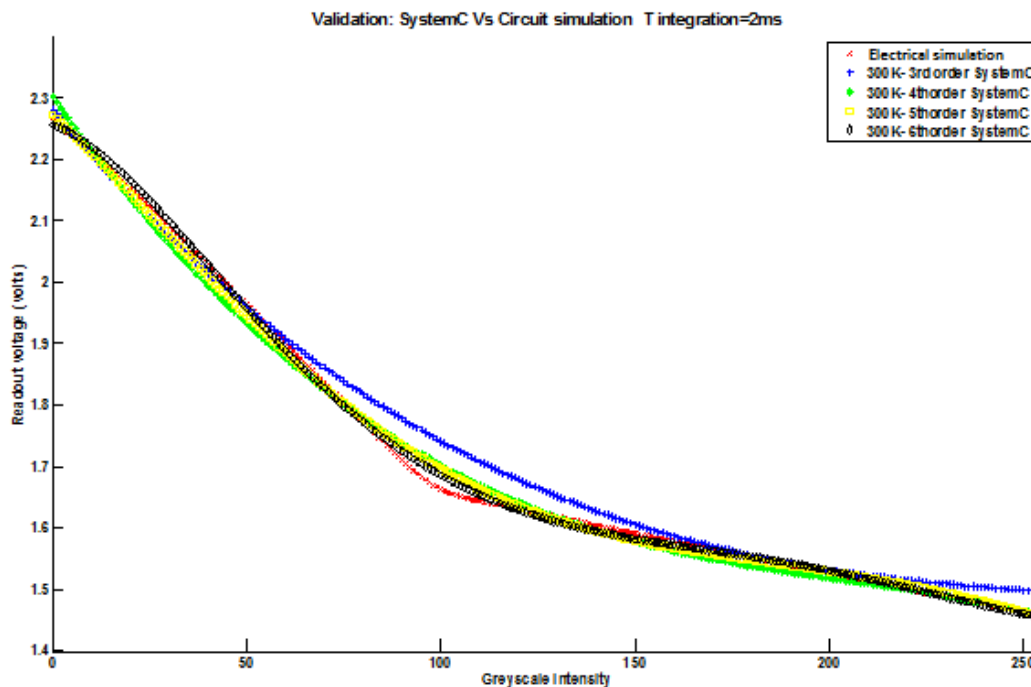


Figure 3.13 Pre-validation model vs Spice simulation

Chapter 3 – Thermal-aware image sensor model

Then the validation performed for various other values of temperature and integration time as indicated in Figure 3.14 (300K, $T_{int}=10ms$), Figure 3.15 ($T=325K$, $T_{int}=10ms$) and Figure 3.16 ($T=350K$, $T_{int}=10ms$).

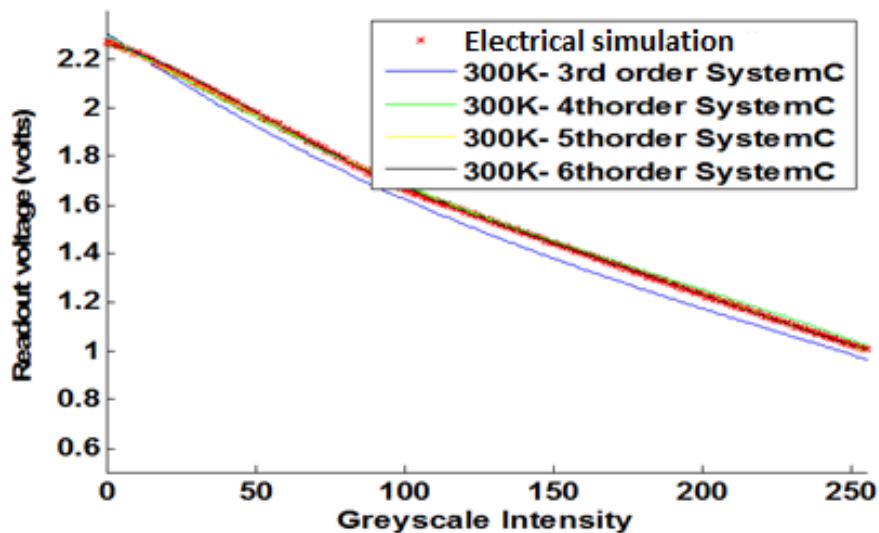


Figure 3.14 Pre-validation ($T=300K$, $T_{int}=10ms$)

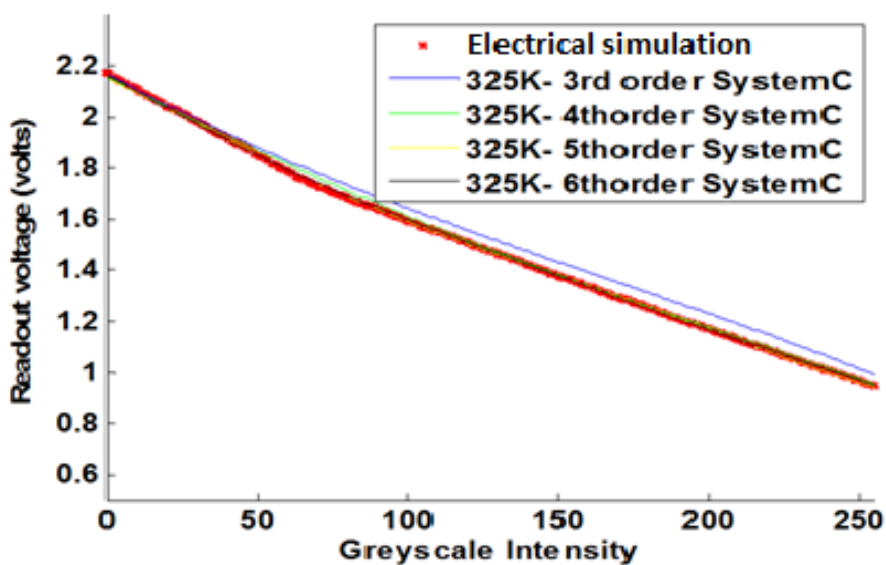


Figure 3.15 Pre-validation ($T=325K$, $T_{int} = 10ms$)

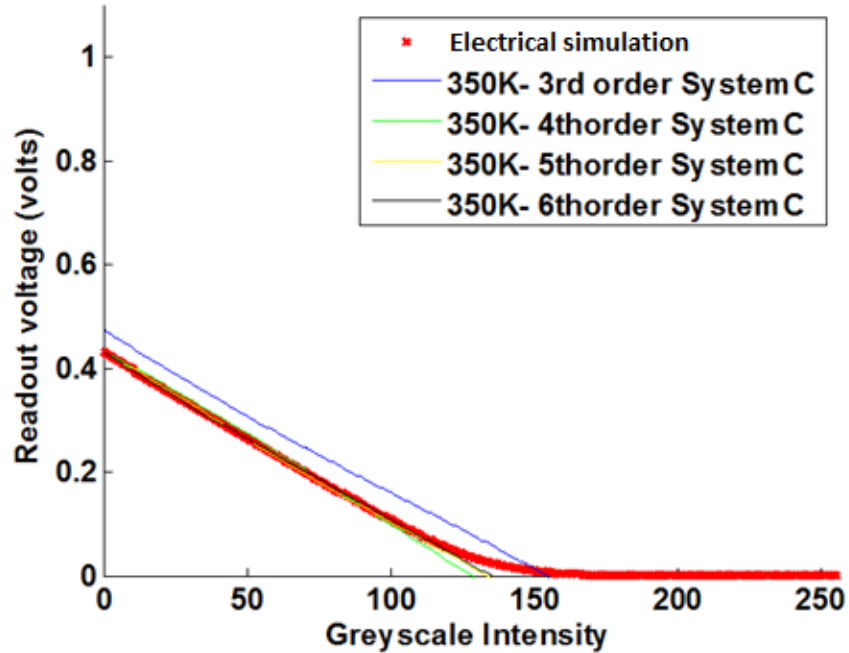


Figure 3.16 Pre-validation ($T=350K$, $T_{int} = 10ms$)

From these figures, it is clear (and intuitively correct) that the accuracy of the model improves as we increase the order of fitting. This pre-validation step proves that the output of the model will not have any influence on the final image output intensity level, since the error is well below the quanta needed to switch between one intensity level to another.

3.5.3 Fitting order accuracy

A pre-validation step has been performed to evaluate the accuracy of the method so as to choose the orders of fitting. The final selection of the order of fitting is performed after evaluating the simulation time in the SystemC environment.

The average error and relative error is calculated using (3.12) and (3.13)

$$\text{Average error (Volts)} = \frac{\sum_{i=1}^{i=N} |\text{Electrical simulation voltage}_i - \text{Model output Voltage}_i|}{\text{Number of values}} \quad \text{--(3.12)}$$

$$\text{Error (\%)} = \frac{\text{Average error}}{3.3V} \times 100 \quad \text{--(3.13)}$$

For this step, several simulations were performed with temperatures of 300K, 325K, 350K and integration times of 2ms to 10ms at regular intervals of 2ms for 3rd, 4th, 5th and 6th orders of fitting. Their average error at each simulation is tabulated in Table 3-3

The behavior of the model for various orders of fitting with respect to electrical simulation are depicted in Figure 3.17 and Figure 3.18.

Table 3-3 Simulation data – Average error (in Volts & in %)

2ms						
300K		325K		350K		
Order	Avg error (Volts)	Error (%)	Avg error (Volts)	Error (%)	Avg error (Volts)	Error (%)
3	0.0193	0.58	0.0233	0.71	0.0382	1.16
4	0.0039	0.12	0.0095	0.29	5.30E-03	0.16
5	9.40E-04	0.03	0.002	0.06	5.11E-04	0.02
6	5.91E-04	0.02	0.0024	0.07	0.002	0.06

4ms						
300K		325K		350K		
Order	Avg error (Volts)	Error (%)	Avg error (Volts)	Error (%)	Avg error (Volts)	Error (%)
3	0.0209	0.63	0.0021	0.06	0.0223	0.68
4	0.0052	0.16	0.0054	0.16	0.0108	0.33
5	5.79E-04	0.02	0.0014	0.04	0.003	0.09
6	8.00E-04	0.02	0.0012	0.04	0.0016	0.05

6ms						
300K		325K		350K		
Order	Avg error (Volts)	Error (%)	Avg error (Volts)	Error (%)	Avg error (Volts)	Error (%)
3	0.0152	0.46	0.0029	0.09	0.0392	1.19
4	0.0065	0.20	0.0041	0.12	0.006	0.18
5	2.91E-04	0.01	0.0024	0.07	6.65E-06	0.00
6	6.85E-04	0.02	0.0012	0.04	8.94E-04	0.03

8ms						
300K		325K		350K		
Order	Avg error (Volts)	Error (%)	Avg error (Volts)	Error (%)	Avg error (Volts)	Error (%)
3	0.0052	0.16	0.0191	0.58	0.0239	0.72
4	0.0054	0.16	0.01	0.30	0.024	0.73
5	0.0016	0.05	3.04E-04	0.01	0.0205	0.62
6	3.92E-04	0.01	1.20E-03	0.04	0.0128	0.39

10ms						
300K		325K		350K		
Order	Avg error (Volts)	Error (%)	Avg error (Volts)	Error (%)	Avg error (Volts)	Error (%)
3	0.0484	1.47	0.0436	1.32	0.046	1.39
4	0.0074	0.22	0.0095	0.29	0.1095	3.32
5	6.18E-04	0.02	0.0018	0.05	0.0911	2.76
6	9.26E-04	0.03	2.64E-04	0.01	0.076	2.30

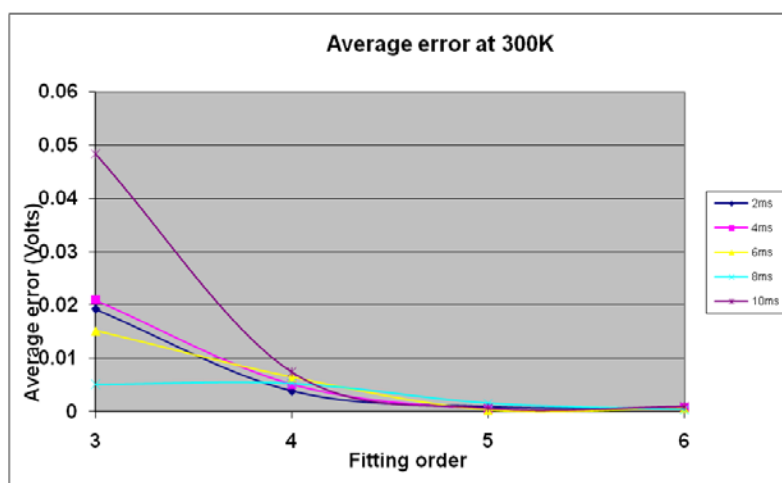


Figure 3.17 Average error at 300K for various values of integration time

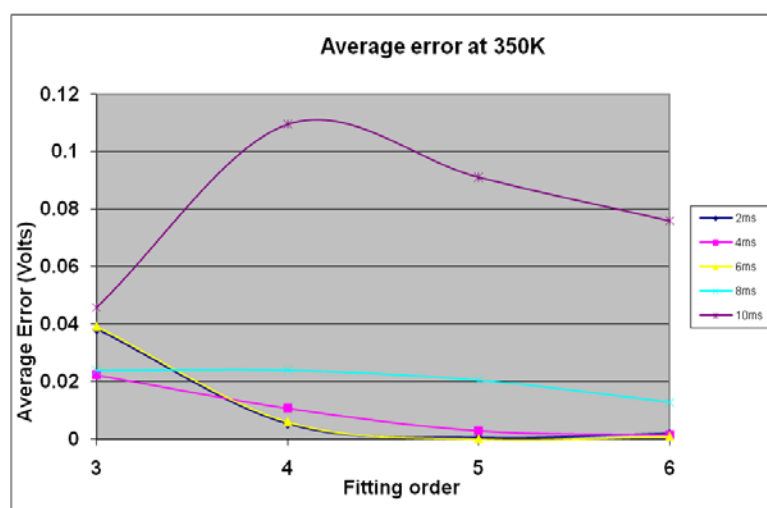


Figure 3.18 Average error at 350K for various values of integration time

The developed model has to perform with as few errors as possible in order not to modify the intensity value. However, there is a lower bound to what can be considered to be a significant level of error, since the number of bits representing the intensity value is known and therefore so is the intrinsic level of accuracy of the data. This level of accuracy is typically expressed in “quanta” (in Volts). Any error below the quanta criterion will not have any influence on the output intensity. For an 8-bit pixel value representation (and 8-bit conversion

at the output), and for a maximum voltage of 3.3V (in a 0.35 μ m CMOS technology), the quanta can be calculated as follows in (3.14)

$$Quanta = \frac{Maximum\ voltage}{Number\ of\ levels} = \frac{3.3V}{256} = 12.89mV \quad \text{--(3.14)}$$

However, there is a drop in voltage in the reset transistor which makes the discharge start below 3.3V and the actual maximum voltage to be below the supply voltage. So an electrical simulation was performed under dark conditions to identify the voltage at which discharge starts in the pixel. It is therefore this value of voltage (2.262V) which must be used as maximum voltage in the quanta criterion. This adds further constraint and requires more robustness and accuracy in the model. The modified values and the equation is as in (3.15)

$$Quanta = \frac{Maximum\ voltage}{Number\ of\ levels} = \frac{2.2622V}{256} = 8.836mV \quad \text{--(3.15)}$$

The average error across the system operational range has been calculated for various orders of fitting and is shown in Figure 3.19. This error quantifies the deviation from the electrical simulation results and it supports in selection of the order of fitting which will not modify the intensity level.

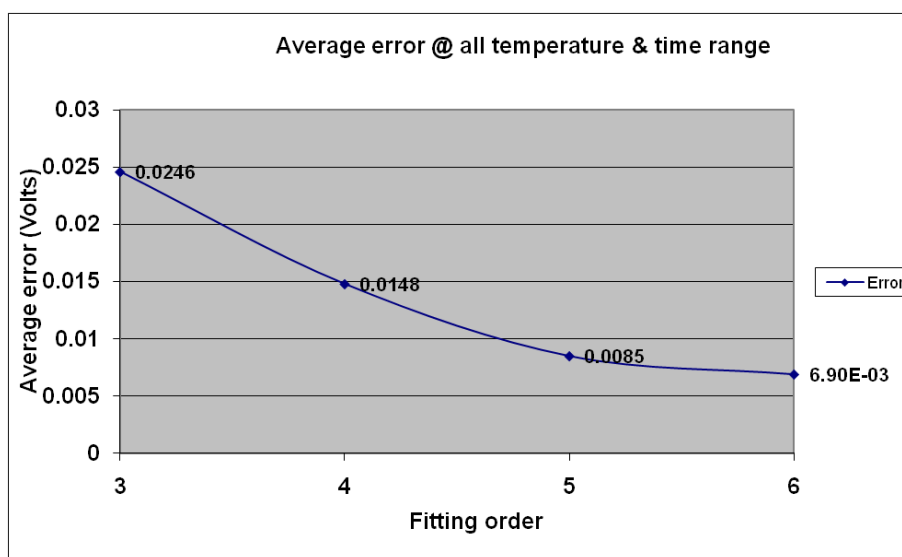


Figure 3.19 Average error across the system operational range for various orders of fitting

Chapter 3 – Thermal-aware image sensor model

It is necessary to use a fifth or sixth order fitting as the average error is close or below the quanta criterion. Final selection of either fifth or sixth could be decided by the simulation time against accuracy tradeoff.

The selection of the fitting order could be improved to achieve higher robustness by adding more constraints to the model. Normally the model tries to converge as close as possible to the realistic behavior of the circuit. This has forced the model to converge closer to 0V in either high temperature conditions (350K) or in maximum light conditions ($200\text{W}/\text{cm}^2$). There are instances in which the discharge voltage reaches zero volts before the prescribed integration time. For example in Figure 3.20 the discharge reaches zero volts before 8ms. If the model needs the voltage at 10ms integration time, it should evaluate to 0V. In the above case, model produced negative voltage or voltages in micro volts or nano volts, which is not a meaningful signal. Results show a maximum error of 76mV (Table 3-3) certain regions (350K , $200\text{W}/\text{m}^2$) even though the average error is below the quanta criterion. The model suffered from such discrepancies in this region of interest where a maximum error is 2% higher than other regions. To overcome this deficiency, a readout voltage threshold criterion is introduced. This threshold criterion not only improves the robustness of the model but also it avoids dealing with data which are not useful signal data. This readout threshold criterion is fixed at 0.1V as explained in section 3.3.3. Any readout voltage below this criterion is converted automatically converted to 0V in the model output. In other words the user could identify that the discharge voltage has reached 0V before the prescribed integration time.

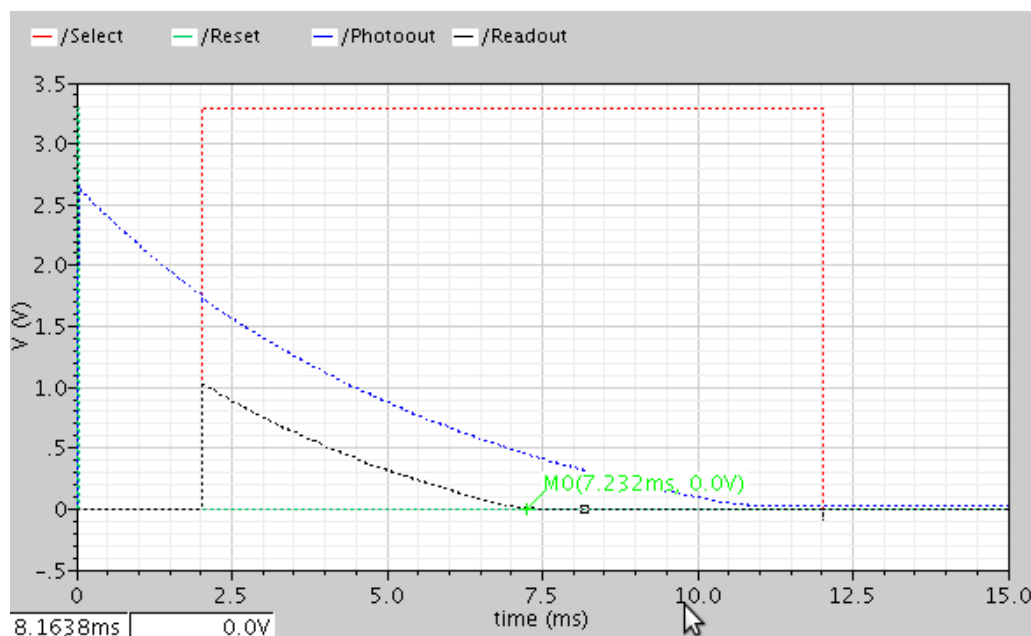


Figure 3.20 Readout voltage at bright light and 350K

Chapter 3 – Thermal-aware image sensor model

This additional constraint has no influence on the low temperature or low light conditions since the discharge voltage is always above the readout threshold voltage. It has improved the model especially for the high temperature (350K) region. This is indicated in Figure 3.21 which proves the absence of influence on operation in the low temperature region (as compared to Figure 3.17) and its influence on operation in the high temperature region shown in Figure 3.22 (as compared to Figure 3.18).

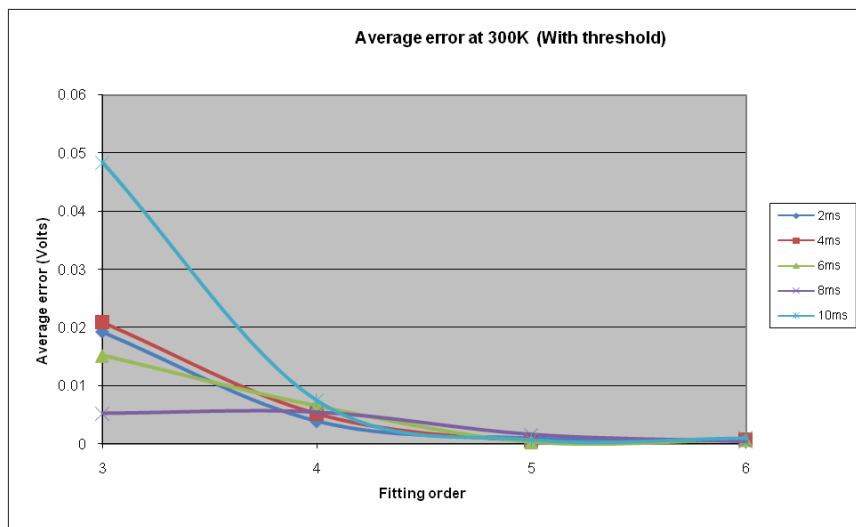


Figure 3.21 Average error at 300K with readout threshold criteria

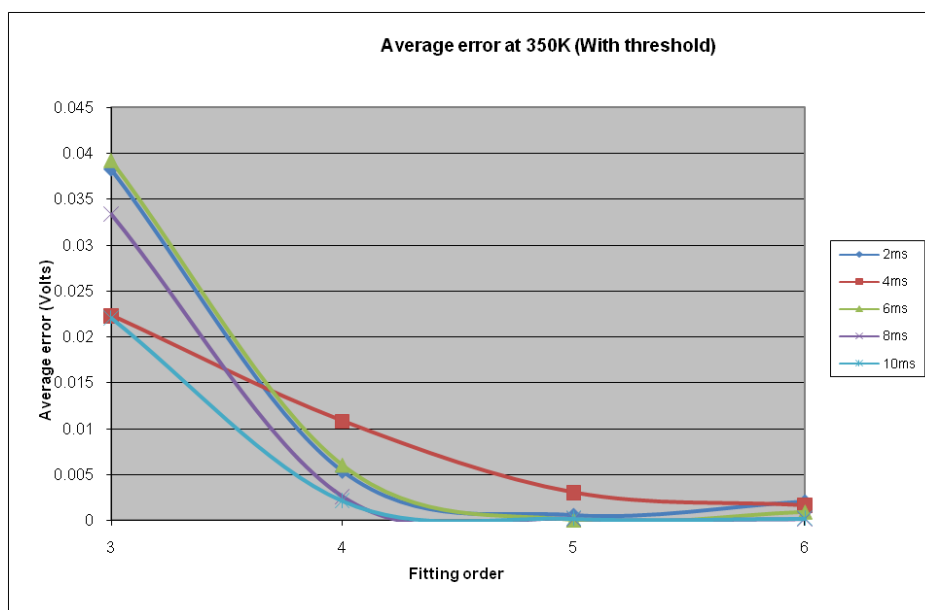


Figure 3.22 Average error at 350K with readout threshold criteria

This criterion has an influence on the overall performance of the model which is indicated in Figure 3.23. It clearly shows the model performing better from the fourth order of fitting compared to fifth order fitting in previous case.

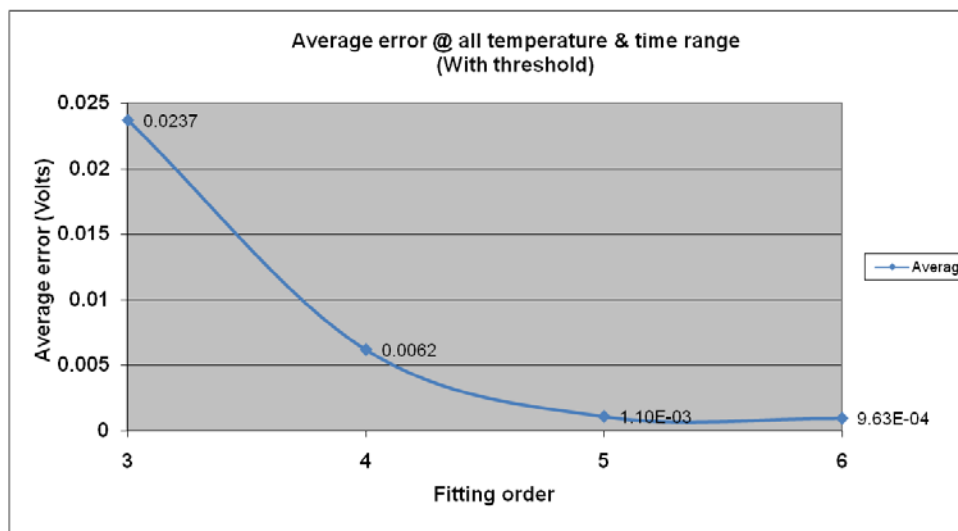


Figure 3.23 Average error for readout threshold voltage over entire system range

Including the threshold criterion into the model provides an improvement of 13.95% over the previous implementation. The maximum error in the region (350K, 200W/m²) explained earlier is reduced from 76mV to 166uV. This also shows that the model could perform much better using a polynomial of at least fourth order - using fifth or sixth order adds a security margin to the results.

3.6 Integrated simulation environment

3.6.1 SystemC

We use SystemC to model our system. SystemC is an open C++ library, the standard of which is defined by OSCI [13]. It allows design exploration at various abstraction levels, from functional to RTL [14] (register transfer language) level. In a System-on-Chip design flow, SystemC allows simulation at a higher level than that provided by typical HDL simulators,

consequently enabling reduced simulation time [15] (or the simulation of larger, more complex systems). The recent SystemC-AMS extension to the existing SystemC library also helps to explore heterogeneous system design, where software components and elements of analog, digital and multi-physics natures can be simulated seamlessly. In our case the application requires only a discrete-time simulation (SystemC) rather than continuous-time simulation.

3.6.2 Image processing

SystemC has the flexibility to allow both hardware and software co-simulation, so the input image processing can be performed using C++ (Figure 3.24).

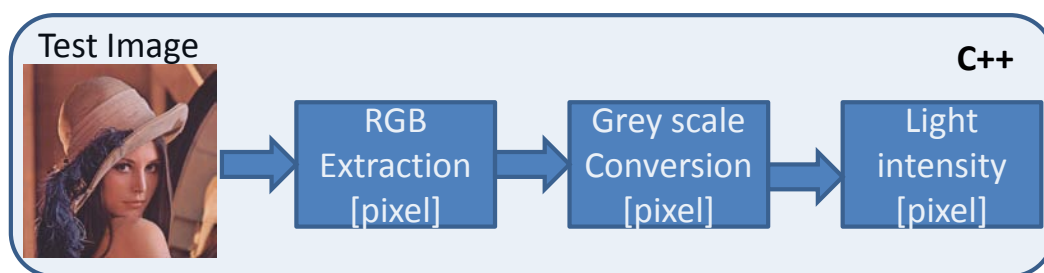


Figure 3.24 C++ based image conversion

Pixel matrix behavior is defined using a test image. A 1024*1024 pixel “lena” picture was considered, while a Bayer filter pattern is considered for simplicity. The bitmap image is processed to obtain the RGB intensity spectrum of each individual pixel. With the obtained RGB spectrum, the overall intensity of each pixel is calculated using two different methodologies: the Hue Saturation Intensity (HSI) method and the Grayscale method. Two different methodologies were considered to view the differences obtained in the final image of the imager in implementing color and black and white pictures. The HSI methodology has intensity representations in color format, while the Grayscale method represents the intensity from black to white in a linearly increasing order of intensity. Our model could use both input methods. However, the Grayscale method is used for simplicity and for easy validation. Their calculations are given by (3.16) and (3.17)

$$HSI\ Intensity = \frac{(R + G + B)}{3} \quad \text{--(3.16)}$$

$$\text{Grey scale intensity} = 0.2989R + 0.5870G + 0.1140B \quad \text{--(3.17)}$$

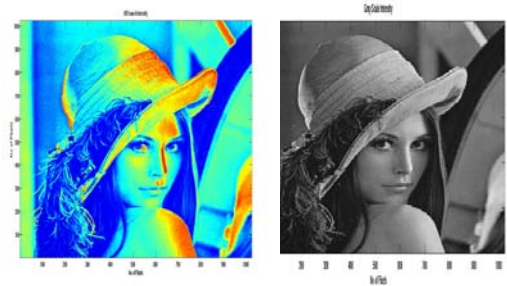


Figure 3.25 Intensity based HIS (Left), Greyscale (Right)

This intensity value, of each image pixel represented in Figure 3.25, is converted to a light intensity value as given by the equation (3.18), considering normal room light condition.

$$\text{Light intensity} = \frac{\text{Greyscale intensity} * \text{Maximum system light range}}{255} \quad \text{--(3.18)}$$

These steps are done to obtain the realistic input light intensity value for each pixel in the matrix, to act as the input to each photodiode in the pixel matrix.

3.6.3 SystemC-based pixel matrix model

The SystemC-based pixel matrix model has to serve the following goals: (i) validate the pixel matrix model developed using the surface fitting methodology, (ii) evaluate the readout voltage for each pixel, (iii) operate for any size of pixel matrix, (iv) be sufficiently flexible to integrate any thermal map generated from external source, (v) run at high speed to evaluate the impact of various input parameters on the output voltage.

The generator module behaves as a virtual decoder. It generates the reset and select signal as per the user requirements. The select signal is used to control the width of the integration time. This model could also disable the generator module and it is possible to fix an integration time globally according to the analytical equation developed using surface fitting.

The pixel matrix module has an array of pixels. This block is developed based on the 3T pixel architecture behavior which includes photodiode, reset transistor and source follower. This block is simulated at transistor level and integrated into SystemC as a behavioral equation developed using surface fitting methodology as discussed previously in this chapter.

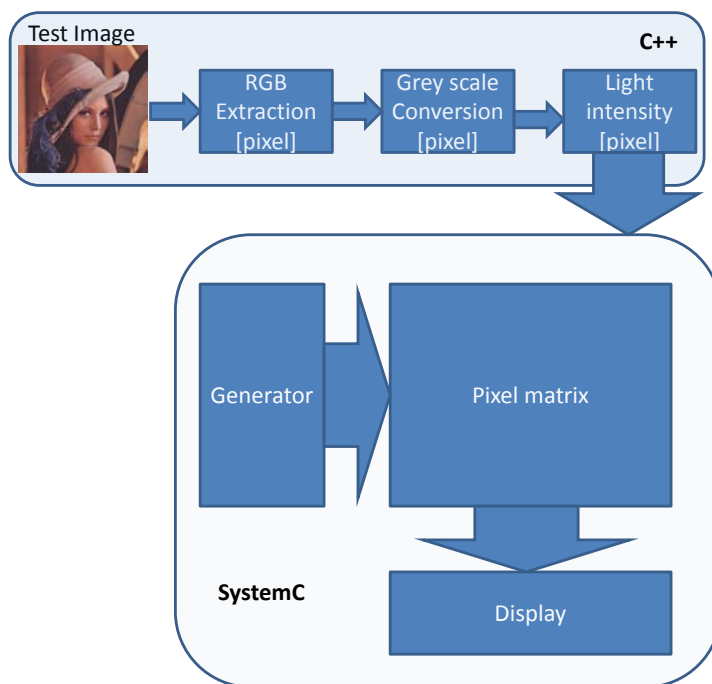


Figure 3.26 SystemC model block diagram

These blocks are described in SystemC modules as *.h* files. A pixel SystemC module consists of control signals ports and analog input/outputs terminals with *float* data type. The photodiode voltage is an internal variable represented with the *float* data type. The reset signal is generated by the generator module and the pixel output is transferred through to the display module as shown in Figure 3.26. In our approach a single pixel model is developed and is instantiated as many times as required according to the pixel matrix size, and each instance is mapped appropriately with the relevant control signals. The image processing toolbox developed using C++ is also integrated into this model to have the input light intensity.

The display module is developed not only to visualize the readout voltage of each pixel, but is also equipped with specific code to save/process the output voltage into the required format. It can also convert the set of analog voltages into a *.pgm* image file to visualize the voltage values as an output image.

3.6.4 Model integration

After development of the SystemC modules, the surface fitting model is integrated into the pixel module. In the current form, the model has four possible orders of fitting (third to sixth order) integrated. This was done intentionally to verify the results produced by each order against both electrical simulation and our image sensor thermal model. All the model parameters, fitting coefficients were ported from the Matlab environment into the SystemC model. In the current form, the model has been used to simulate from 2*2 to 1024*1024 matrix size. Extension of the model to allow the simulation of larger matrices would need negligible modifications (inclusion of new matrix size, appropriate picture input).

Since the pre-validation step has provided enough information in terms of fitting accuracy, the model integration has certain other goals to fulfill. They are

- Simulation of entire pixel matrix with appropriate inputs
- Measurement of the speed of simulation for all the orders of fitting
- Validation with electrical simulation

These steps could help in narrowing down to a single order of fitting for future simulations and validate the entire model.

To simulate with the pixel matrix thermal map, the model is equipped to read *.txt* and *.m* file formats with double data type to read in the thermal map with high precision. This high precision helps in improving the accuracy of our model to the reference simulation. The input data (temperature, image data) needed for the model to simulate is read into memory arrays in order to avoid continuous opening, reading and closing of files. This avoids time consumed for file operations.

3.6.5 Simulation speed

As discussed earlier, the main goal is to identify the simulation time of various orders of fitting, as indicated in Figure 3.27. The reference simulation to identify the speed of various orders of fitting are performed using a 256*256 pixel matrix size. The input to the SystemC model is the "*lena*" picture, with the same resolution. As it can be clearly seen and as dictated by intuition, a higher order of fitting results in a longer simulation time. At the sixth order fitting the simulation time is at 630ms.

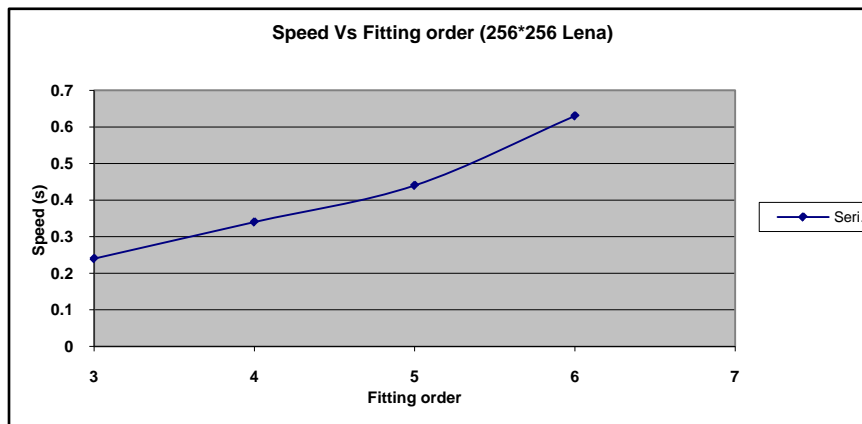


Figure 3.27 SystemC model simulation time

The main focus of this work is to have the model behave in a robust way in the entire region of operation. The selection of fitting order is a tradeoff between accuracy and simulation time. Overall relative error percentage in the entire region of operation for the fifth order is 0.015% and for the sixth order is 0.014% with a constrained upper bound voltage at 2.262V (from eq.3.13). Sixth order fitting exhibited an accuracy both in the lower temperature and higher temperature region along the entire region of integration time of same order. On the contrary the accuracy of fifth order is lower (0.04%) in the region with 4ms integration time (Figure 3.22) compared to sixth order. So we have chosen sixth order of fitting: 1. To have a robust behavior in the entire region of operation of the pixel, 2. Accuracy remained as main concern 3. This selection allows the model utilizable (scalability) from 8 to 14 bit resolution, although this work only 8 bit resolution is used. Nevertheless, the SystemC model is completely equipped to use any order of fitting as per the user requirement.

To compare the simulation time of the SystemC model with that of the electrical simulation, several pixel matrix sizes were simulated (Table 3-4, Figure 3.28). The simulations were performed on an Intel Xeon server running at 2.4GHz with 4GB of RAM.

Table 3-4 Simulation time comparison

Matrix Size	Simulation time (in seconds)	
	Classical	SystemC
6*6	141	0.01
32*32	4249	0.02
48*48	8678	0.03
128*128	88380	0.17
256*256	345960	0.63

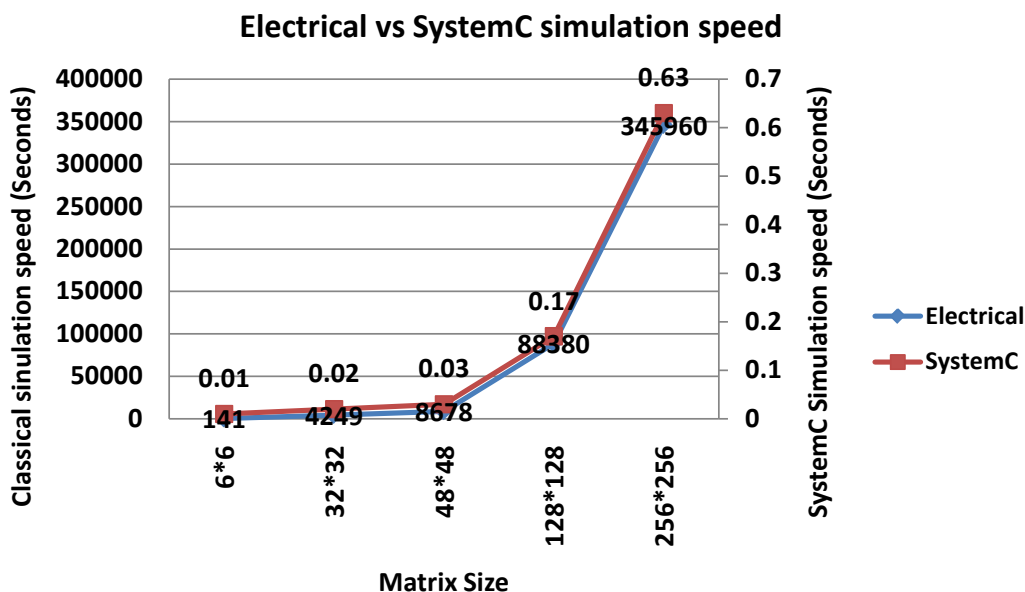


Figure 3.28 Simulation time comparison

Figure 3.28 clearly depicts the huge speedup obtained by the simulation approach using SystemC. A typical classical simulation took around 4 days to simulate the 256*256 pixel matrix, while the SystemC approach simulated the same pixel matrix in 630ms. The SystemC simulation therefore achieves approximately **500,000X** speedup compared to the electrical simulation. A 1024*1024 megapixel (1MP) array is simulated to verify the feasibility to simulate large pixel matrices. It took 9.5 seconds to simulate the 1MP array. We can therefore also conclude that the SystemC model has greater capability for the simulation of

large pixel matrices. This size cannot be simulated using Cadence Spectre (or any Spice-based simulator).

SystemC simulation time for the 6*6 or 32*32 is much faster but they are having an influence from the image, thermal map read/write/open/close operations involved which takes significant amount of time. This simulation model not only alleviates the problem of simulating large pixel matrices, but also helps the designer to analyze the impact of pixel behavior at early stages of system design, due to the high speed simulation and the tunable accuracy available from the model.

3.7 Post-validation

3.7.1 Matrix simulation

The pre-validation step provided the necessary behavior of the pixel for grey scale intensity (image) and the temperature impact (thermal map). The integration step provided the simulation behavior and its speed for different pixel matrix sizes. The next step is to simulate an entire pixel matrix with a test image input and several thermal maps. This will enable the evaluation of the robustness of the model integrated into the SystemC environment. To start the preliminary post validation, a homogenous distribution of temperature is taken across the pixel matrix. This is performed to validate the model and to see if all the pixels behave the same way with homogenous temperature distribution.

To perform this validation, several electrical simulations were performed for the same input image at different homogeneous temperatures, as depicted in Figure 3.29.

For the Cadence Spectre reference simulation, a Skill™ function based interface [16] was developed to decode the image into light intensity values to be fed into the pixel matrix. This toolbox was developed to help designers handle millions of pixels easily. The toolbox uses the same resolution as the image sensor. Sampling times can be fixed to fetch the readout voltage of each pixel. This toolbox helps in feeding the image input and obtains the readout voltage of each pixel. Generally, designers tend to simulate only small groups of pixels to validate the global simulation, using approaches based on TCAD at the physical level [16].

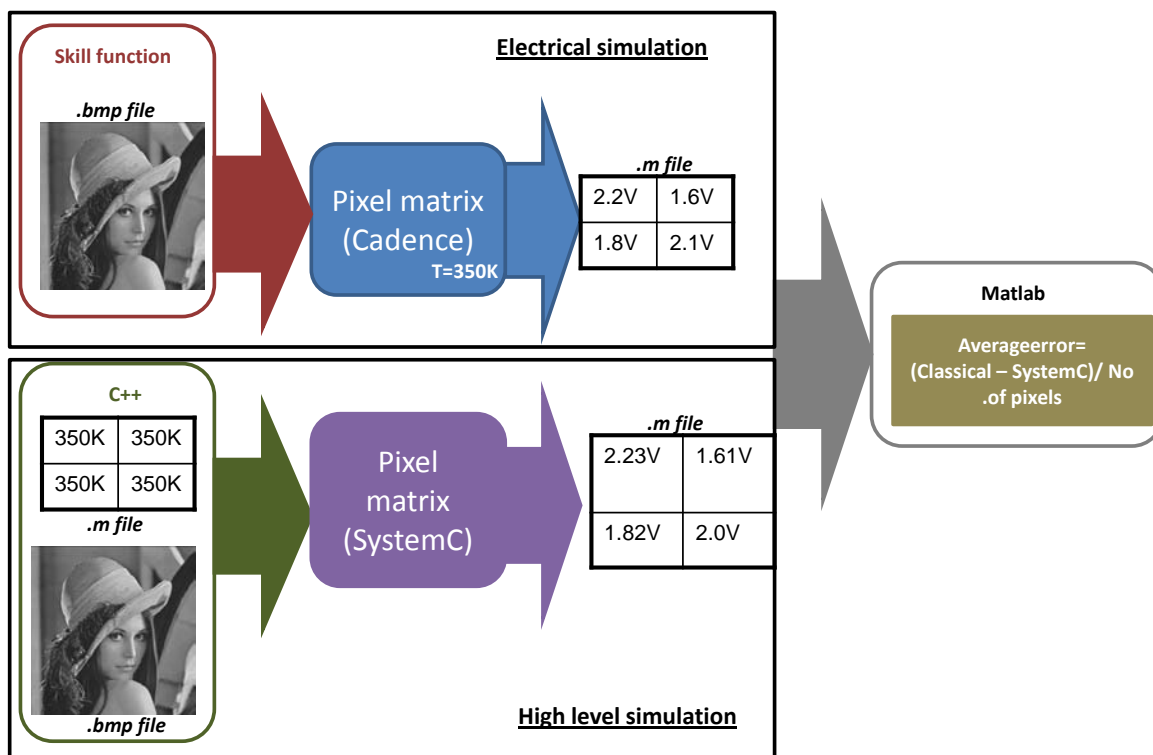


Figure 3.29 Post validation steps and used tools

Both the electrical simulation and high-level simulation results are obtained in *.m* to feed into Matlab for further processing. In the Matlab environment both the data are collected and applied with the following equation (3.19) is used to calculate the average error across the picture.

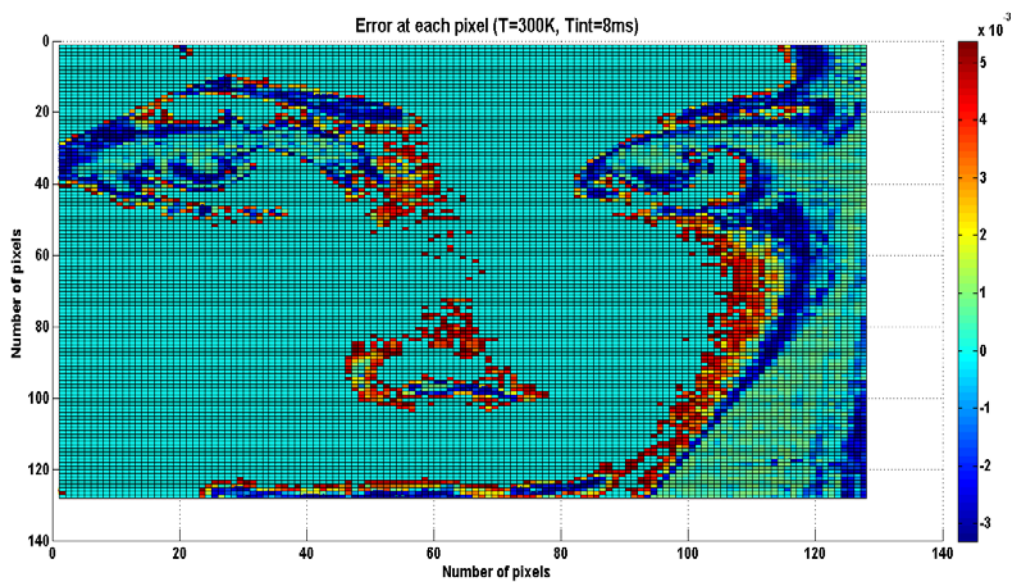
$$\text{Average error} = \frac{\text{Classical [pixel voltage]} - \text{SystemC[pixel voltage]}}{\text{Total number of pixels}} \text{ (in volts)} \quad \text{--(3.19)}$$

3.7.2 Test case I (128*128 “lena”)

Classical and SystemC based simulations were performed for the 128*128 size “lena” picture. Several simulations and their average error results are shown in Table 3-5. Some examples in Figure 3.30 and Figure 3.31 depict the error for each individual pixel across the “lena” picture. In both figures the Z-axis is the error in Volts and X-axis, Y-axis is number of pixels. The colors in the figure indicate error at different pixels.

Table 3-5 Average error – 128*128 lena picture

	Average error (Volts)				
	Tintegration				
Temperature	2ms	4ms	6ms	8ms	10ms
300K	0.000448	7.20E-05	0.000246	0.000137	0.000236
325K	0.000945	0.000276	0.000804	0.001079	6.20E-05
350K	0.001308	0.000168	0.000459	0.000139	0.001364
Average	0.0009	0.000172	0.000503	0.000452	0.000554

Figure 3.30 Post validation at $T=300K$ and $T_{int}=8ms$ (Average error = 139 μ V)

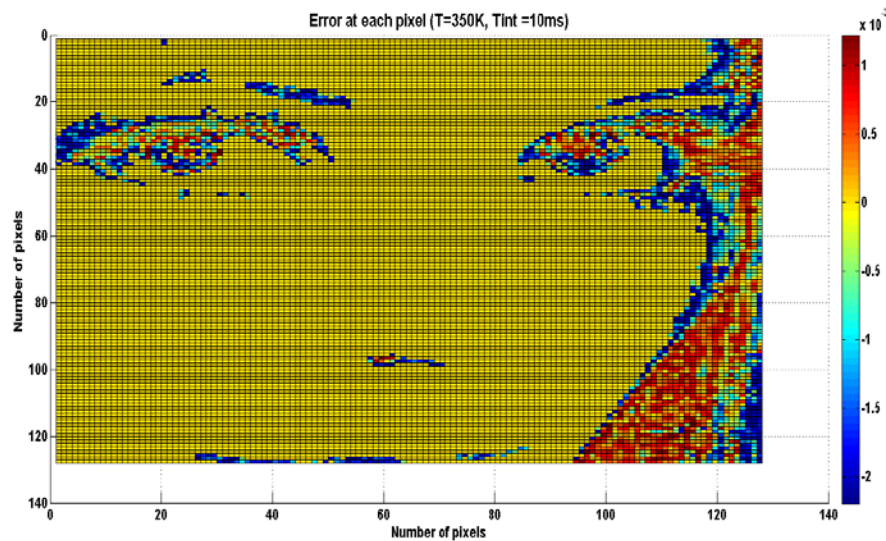


Figure 3.31 Post validation at $T=350K$, $T_{int} = 10ms$ (Average error = $101\mu V$)

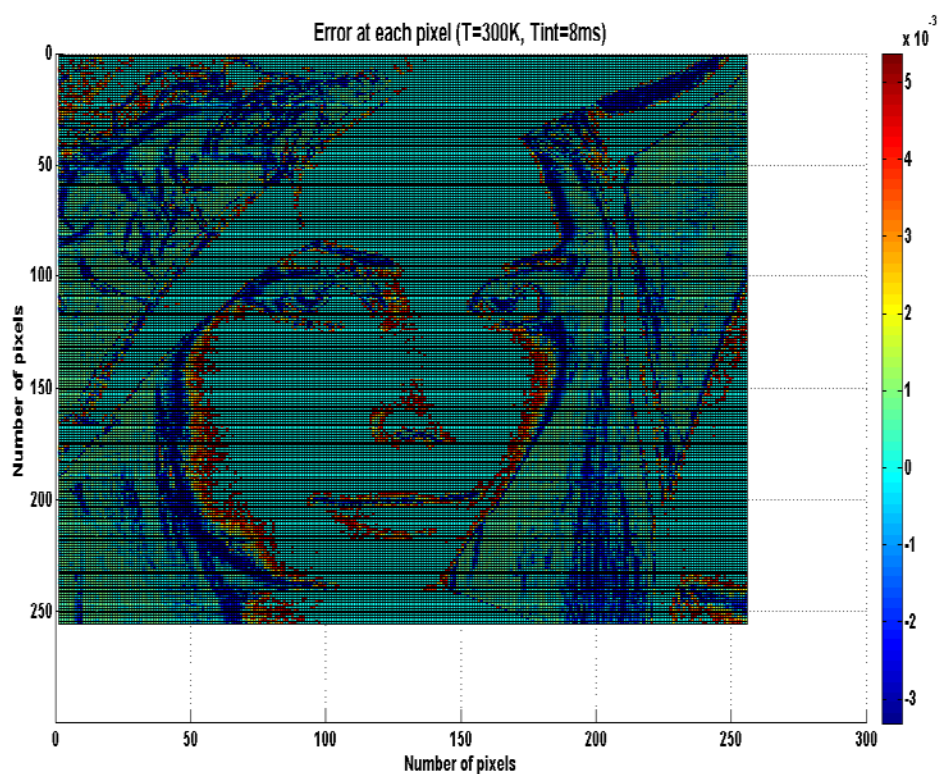
A relative error of 4% is seen across the entire range of temperature and integration time. The average error across entire region of operation of pixel matrix is $516\mu V$ for quanta of $8.83mV$.

3.7.3 Test case II (256*256 lena)

Classical and SystemC based simulations were performed for the 256*256 size “lena” picture. Several simulations and their average error results are shown in Table 3-6..Some examples in Figure 3.32 and Figure 3.33 depicts the error for each individual pixel across the “lena” picture. In both figures the Z-axis is the error in Volts and X-axis, Y-axis is number of pixels. The colors in the figure indicate error at different pixels.

Table 3-6 Average error – 256*256 lena picture

	Average error (in Volts)				
	Tintegration				
Temperature	2ms	4ms	6ms	8ms	10ms
300K	0.000998	0.000104	0.000615	0.000742	0.0013
325K	0.000152	0.000303	0.000425	0.000895	0.000104
350K	0.0013	0.000181	0.00032	2.06E-05	0.000129
Average	0.000817	0.000196	0.000453	0.000552	0.000511

Figure 3.32 Post validation at $T=300K$, $T_{int}=8ms$ (Average error = $20.55\mu V$)

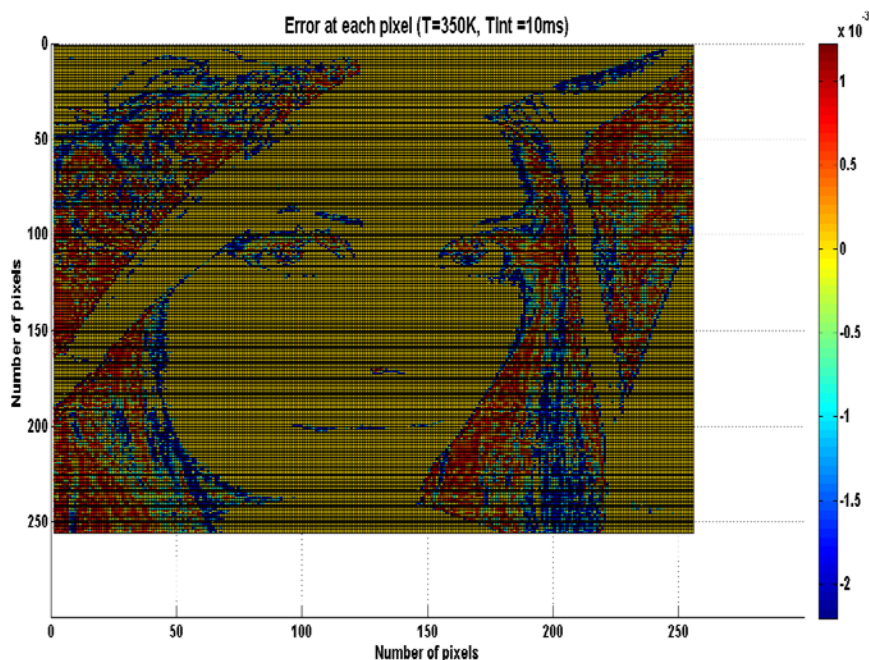


Figure 3.33 Post validation at $T=350K$, $T_{int}=10ms$ (Average error = $129.4\mu V$)

Overall average error across the entire range of temperature and integration time is $506\mu V$. Relative error is less than 4% is seen across the SystemC model for this specific test case.

3.7.4 Test case III (White picture)

The previous test case used a complete distribution of the light intensity from white to black colors. A test case with one single light intensity distribution across the pixel matrix is also necessary to verify if the behavior is the same across the entire pixel matrix. A bright light (white color intensity) test case was chosen to verify the behavior of the pixels with a steep discharge behavior. This post-validation is used as reference for future simulations, to be described in Chapter 4. Classical and SystemC-based simulations were performed for a 256×256 size white picture. This simulation is performed at $300K$ at $10ms$ integration time.

Chapter 3 – Thermal-aware image sensor model

The error distribution across the picture is shown below in Figure 3.34. In both figures the Z-axis is the error in Volts and X-axis, Y-axis is number of pixels.

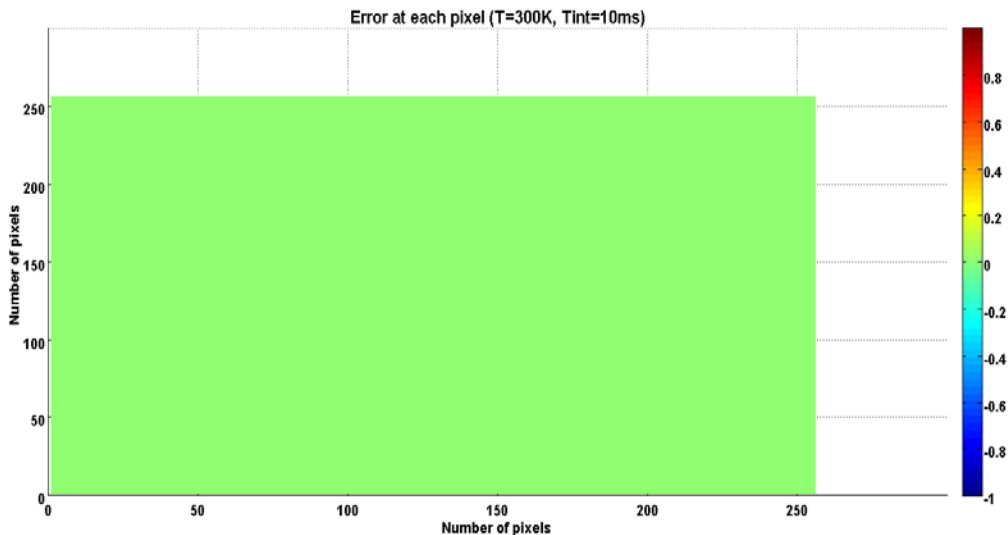


Figure 3.34 Post validation at $T=300K$, $T_{int}=10ms$ (Average error = $1.2mV$)

The error for each pixel, compared to the reference electrical simulation is $1.2mV$. This is far below the $8.83mV$ criterion established with the 8-bit quanta calculation.

This post-validation step is also extended by performing more simulations to cover the entire range of temperature. Figure 3.35 depicts the simulation performed under bright light conditions at $325K$ and for $T_{int} = 10ms$.

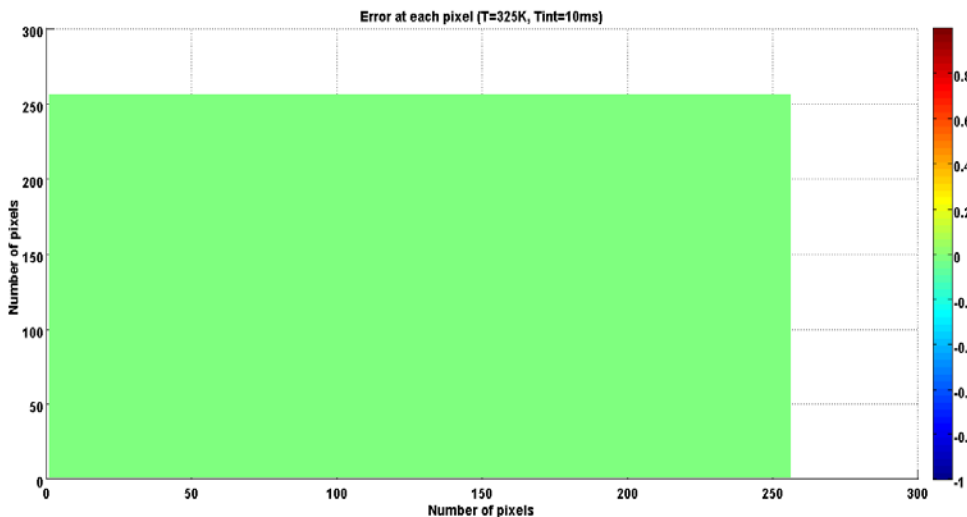


Figure 3.35 Post validation at $T=325K$, $T_{int}=10ms$ (Average error = $1.3mV$)

The error for each pixel compared to the electrical reference simulation is 1.3mV. The model still holds very well to the prescribed behavior expected from the simulation model.

A final test case, to satisfy the robustness of the simulation model as explained in section 3.5.3, applies the additional constraint to the model to avoid reporting noise voltages once the discharge node reaches zero volts.

Electrical simulation indicated a readout voltage of 2.625uV (Figure 3.36) which is clearly a noise voltage with no meaningful value in this context. SystemC simulation produced the readout voltage as 0V as expected.

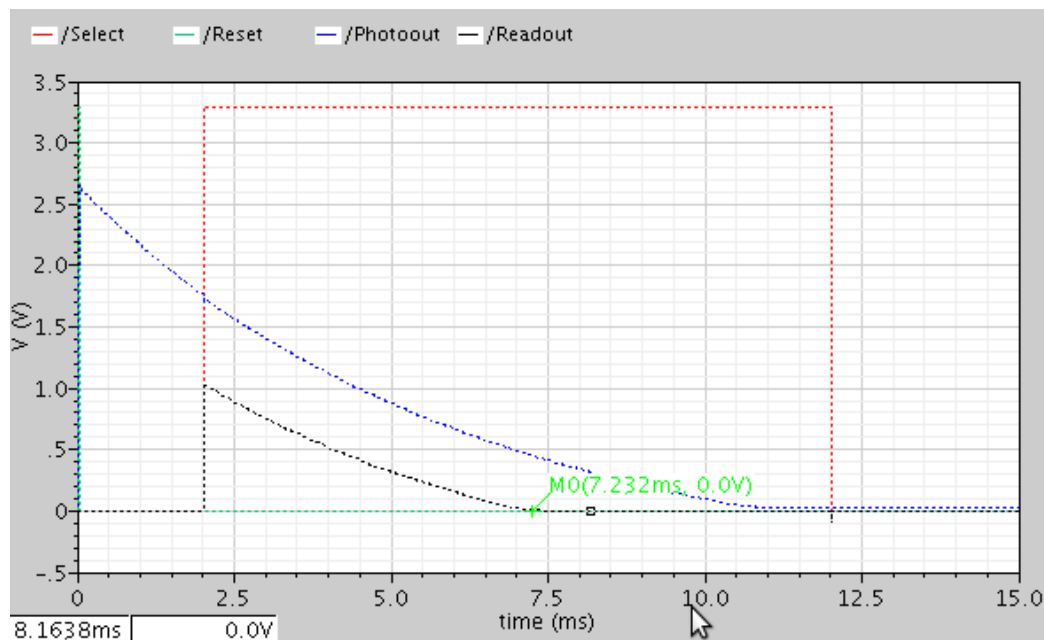


Figure 3.36 Electrical simulation ($T=350K$, $T_{int}=10ms$)

The error for each pixel compared to electrical reference simulation is 2.625uV. Figure 3.37 depicts the error across each of the pixels in the 256*256 white picture test case. To conclude, this test case clearly ascertains that the SystemC model behaves as expected indicating 0V.

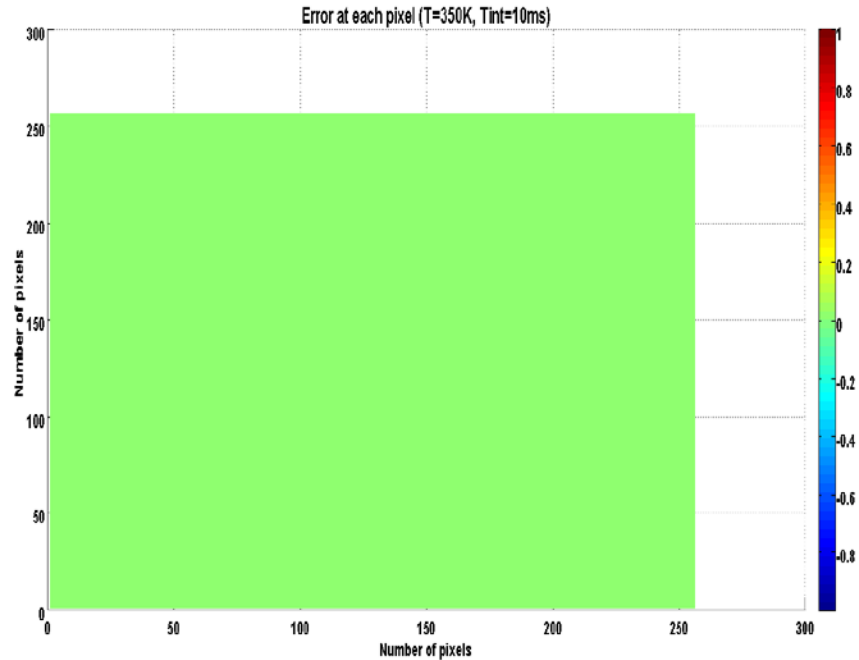


Figure 3.37 Post validation at $T=350K$, $T_{int}=10ms$

3.8 Inference

The thermal-aware image sensor model has been fully developed and integrated into the SystemC environment for simulating any size of pixel matrix. The model has fulfilled the following

- Several orders of fitting is realized (Surface fitting) - third to sixth order fitting deemed a useful range
- Fulfilled the expected accuracy (Pre-Validation):
- Average error of 963 μ V (improvised model) and 690mV (standard model)
- Achieved the speed requirement (SystemC Integration):
- 630ms for 256*256 pixel matrix
- SystemC pixel matrix behaves as expected (Post validation)
- Several pixel matrix sizes have been verified
- Testcases with “lena” and “white” pictures have been validated

The above results and validation have provided a model which is flexible to be integrated with other tools such as Hotspot [5] (thermal simulator) or a floorplanner to perform various experiments. This will be dealt in the next chapter.

Bibliography

- [1] H.Tian, “Noise analysis in CMOS Image sensor” August 2000, Thesis, Stanford university
- [2] S. Decker, D. McGrath, K. Brehmer, and C. G. Sodini “A 256x256 MOS Imaging Array with Wide Dynamic Range Pixels and Column{Parallel Digital Output. IEEE J. Solid-State Circuits, 33(12):2081{2091, 1998.
- [3] O. Yadid-Pecht, B. Mansoorian, E. R. Fossum, and B. Pain. “Optimization of Noise and Responsivity in CMOS Active Pixel Sensors for Detection of Ultra Low Light Levels”, In Proc. SPIE, volume 3019, pages 125{136, San Jose, CA, Feb. 1997
- [4] S. K. Mendis, S. E. Kemeny, R. C. Gee, B. Pain, C. O. Staller, Q. Kim, and E. R. Fossum. “CMOS Active Pixel Image Sensors for Highly Integrated Imaging Systems”, IEEE J. Solid-State Circuits, 32(2):187{197, 1997.
- [5] K. Skadron, K. Sankaranarayanan, S. Velusamy, D. Tarjan, M.R. Stan, and W. Huang. “Temperature-Aware Microarchitecture: Modeling and Implementation.” ACM Transactions on Architecture and Code Optimization, 1(1):94-125, Mar. 2004
- [6] S.Mendis, S.E.Kemeny, E.Fossum, “CMOS Active pixel image sensor » IEEE transactions on electron devices, vol 41, No.3, March 1994
- [7] M.Bigas, E.Cabruja, J.Forest and J.Salvi, “Review of CMOS image Sensors” Microelectronic Journal,2006,37,433-451
- [8] S.Kavusi, A.El Gamal, “Quantitative study of high dynamic range image sensor architecture”, Proc. of SPIE-IS&T Electronic Imaging, SPIE Vol. 5301 ,2004

- [9] J.Krammer, Luc Hebrard, “Pixel schematic accessed through 3D IDEAS collaboration”
- [10] M.G. Cox and J.G.Hayes, “Curve fitting: A guide and suite of algorithms for the non-specialist user NPL report NAC 26 National physical laboratory, 1973
- [11] Wolfram Mathworld: “Polynomial”
- [12] <http://www.mathworks.com/moler/interp.pdf>
- [13] Open SystemC Initiative: <http://www.systemc.org>
- [14] Yarom.I., Glasser G., ,Proceedings of ICECS 2004, 13-15 Dec. 2004 p.:507 - 510.
- [15] Habibi A., Moinudeen H et al., “ Towards faster simulation of SystemC designs “, Emerging VLSI Technologies and Architectures, IEEE, 2-3 March 2006, Vol.00 p:2 pp
- [16] Navarro.D, Feng.Z,Viswanathan.V et al., “Imager toolbox for CMOS image sensors in Cadence ADE “, Demset 2011, Orlando, Florida, USA, Nov 29th – Dec2nd, 2011

Chapter 4

3D Integrated design flow

4.1 Introduction

The thermal aware image sensor model (introduced in Chapter 3) developed and integrated in SystemC can be used in a more sophisticated way to analyze the temperature of a 3D stacked chip (Figure 4.1). The integration of a stacked chip floorplan coupled with analysis of the thermal behavior supports improvements in the imager performance when moving to complex architectures such as 3D. 3D technology is not only complex in fabrication but also suffers from a greater and more complex dependency on thermal behavior, which impacts specifically noise performance, aging, leakage issues. These factors could have a direct influence on the performance of the imager (e.g. shot noise, dark current, reset noise etc.).

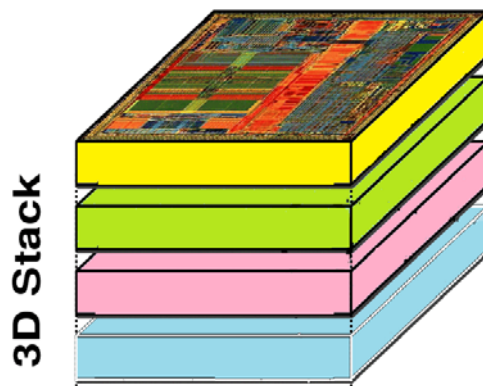


Figure 4.1 3D stacked chip

4.1.1 3D stacked chip

3D stacked chips have been the topic of both academic and industrial research development due to its promise to extend the life of Moore's Law. 3D technology has the potential to alleviate performance limitations present in 2D chips where there is a continued CMOS scaling

trend [1][2][3], and in particular to overcome the interconnect bottleneck which exist in 2D chips. By using the vertical dimension, chip size is automatically reduced by a factor equivalent to the number of stacked levels, such that the maximum length of wires is reduced, leading to a lower number of repeaters or buffer and consequently better circuit speed performance. The 3D integration approach further has the potential to combine different technology layers [4] such as digital, analog, optical in a single chip.

Although there are many advantages in using 3D, it does suffer from issues such as power density, integration yield and test coverage. In particular, power density increases with the number of layers integrated on top of each other, the natural consequence being that the temperature dissipation also increases many-fold [5]. In a conventional 2D chip the heat sink area evacuates heat over the entire surface of active elements, but 3D integration decreases the chip footprint (and stacks layers of active elements above each other) and therefore increases the power density while at the same time reducing the area of the heat sink interface, so the heat sink cannot evacuate the high temperature. The analysis and reduction of the thermal impact is therefore mandatory in any consideration of 3D technology.

In this chapter we will discuss in more detail the thermal model integration into the 3D platform. In section 4.2 we will detail the floorplanner, followed by the thermal evaluation tool in section 4.3. The integration of the thermal-aware imager model in the integrated environment will be discussed in section 4.4 followed by results of the tool in section with various test cases in section 4.5. The thermal impact and its effects will be correlated with the imager performance as and when required. Finally, inferences will be drawn from the test cases in section 4.6.

4.1.2 Integrated design flow

The thermal aware image sensor model demonstrated in Chapter 3 is accurate, and simulates at a speed compatible with system-level simulation. In order to simulate the performance of the imager level in the 3D stack, we require a tool which will extract a thermal map from the 3D stack thermal model, and inject this thermal map into the thermal-aware image sensor model. In addition to the thermal map and as we have seen in the previous chapter, the imager thermal model needs light intensity and integration time inputs as shown in Figure 4.2.

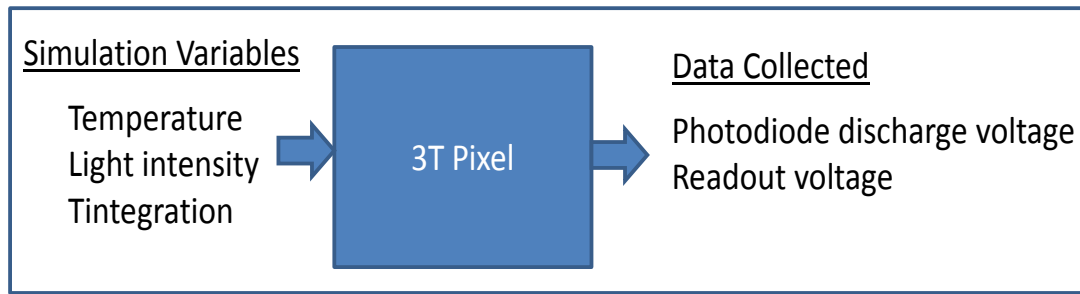


Figure 4.2 Imager thermal model input/output

The input light intensity necessary for the model is available through the input picture which is decoded into individual pixel light intensity as explained in section 3.6.2. As described in the previous chapter, the thermal map used to test the model had a homogenous distribution of temperature; this is of course not the case in 3D stack scenarios. In this case, it is necessary to use the actual thermal map of the underlying layer(s) to provide a realistic temperature value to each pixel, and causing a proper evaluation of each pixel discharge. This is not feasible in conventional simulators such as Spice, since temperature is a global parameter.

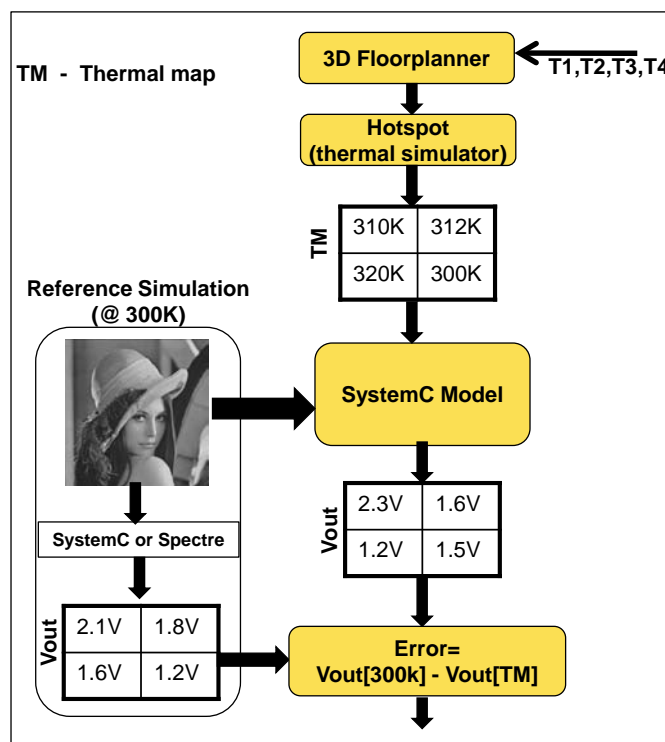


Figure 4.3 Integrated design flowchart

A further consequence of the combination of a thermal map with the thermal-aware imager model is that it can also be used in the design cycle (Figure 4.3) to help adjust the placement of blocks in underlying layers according to their power density and in order to minimize their impact on the imager performance. Indeed, the availability of many layers supports a greater freedom of movement to enable the movement of high-power blocks away from temperature-sensitive areas or layers in the final placement. This temperature-aware placement is however of course constrained by interconnect length, technology, area, power density.

T1-T4 represents different scenarios (e.g. compact area, minimum temperature etc.) to analyze the imager performance in the design cycle. Each scenario acts as a configuration setting for the thermal simulator to run the optimization. At the end of the optimization, the output is a thermal map which is fed into the imager thermal model. The average error compared to the reference simulation is calculated. We select suitable scenario manually at the end of simulation based on the average error (thermal impact) on the imager performance.

4.2 3D Floorplanning

4.2.1 Thermal floorplanning

There are several approaches to reduce the temperature in a 3D stacked chip [6]:

- Thermal-aware Floorplanning
- Thermal via insertion, cooling microchannel insertion
- Heat sink and package design

The latter two have been proved to help heat dissipation by fabrication techniques and external components, but also increase cost. Thermal-aware floorplanning moves consideration of the thermal issues upstream of fabrication and can, through design, lower the temperature and consequently the need for and cost of thermal vias, heat sinks and heat extracting packaging.

The floorplanning algorithm used in this work is a fine-tuned version [6] of the simulated annealing based floorplanning algorithm, adapted to reduce the peak temperature as well as thermal gradients. It also uses smart heuristics that help the search algorithm to

converge to thermally efficient solutions. Since our objective is to achieve a better imager performance through reduction of the influence of temperature, we explore the use of this floorplanning algorithm in conjunction with the 3D integrated design flow. In the following paragraphs we give a brief description of the algorithm and its use.

4.2.2 Floorplanner algorithm

Primarily this work is a parallel research work going on in our group which focuses on architectural exploration using Parquet 2D floorplanner and HotSpot tool. Part of this work and its improvements are utilized to realize the 3D integrated design flow.

The floorplanner tool is adapted from the Parquet 2D floorplanner [7], where the floorplanning algorithm is based on simulated annealing. The problem is formulated for the 3D case [6] as follows: $B=\{b_1, b_2, \dots, b_m\}$ are the set of rectangular blocks with height h_i and width w_i having terminals $T=\{t_1, t_2, \dots, t_p\}$. P_i are the pins that connect the various blocks and terminals, while $L=\{l_i | 1 \leq i \leq n\}$ are the set of n layers.

Let (x_j, y_j, l_j) denote the coordinates of terminal t_j and (x_i, y_i, l_i) denote the coordinates of block b_i . The 3D floorplanning problem is to find a solution S for the assignment of blocks coordinates (x_i, y_i, l_i) so that no two blocks overlap and a cost function $C(S)$ is minimized. In the implemented optimization, the solution is initialized to a random floorplan. The solution is incrementally improved until the optimization times out. The solution quality depends on the starting point and how much time the algorithm is allowed to spent refining it. Increasing the optimization time reduces the dependency of the solution quality on the starting point.

For a 3D stacked IC problem, the circuit and the stack descriptions are necessary. The circuit description indicates the size, power and connectivity of the blocks, while the stack description indicates over how many and of what types of layers the blocks can be arranged. It is important to be able to realise various kinds of optimization (area, wirelength, temperature) for the technology nodes used in each layer. Apart from area minimization, the connectivity between blocks as well as the I/O pad positions are required in order to be able to optimize the wirelength. Material conductivities, and stack geometries are necessary for temperature minimization. The workflow is illustrated in Figure 4.4.

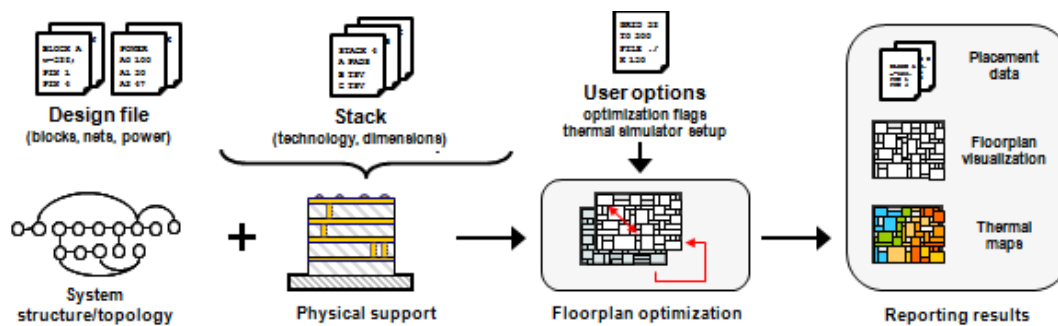


Figure 4.4 Workflow [8]

The file input/outputs in this workflow are:

Design files cover the circuit description: a set of blocks defined by their dimensions, power figures and connectivity with other blocks and I/O pads. File extensions: .blocks, .nets, .power, .pl, .wts

Stack files cover the physical stack description. There are three stack files in total: one for the floorplanner, indicating the number of layers and their associated technology, while the other two are used by the thermal simulator. They define the geometry and thermal properties of the tiers in both detailed and simplified manners. One is then used during the floorplan optimization and the other is reserved for a detailed analysis. File extensions: .stack, .lcf, .lcf.eval

The following section describes in detail the floorplanner options and implementation details.

4.2.3 Floorplanner options

In the following, we present the command line options (**bold** letters) to run the floorplanner. The basic command line should always contain the following options:

-f <designName> loads a given design. The argument designName is the prefix of the design files. All design files must be placed in the same folder. .power and .wts files are optional.

-stack <stackName> specifies the use of a given stack. The only stack file mandatory is the .stack. The other two files are necessary if thermal simulation is activated. Again, all files describing a stack must be in the same folder.

Apart from the basic command line arguments there are other user options which give means to control the optimization process. The user can control the random seed generator and runtime (number of iterations), change the optimization objectives or modify the thermal simulator setup. With these options the user has the possibility to achieve better solutions and/or repeat experiments.

-n <p> produce p independent runs (different seeds). The console output reports the minimum, average and maximum values attained for the various quality measures (wirelength, temperature, etc). *Default 1.*

-s <q> set the random generator to use the seed q (integer). To reproduce a given result, we initialize the random generator with same starting point and store all the seeds generated. The stored file is used in the optimization to guarantee the result reproduction. *Default random.*

-seedlist <seedsFile> is a combination of the first two options. The tool runs for each seed value declared in *seedsFile*. This mechanism allows the impact of different options to be compared in a statistical manner. *Default not used.*

-maxIter <k> sets the maximum number of iterations (solutions visited) before the algorithm stops. To scale with the size of the problem, the actual maximum number of iterations is obtained multiplying k by the number of blocks ($\text{maxIter} = k * n_{\text{blocks}}$). *Default 2000.*

The position [8] of the I/O terminals (pads) is an important factor for floorplanning. Different assignments will lead to different floorplan solutions, with the placement of the blocks close to the terminals to which they are connected.

In a first approach, the actual pad position may not be known, as well as the dimensions of the floorplan outline (core outline). Therefore, three ways to process the terminal positions are available.

-noScaleTerms The positions declared in the placement file are used and kept unchanged (Figure 4.5(a)). The actual floorplan outline can either be contained in or exceed the outline

delimited by the terminals. This is useful when the dimensions of the I/O pads are known and impose the outline of the chip (pad-limited instead of core-limited).

default The positions declared in the placement file are scaled to fit the floorplan outline (Figure 4.5(b)). In a real design, scaling these locations can cause pads to overlap, but here pads are considered to have zero area. In all simulations performed the default option is used.

-centerTerms All terminals are placed at a single point at the center of the chip (Figure 4.5(c)). This option is useful when the designer has not yet defined the I/O pad positions, although it will lead to solutions that are different from those with the I/O's at the boundary.

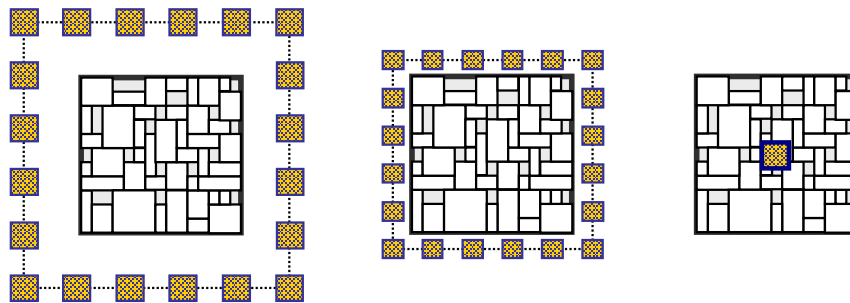


Figure 4.5 (a) No scaling (b) Scaled –default (c) Centered [8]

Plotting the output is possible using the option **-plot**. The output is generated using `out.plt` and visualized in `gnuplot`. The header of the output file lists the numerical results of the solution. The random seed used is listed, giving the means to reproduce the same result again. In the case where multiple runs are performed, only the best result is plotted (i.e. the result that best minimizes the cost function).

The block labels can be sometimes cumbersome. In these cases, a cleaner output can be generated with the alternative `-plotNoNames`. Also, `out.plt` is a `gnuplot` script that can be modified if other plot layout is needed or to save the image in other formats. The results can be saved in the same format used for input to exploit the placement information in another tool. This is achieved by

-save <baseFileName> This saves all the solution information (`.blocks`, `.pl`, `.nets`, `.wts`, `.power`) with the prefix `baseFileName`. Example command line: `> ./mofp -f oldDesign -stack 4layerStack -save newDesign`

4.3 Thermal Simulation

4.3.1 Thermal-aware floorplanning

Thermal-aware floorplanning problem is formulated using the area-wirelength minimization problem and adding the maximal temperature (T_{max}) in the weighted cost function (4.1):

$$C(S) = \alpha * Area + \beta * WL + \chi * T_{max} \quad \text{--(4.1)}$$

Firstly, the solution with optimal wirelength usually does not correspond to the solution with optimal area. But, in a general way, wirelength benefits from area reduction. On the other hand, temperature and area are completely opposite objectives: compact floorplans present high temperature while sparser arrangements are cooler. The objective of this thermal aware floorplanner is to find a balance between these opposite objective.

During floorplanning process needs a significant number (millions) of iterations until the search converges to thermally efficient solutions. Due to this high number of iterations and corresponding candidate solutions to evaluate, it is not feasible to run a detailed finite element simulation to evaluate the thermal profile of each one. Simplified thermal models that are suitable for use in a floorplanning algorithm have been proposed by several research groups [9][10]. Two models are identified that represent different degrees of accuracy. Both rely on the thermal-electrical analogy and use cubes to mesh the chip volume. The temperature values are obtained solving the linear system $T = P * R_{th}$, where R_{th} is the thermal resistivity matrix and P is the power vector.

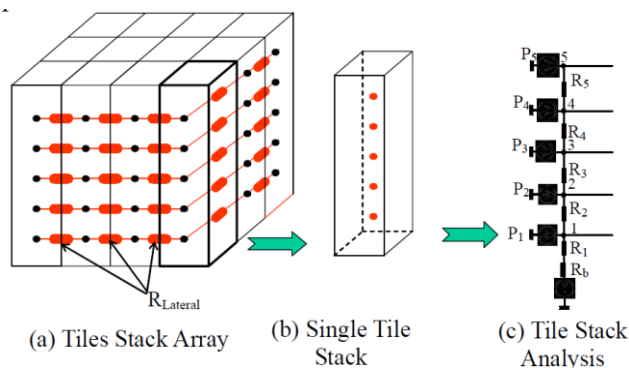


Figure 4.6 Simplified thermal model [10]

Among the identified models, HotSpot [9] is the most refined. It solves the linear system with an iterative multi-grid method, starting with a coarse mesh and then successively refining the solution. HotSpot also models the heat flow from the chip to the heat sink and the board. A faster alternative was used in [10]. Instead of solving the complete linear system, the lateral heat flow is neglected and tile stacks are analyzed individually (Figure 4.6). Because there is no interaction between tile stacks, this approach is less accurate and can produce a noisy thermal profile. Nevertheless, in [11] it is shown that the correlation between this model and HotSpot is 0.82, making it a reasonable choice for floorplanning. In the implementation for the current work, both approaches are used, neglecting lateral heat flow during the optimization and using Hotspot with a fine mesh to evaluate the final solution.

Floorplanning algorithms are usually initialized randomly. Random initializations generally produce disorganized (sparse) floorplans. This largely favors the T_{max} objective and can impede the search algorithm to move to solutions of smaller area and wirelength. Moreover, the thermal conductivity of the bonding interface material (epoxy, 0.05W/mK) is much lower than that of silicon (150W/mK) and copper (285W/mK). This large difference creates a barrier to heat flow, leading to significant temperature increases at each bonding interface. Consequently, it disturbs the search and impedes the efficient use of the upper layers. As an example, in [10], where the formulation (4.1) is used, the temperature reduction comes at the expense of area increase, of the order of 16%. An alternative to this problem is proposed in [11], using a two-phase algorithm. As described in the next section, this approach has been adapted in our implementation with different characteristics to improve its efficiency.

4.3.2 Two-phase algorithm

Floorplanning specialized in temperature minimization is carried out once the area is sufficiently compact. Floorplanning is performed in two phases, where temperature is minimized implicitly during the first phase and then explicitly during the second. Switching between different phases of the algorithm is based on area and a heuristic supporting the search algorithm to converge to cooler solution. Switching between phase one to phase two does not involve restarting the annealing schedule. The cost function for phase two keeps all the objectives of phase one, in contrast with [11] in which the wirelength objective is not considered when optimizing temperature.

Phase I – Power density distribution

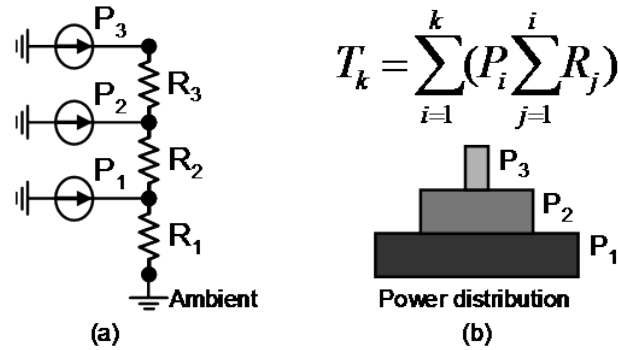


Figure 4.7(a) Vertical heat flow model (b) Power distribution profile that minimizes temperature

In the first phase a thermally efficient power density distribution is performed as explained below. From a 1D approximation, the vertical heat flow on the chip as indicated in Figure 4.7(a) it can be ascertained that a power distribution with a pyramidal shape (Figure 4.7(b)) will implicitly reduce peak temperature.

Therefore, during the first phase, we arrange the blocks in n layers so that the power density is maximized and the more power-hungry blocks are placed closer to the heat sink. For this purpose the cost function is written as:

$$C(S) = \alpha * Area + \beta * WL + \delta * (1/P_{Density}) \quad --(4.2)$$

where $P_{Density}$ is a weighted sum of the power density[6] of each layer:

$$P_{Density} = \sum_{i=1}^n \frac{P_i}{Area} \cdot q_i, \text{ with } q_i = R_1 / \sum_{j=1}^i R_j \quad --(4.3)$$

The q_i weighting factor decreases for layers further away from the heat sink. In this formulation, the term $P_{Density}$ is maximized both when the area is reduced and when the power-hungry blocks are moved to the lower layers. This formulation provides a means to combine the opposing objectives of area and temperature reduction in the same direction.

Phase 2 – Minimize thermal gradients

Once the area value threshold is achieved and all layers are appropriately occupied, the second phase commences involving thermal simulations. This threshold must be at least

$\lambda \leq A_{2D}/(n-1)$, where A_{2D} is the area of the design in a 2D configuration and n is the number of available layers (Figure 4.8).

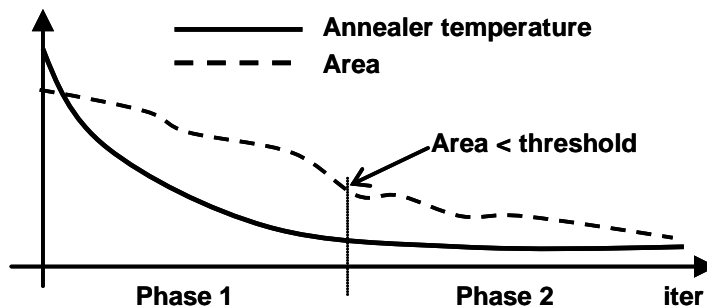


Figure 4.8 Two-phase algorithm and the switching criteria

During the second phase, the cost function is augmented with a temperature term:

$$C(S) = \alpha * Area + \beta * WL + \delta * (1/P_{Dens}) + \chi * \Sigma Tmax \quad --(4.4)$$

Our approach minimizes the sum of maximal temperatures on each layer instead of minimizing the maximal temperature. This formulation is motivated by the observation that the x - y coordinates of the hottest spot in each layer does not always coincide. If these situations occur, the formulation is able to reward the improvements in the thermal profile of each internal layer (i.e. gradient reduction). Furthermore the temperature on the top layers is naturally higher than that in the lower layers and, consequently, a higher reward is given to improvements at the top-most layer.

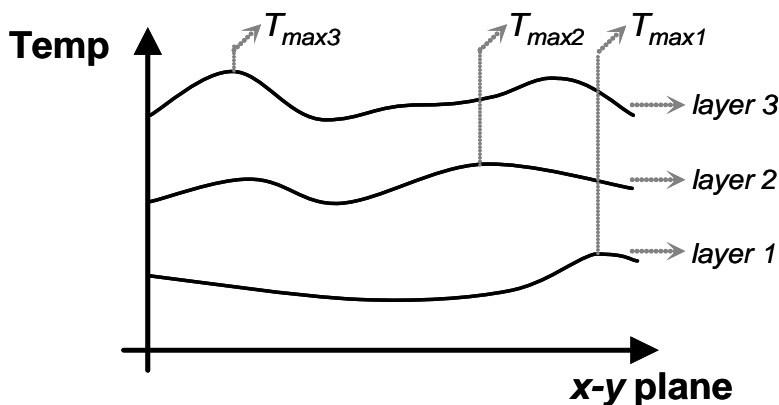


Figure 4.9 Thermal profile of each layer along a cross section of the x - y plane.

The power density heuristic consists of biasing all the inter-layer moves in the direction of attaining a pyramidal power distribution. Therefore, a block b_i in layer l_k is only allowed to move to a lower (resp. upper) layer l_p if it meets the condition of having a power density greater (resp. lesser) than the average power density of the blocks in l_k . When performing a 3D move, we randomly select a block in l_k until this condition is satisfied.

The next section describes in detail the various options used in the thermal-aware floorplanner and its implementation.

4.3.3 Thermal simulation options

When power information is available through the .power file, the user can activate the thermal simulation with three options:

- evalT** Performs a detailed thermal simulation at the end of the optimization. No temperature minimization is performed. *Default off.*
- minT** Minimizes the temperature using the two phase algorithm. *Default off.*
- useHeur** Activates the use of the power density heuristic. This option enables `-evalT` and can either be used alone for a fast thermal-aware floorplanning, or be combined with `-minT` to further improve the solution quality. *Default off.*

The grid size used to discretize the volume can be adjusted to obtain better accuracy. It can be adjusted to a finer granularity for detailed evaluation and to a coarser granularity during the iterative optimization process:

- gridEval <size>** The grid size used for the detailed evaluation. The value must be a power of 2. *Default 32 (32x32 grid).*
- gridOpt <size>** The grid size used for the simplified vertical model. The value must be a power of 2. *Default 8 (8x8 grid).*
- hsConfigFile <filename>** is used to replace the default simulator configuration file by a user defined file.

Using a very fine grid does not imply better results because the simplified thermal model neglects the lateral heat flow and only takes into account the vertical alignment of heat

sources. A very fine grid can map to regions of the floorplan where there are no blocks or heat sources. Since the model neglects lateral heat flow it can thus lead to very low or quasi-zero temperature difference with respect to ambient temperature and can cause the gradient computation to be very high. Finally, the minimum grid size is the area of the smallest block: below this value, there is of course no improvement in optimization results. In practice, the grid size (number of rows * number of columns) of the mesh used during optimization is set to be slightly larger than the smallest block area. To calculate the number of rows and number of columns we consider a perfect square floorplan over n layers with zero white space ($A_{\text{flp}} = A_{\text{blocks}}/n$) and let the A_{min} be the area of the smallest block considering this as square. Then the minimum grid size [8] is given by ratio of the square sides (4.5)

$$\text{gridsize} \geq \sqrt{\frac{A_{\text{blocks}}}{A_{\text{min}}}} \quad \text{--(4.5)}$$

We utilize 32*32 grid size in our simulation.

Saving and plotting the thermal data is done in the command line. Files with prefix "*thermal_grid*" contain temperature values for the grid, while those with prefix "*thermal_flp*" describe placement values. All filenames have a numerical suffix to indicate their layer number. The plot command used in HotSpot generates an SVG image from the aforementioned output files, where the temperature values in the plot (Figure 4.10(a)(b)) are in Kelvin. The temperature scale of each plot is set automatically.

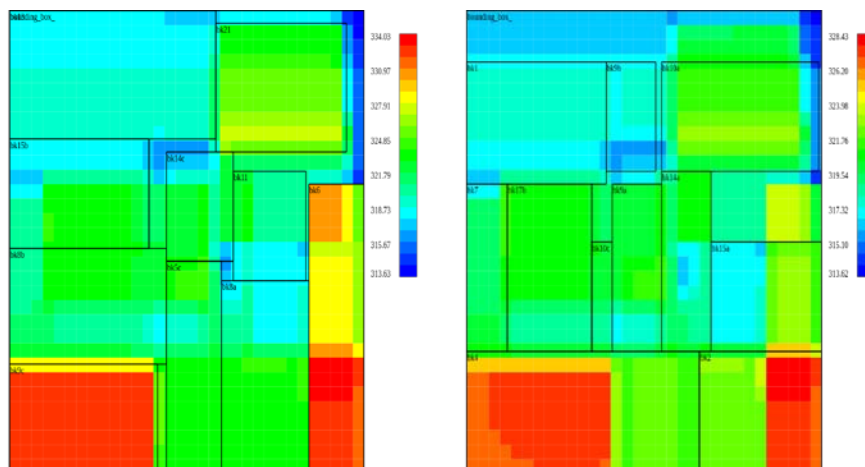


Figure 4.10 (a) Layer 0 (top) (b) Layer 1 (bottom)

The configuration settings of the floorplanner and the hotspot tool is elaborated in the Appendix V.

4.4 3D Integrated design flow

4.4.1 Design flow characteristics

The 3D integrated design flow combines all the characteristics explained in the previous section taking into account underlying system floorplanning and thermal map via Hotspot simulation, and is integrated into the imager thermal model to simulate the complete pixel matrix in the 3D environment as developed and explained in Chapter 3 (Figure 4.11). This 3D integrated tool can provide a complete analysis of the 3D stacked IC mainly in terms of thermal behavior, as well as area and interconnect data. In this work, we focus mainly on the thermal behavior and its impact on the pixel matrix output performance.

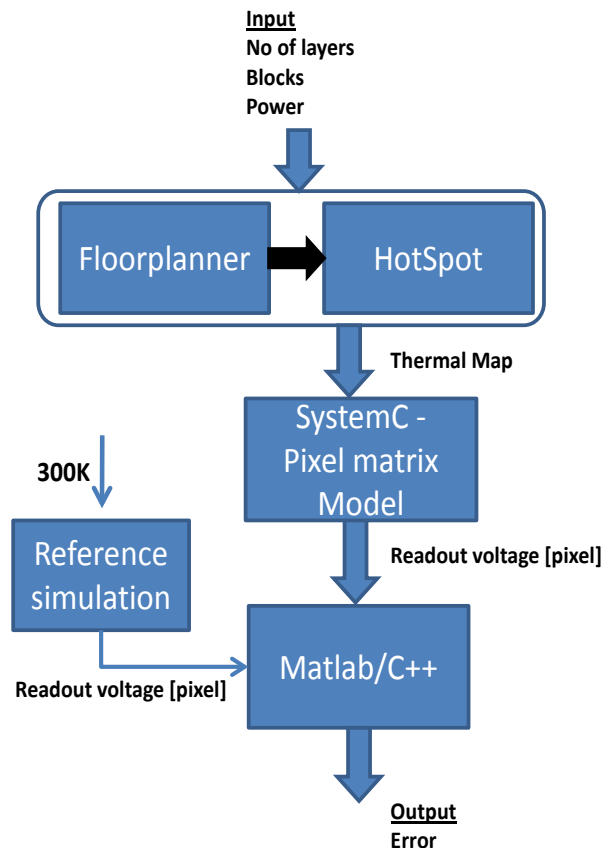


Figure 4.11 3D integrated design flow

Figure 4.11 depicts the flow of information throughout the complete evaluation process. Initially, the number of layers, the blocks available in the entire system and their power values are set. As explained in the previous section, the floorplanning algorithm is run to obtain a suitable set of layer floorplans with block positions, along with the approximate thermal profile of each layer. Then the HotSpot tool is run to obtain a more accurate thermal profile of each layer of the 3D chip.

Both the floorplanning and HotSpot tools were run using a 32*32 grid size. The thermal map thus obtained is adapted according to the imager pixel matrix size. This process helps to determine the operating temperature of each pixel.

Simulation of the 3D integrated design flow is necessary to choose the floorplan which has the lowest thermal influence on the output performance of the imager pixel matrix. The thermal map obtained from HotSpot is used to provide realistic thermal data per pixel as input to the SystemC-based imager pixel matrix thermal model. Only the thermal map from the layer 0 (top most layer) is taken into account for the thermal simulation of the pixel matrix. The model calculates the readout voltage of each pixel based on the input from the thermal map and set of input image intensity values.

To verify and select the floorplan which has the lowest influence on the output performance, a validation step is performed. The validation step involves calculating the error taking the average of absolute differences of each pixel readout voltage V_{out} from the reference simulation. This is given by

$$Average\ error\ (V) = \frac{\sum_{i=1}^{i=N} |V_{out_i}[300K] - V_{out_i}[T_M]|}{N} \quad --(4.6)$$

where T_M represents the temperature value for the given pixel at the relevant point in the thermal map of the pixel matrix.

In this case, we have taken the readout voltage error as sole criterion for selection of the best floorplan. Of course, the overall process can also introduce other metrics for selection, combining for example temperature impact minimization with area minimization, resulting in a more complex and longer design cycle. This topic will be covered in detail in the following sections.

4.5 Results

4.5.1 Test cases

The integrated design has been verified using the following test cases. Test cases were carefully chosen to prove the robustness, flexibility and capability of the 3D integrated design flow. All the test cases are simulated with MCNC benchmark suite utilizing the ami33 with 33 blocks[13]. Power values for all the blocks are used as per the benchmark without any modification. The 3D structure which has been used for the simulation has three active layers below the pixel matrix as indicated in Figure 4.12.

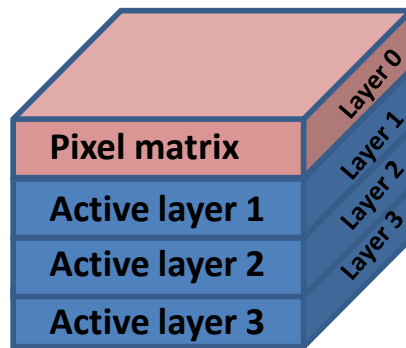


Figure 4.12 3D stack – ami33 – 4 layer structure

During the floorplanning optimization process the solution is initialized to a random floorplan. Then the process searches for improved solutions until the optimization times out (reaches the maximum number of iterations). As previously mentioned, the quality of the final solution depends on the starting point and on how much time the optimization process is allowed to refine it (with increased time, the dependency on the starting point decreases). Typically the initialization is random but it could also be fixed to the same starting point. Fixing the same starting point helps to analyze the impact of setting optimizations with different objectives and/or different algorithm parameters such as weights on temperature minimization or area minimization, or raising the maximum number of iterations. During the proposed test cases, and since the objective at this stage is to determine the best tool configuration, the floorplanning tool is set to use a number of fixed seeds q (integer) to ensure the use of the same starting points for all test cases. This approach is typically used to reproduce a given result, and here enables the comparison between different test cases. In all test cases the simulations run through five seeds. The test cases considered are as follows (Table 4-1):

- T1 - Compact area, ignore temperature impact, 2000 iterations, no heuristics
- T2 – Ignore area, minimize temperature impact, 2000 iterations, no heuristics
- T3 – Ignore area, minimize temperature impact, 4000 iterations, no heuristics
- T4 – Compact area, minimize temperature impact, 2000 iterations, use heuristics

Table 4-1 Test cases

Test case	Area	Temperature	Iteration
T1	😊	😞	2000
T2	😞	😊	2000
T3	😞	😊	4000
T4	😊	😊	2000

A simple pixel matrix size of 128*128 is considered in all test cases. To verify the robustness of the model we have chosen two input pictures. Part of the “lena” (it will be called as *lena* in future sections) picture (Figure 4.13) has different intensities at different pixels of the picture. The “white” picture (Figure 4.14) has uniform intensity over all pixels. These pictures are fed into the imager thermal model with a uniform temperature distribution set at 300K. The colors represented in the figures are the actual 8-bit pixel integer values rather than intensity levels.

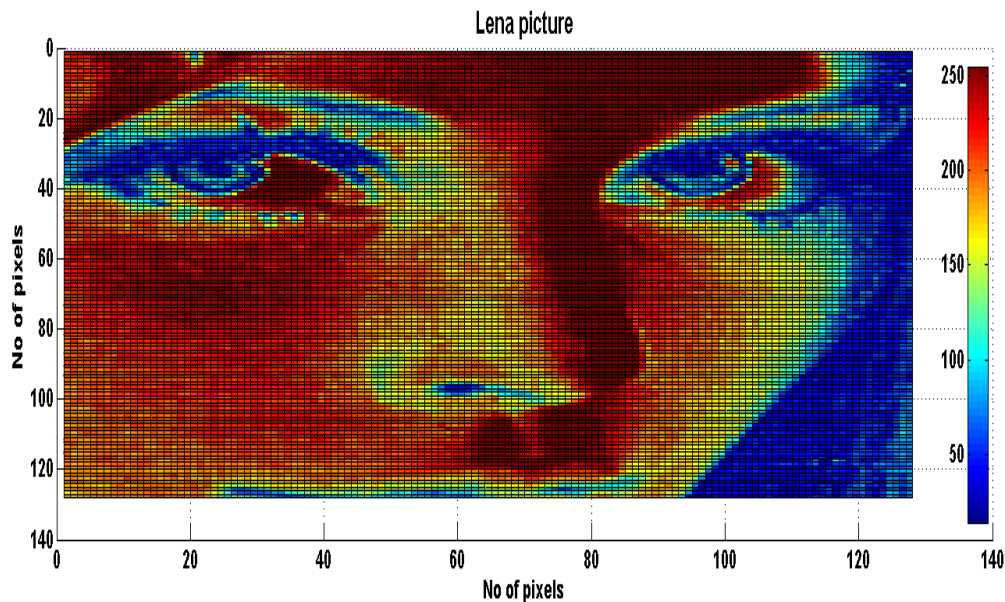


Figure 4.13 “Lena” picture input to imager thermal model

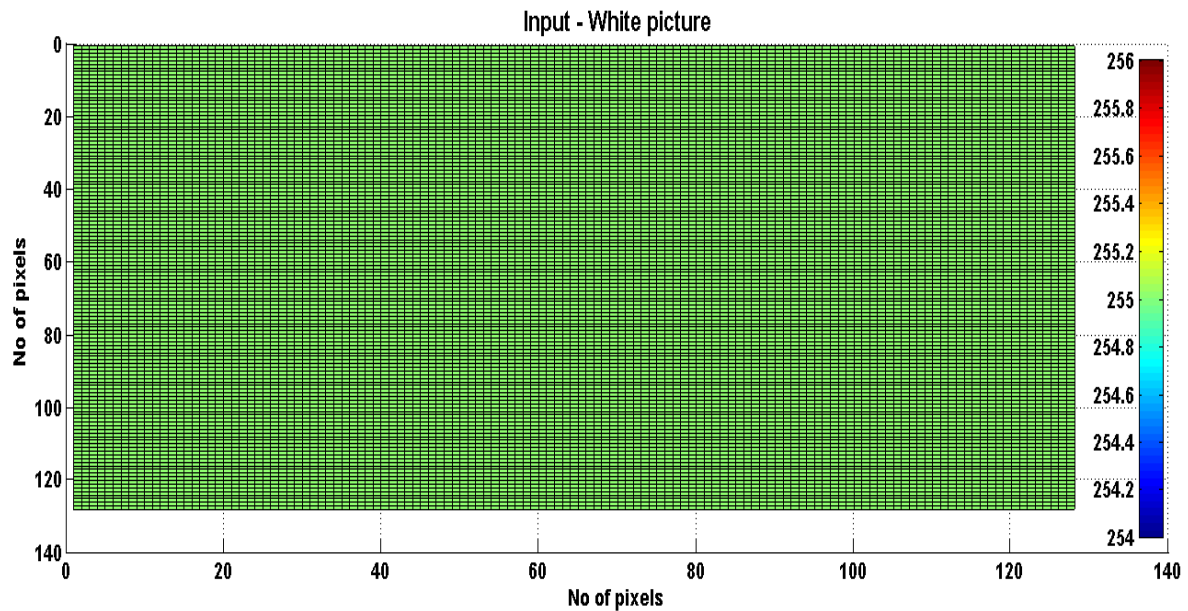


Figure 4.14 Input intensity of “White picture” to imager thermal model

The imager thermal model output gives the readout voltage of each individual pixel in the pixel matrix at 300K and for 10ms integration time. Figure 4.15 and Figure 4.16 represent the reference simulation results to be used in all test cases to evaluate the performance variation due to temperature.

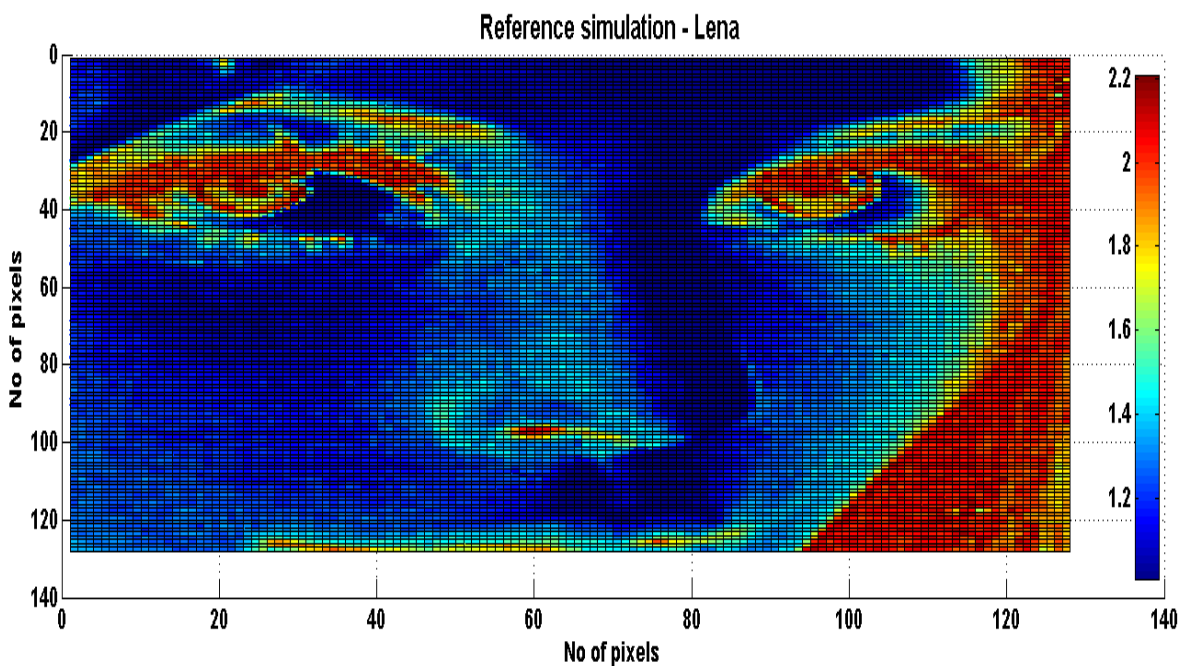


Figure 4.15 Readout Voltage - Reference simulation ($T_{int}=10ms$, Temperature=300K)

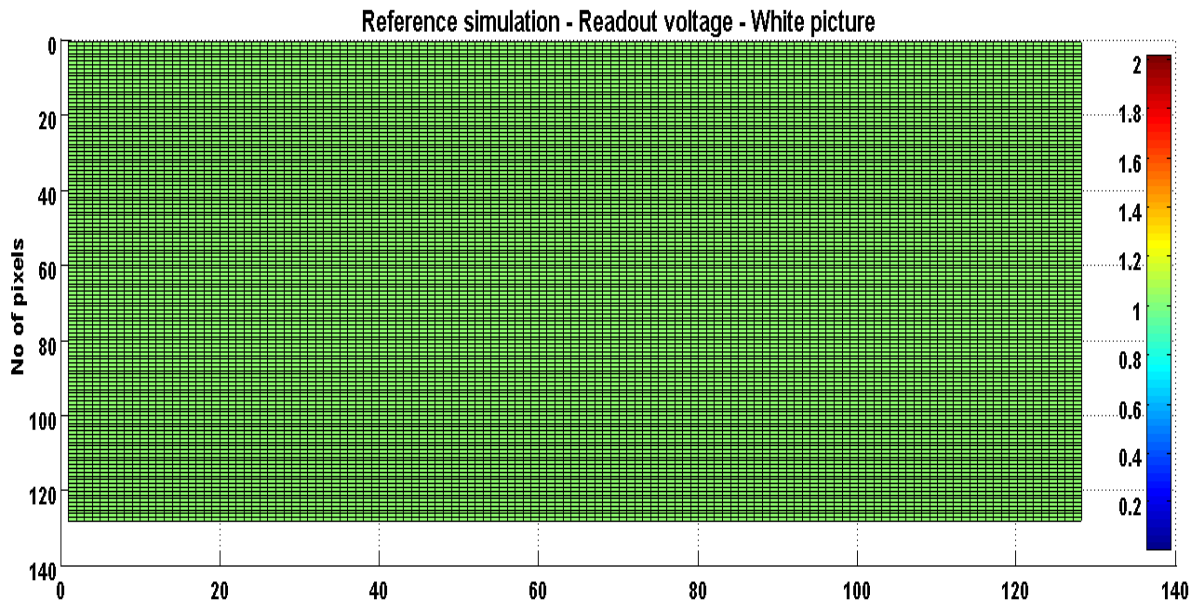


Figure 4.16 Readout voltage – Reference simulation ($T_{int}=10ms$, $Temperature=300K$)

Each test case is detailed on a case by case basis, along with their relevant results in the next section. While considerations such as area and wirelength optimization are also possible, this work mainly concentrates on temperature minimization and temperature based floorplanning.

4.5.2 Test case I – Compact area

The main goal of this test case is to obtain a compact area for the four layered chip stack. Temperature minimization is not performed. The top layer is occupied entirely by the pixel matrix, the layout of which is fixed. The floorplanner handles movement only on the three lower layers, where blocks undergo both intra- and inter-layer movements.

As discussed earlier, the flow begins initially with floorplanning, at the end of which the thermal maps are produced for each layer as indicated in Figure 4.17.

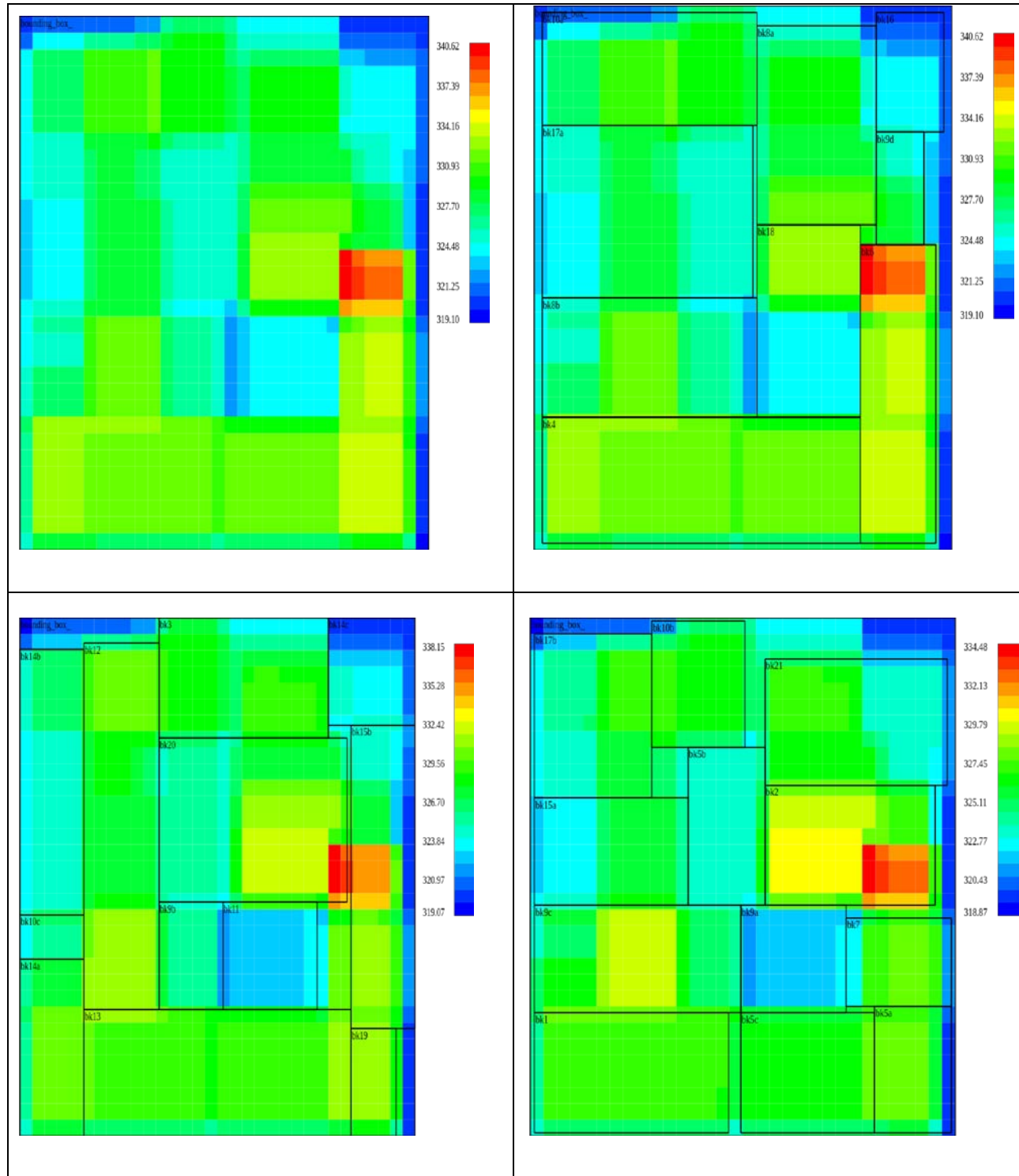


Figure 4.17 Test case 1 result – Thermal map
 Layer 0 (Top-left), Layer1 (Top-Right), Layer2 (Bottom-left), Layer 3(Bottom-Right)

During the optimization process reports were generated individually for each seed and they are tabulated as in Table 4-2. Each column represents either the geometry (area, height, width, wire length) or temperature (maximum temperature, gradient) and power density data. AR is the ratio between the height and width values. Gradient is the difference between the maximum temperature and minimum temperature value. Power density is calculated by (4.2). The thermal maps shown in Figure 4.17 are shown for Seed 2, which resulted in the best area (objective of this test case).

Table 4-2 Test case I – Compact area - Report

Seed	Area (um ²)	Height (um)	Width (um)	AR	WL (um)	Temperature (K)	Gradient (K)	Power density (W/m ²)
1	429828	1428	301	4.74419	95996.5	325.317	19.8503	1636680
2	421890	735	574	1.28049	67311.5	340.617	21.5142	1667480
3	425320	868	490	1.77143	69756.2	332.1	18.9416	1654030
4	434042	1442	301	4.7907	89115	323.845	18.084	1620790
5	422037	693	609	1.13793	71983	340.253	19.642	1666900

Once the optimization process was completed, the thermal map of the pixel matrix layer is decoded into the temperature values of individual pixels and fed into the imager thermal model with 10ms integration time to obtain the set of actual readout voltages. With the same thermal map, two different simulations were performed: one with light intensity values coming from the *lena* image, and the other with uniform and non-zero intensity across the picture. The readout voltage distribution obtained for the *lena* picture is indicated in Figure 4.18 and readout voltage distribution obtained for the white picture is indicated in Figure 4.19.

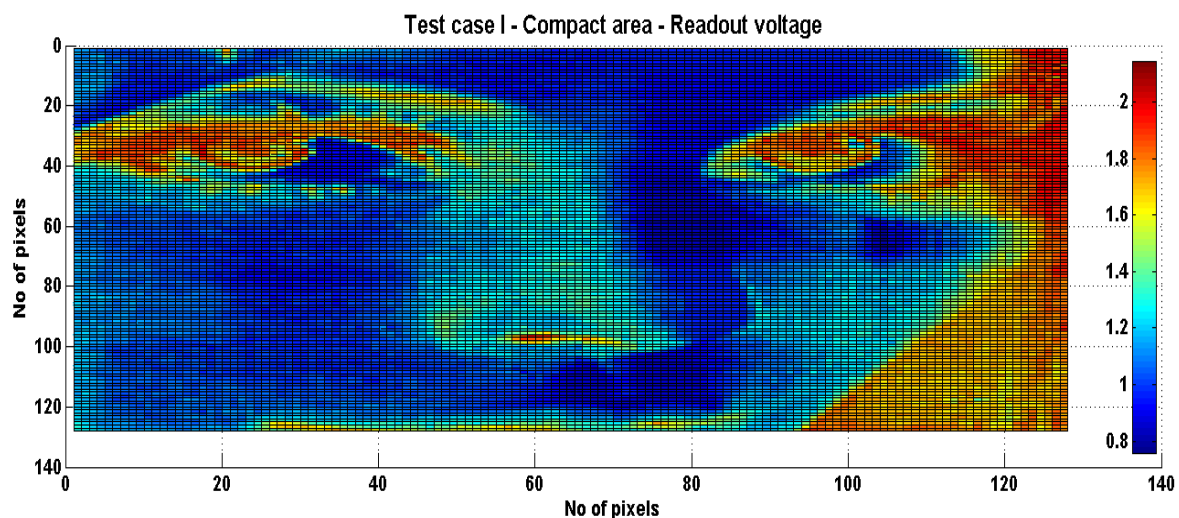


Figure 4.18 Testcase I result – Lena picture – Readout voltage

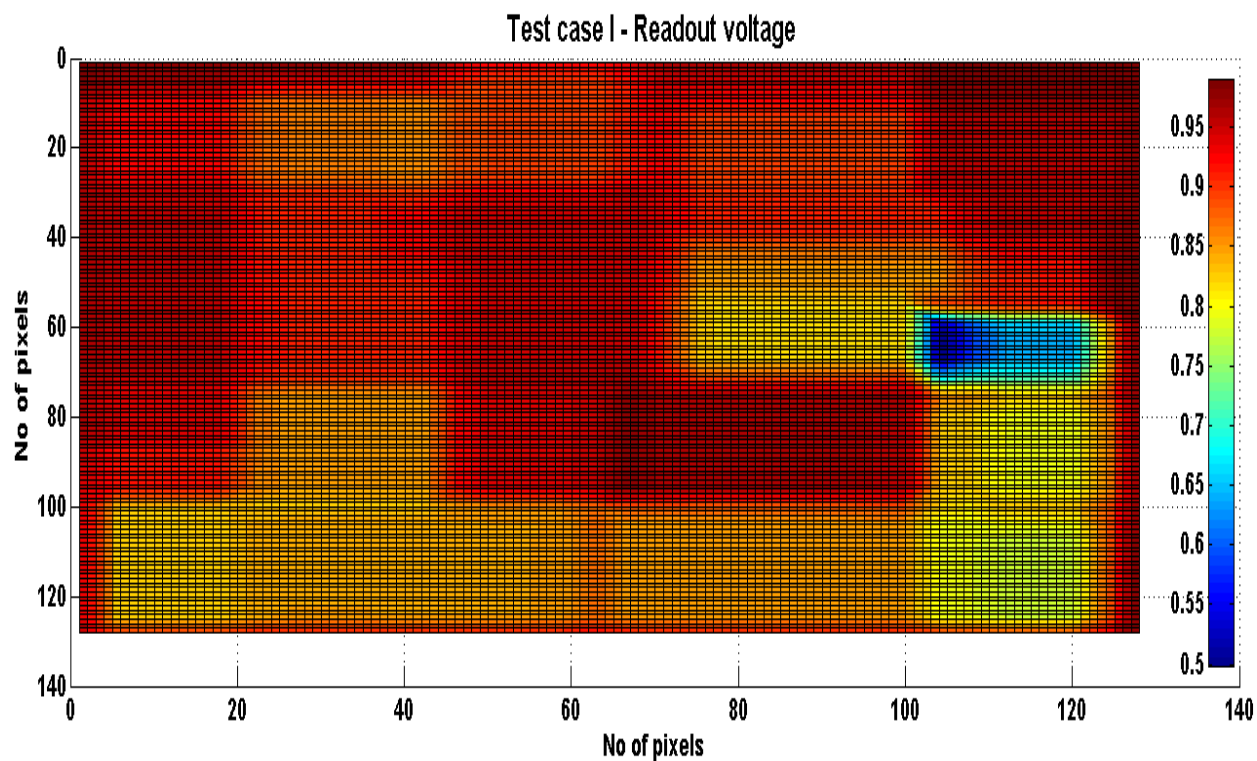


Figure 4.19 Testcase I result- White picture – Readout voltage

Table 4-3 depicts the maximum and minimum temperature values and readout voltages as extracted from the pixel matrix. Temperature distribution is depicted in Figure 4.20. The mean value for this test case is 328.28 K with standard deviation is 3.5219 and 3σ value is 10.5657.

Table 4-3 Comparative results (Reference vs Testcase I)

	Temperature (K)		Readout voltage (Volts)	
	Min temp	Max temp	Min Voltage	Max Voltage
Ref. Lena	300	300	1.0072	2.2088
Lena	319.1	340.36	0.7583	2.1457
Ref.White	300	300	1.0072	1.0072
White	319.1	340.36	0.4987	0.9892

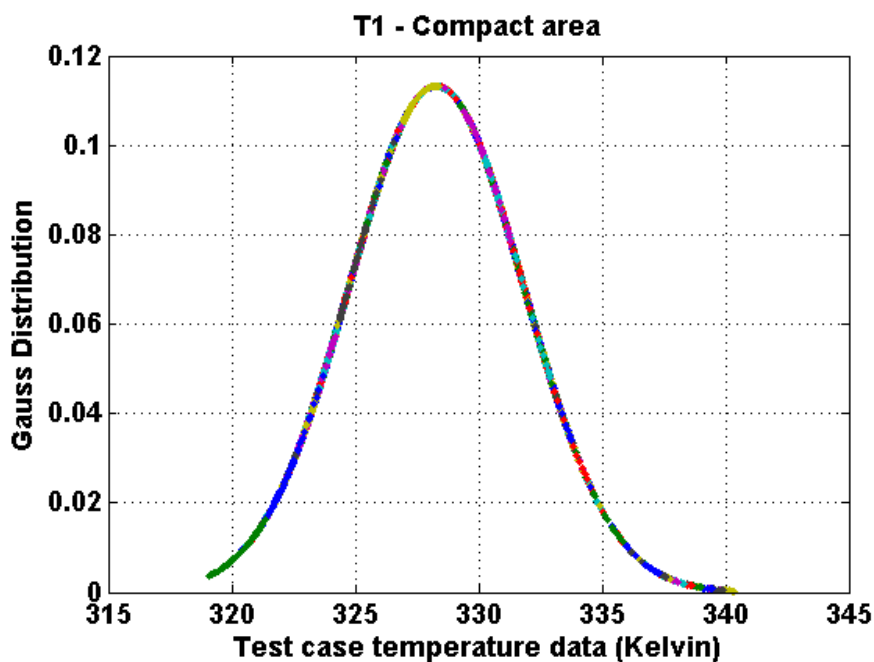


Figure 4.20 Test case I temperature distribution

Using equation 4.6 we find an average error over the pixel matrix of 0.1367V for the *lena* picture and 0.1138V for the white picture due to the temperature increase in test case I (best compact area). As previously calculated, the allowable error based on the quanta calculation is 12.89mV, so the above error will lead to a shift of 10 levels in intensity (Eq 4.7).

4.5.3 Testcase II – Minimizing temperature

The main goal of this testcase is to minimize temperature (area is not part of the objective function). It uses the two phase algorithm as explained in section 4.3.1. The model produces the following thermal map as in Figure 4.21.

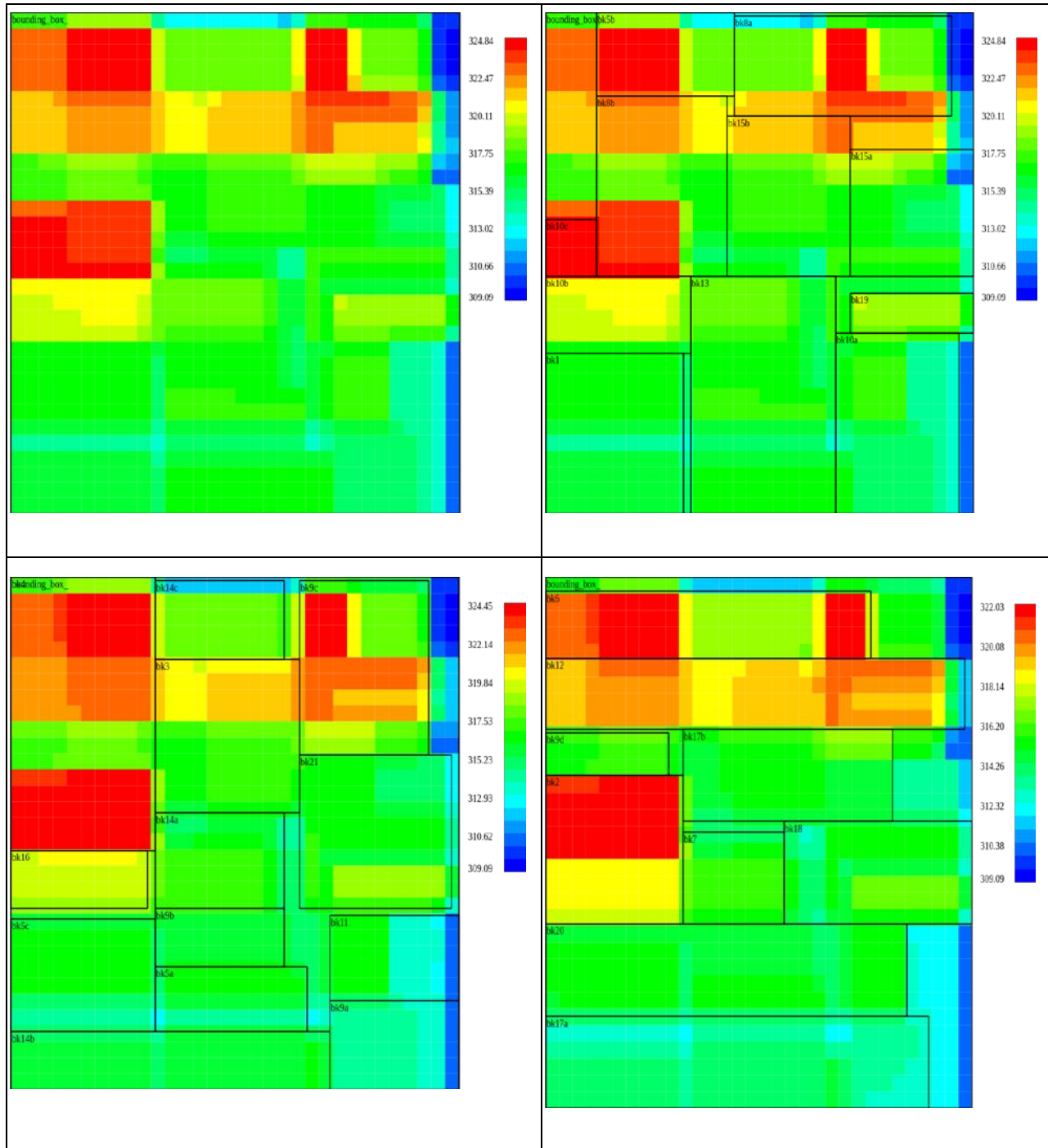


Figure 4.21 Test case II results – Thermal map
 Layer 0 (Top-left), Layer1 (Top-Right), Layer2 (Bottom-left), Layer 3(Bottom-Right)

During the temperature minimization optimization process reports were generated for each seed and they are tabulated as in Table 4-4. The thermal maps shown in Figure 4.21 are shown for Seed 1, which resulted in the lowest temperature (objective of the test case).

Table 4-4 Testcase II – Minimization temperature - Report

Seed	Area (um ²)	Height (um)	Width (um)	AR	WL (um)	Temperature (K)	Gradient (K)	Power density (W/m ²)
1	433650	413	1050	0.39333	82664.5	324.838	15.7494	1622260
2	462560	826	560	1.475	74231.9	330.978	15.969	1520870
3	454279	889	511	1.73973	85262.8	328.032	13.2272	1548590
4	459375	875	525	1.66667	69264	325.554	12.1655	1531410
5	444136	616	721	0.85437	65395.9	331.584	12.5326	1583960

The layer 0 thermal map obtained after the optimization process is fed into the Imager thermal model. The Imager thermal model produces readout voltage of individual pixels. With the same thermal map two different simulations have been performed, one with intensity distribution coming from *lena* picture and other with white picture. The readout voltage distribution obtained for the *lena* picture is indicated in Figure 4.22 and the readout voltage distribution obtained using white picture is indicated in Figure 4.23

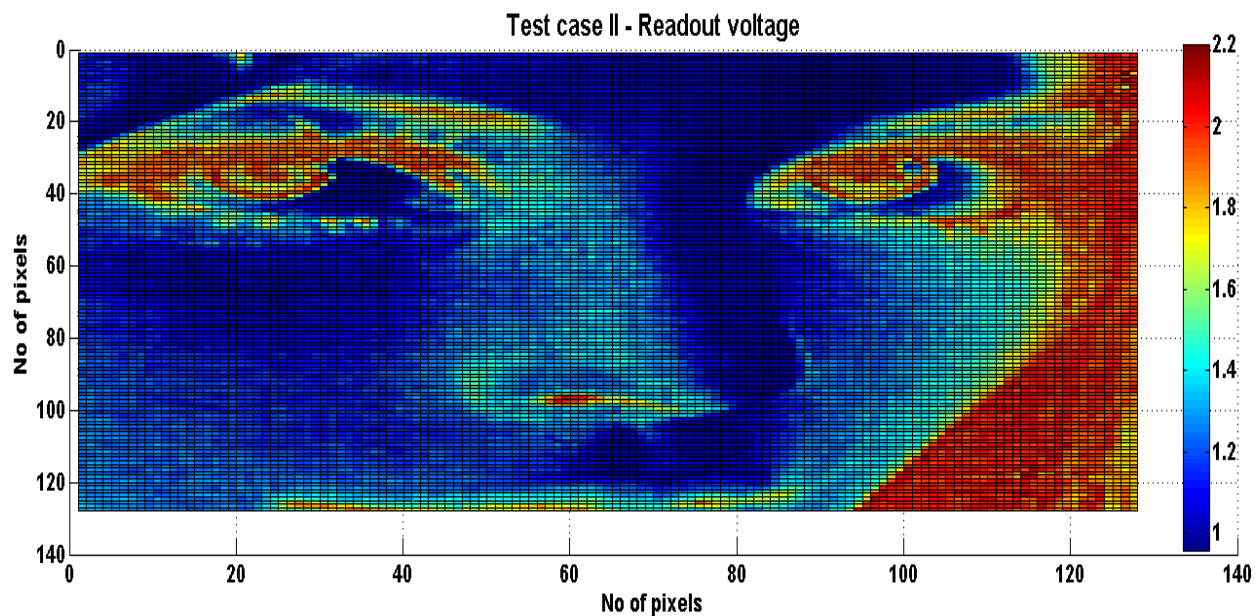


Figure 4.22 Testcase II results – Lena picture – Readout voltage

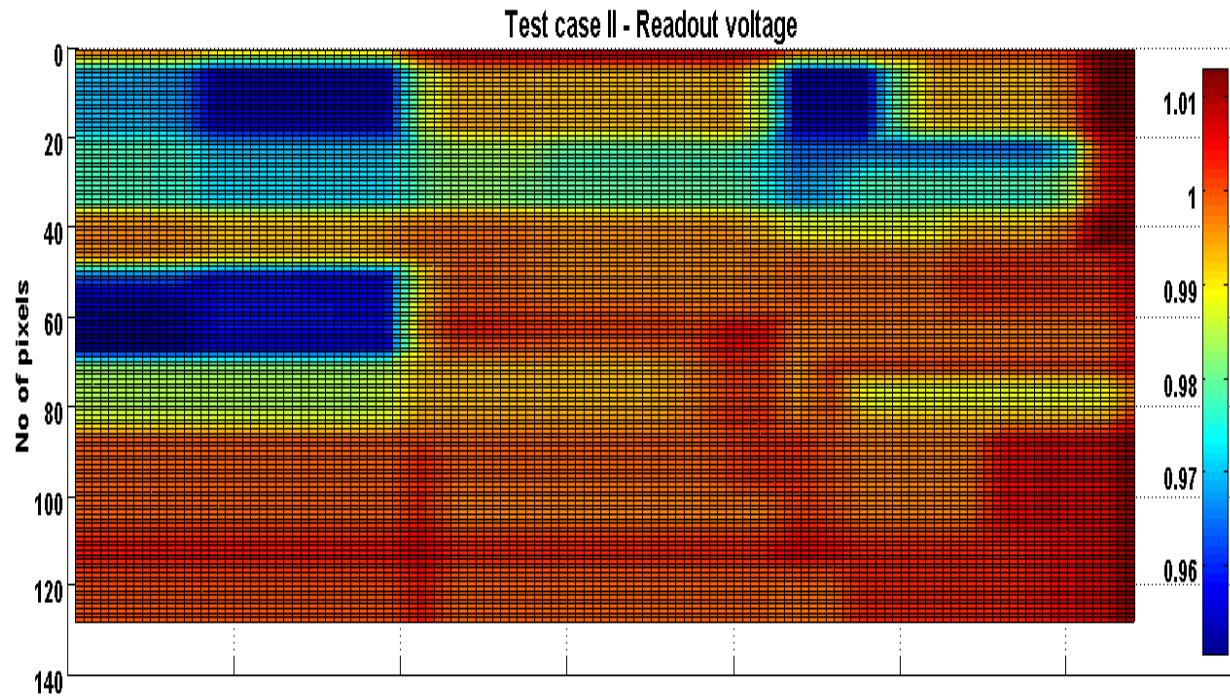


Figure 4.23 Testcase II results – White picture – Readout voltage

During the above results generation, few comparative results has been noted down and tabulated as in Table 4-5. Temperature distribution is depicted in Figure 4.24 . The mean value for this test case is 317.99 K with standard deviation is 3.0156 and 3σ value is 9.0467.

Table 4-5 Comparative results (Reference vs Testcase II)

	Temperature (K)		Readout voltage (Volts)	
	Min temp	Max temp	Min Voltage	Max Voltage
Ref.Lena	300	300	1.0072	2.2088
Lena	309.09	324.81	0.9574	2.2028
Ref.White	300	300	1.0072	1.0072
White	309.09	324.81	0.9504	1.0129

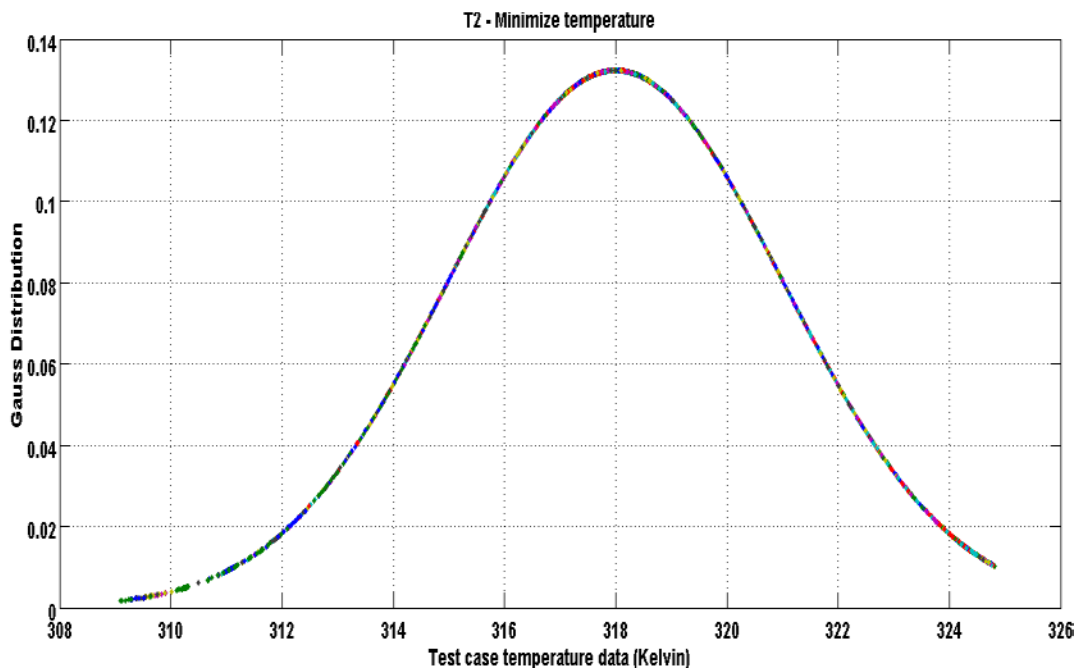


Figure 4.24 Test case II temperature distribution

Seed 1 which is selected based on lowest maximum temperature among all the seeds. An average error calculated for the pixel matrix stand at 0.0241V for *lena* picture and 0.0163V for white picture. Based on quanta (Eq 4.7) calculation shift in two levels will be seen for *lena* picture and one level for white picture because of temperature. From this calculation and the above tabulation there is a clear improvement in performance compared to the previous testcase.

4.5.4 Testcase III - Longer iteration

In this testcase minimization of temperature across the layer is the main objective but additionally we allow the optimization process to run longer than the default condition. In the previous testcases default iteration of 2000 times was used. In this test case 4000 iterations is performed.

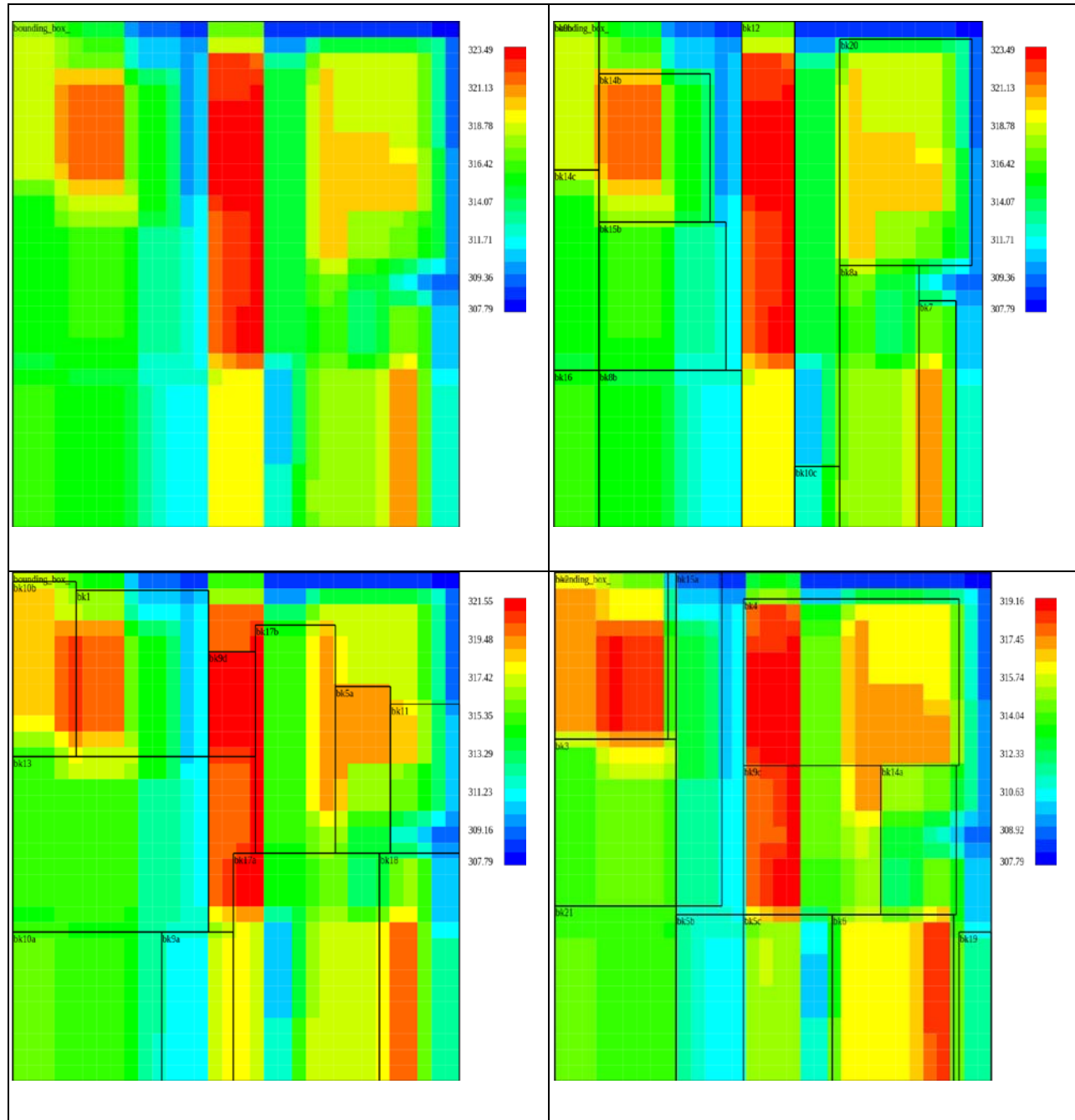


Figure 4.25 Test case III results – Thermal map
 Layer 0 (Top-left), Layer1 (Top-Right), Layer2 (Bottom-left), Layer 3(Bottom-Right)

Reports for various seeds were generated during the process of this optimization and they are tabulated in Table 4-6. The thermal maps shown in Figure 4.25 are shown for Seed 3, which resulted in the lowest temperature with long iteration (objective of the test case).

Table 4-6 Testcase III – Longer iteration with temperature minimization - Report

Seed	Area (um ²)	Height (um)	Width (um)	AR	WL (um)	Temperature (K)	Gradient (K)	Power density (W/m ²)
1	446880	560	798	0.70174	74350.2	331.445	15.8771	1574230
2	445214	826	539	1.53247	67404.3	327.486	11.4272	1580120
3	460404	1134	406	2.7931	83174.8	323.492	15.7018	1527990
4	448791	903	497	1.8169	65374.7	324.126	10.544	1567530
5	470008	616	763	0.8073	69118.2	329.716	12.273	1496760

The layer 0 thermal map obtained after the optimization process is fed into the Imager thermal model. The Imager thermal model produces readout voltage of individual pixels. With the same thermal map two different simulations have been performed, one with intensity distribution coming from *lena* picture and other with white picture. The readout voltage distribution obtained for the *lena* picture is indicated in Figure 4.26 and the readout voltage distribution obtained using white picture is indicated in Figure 4.27

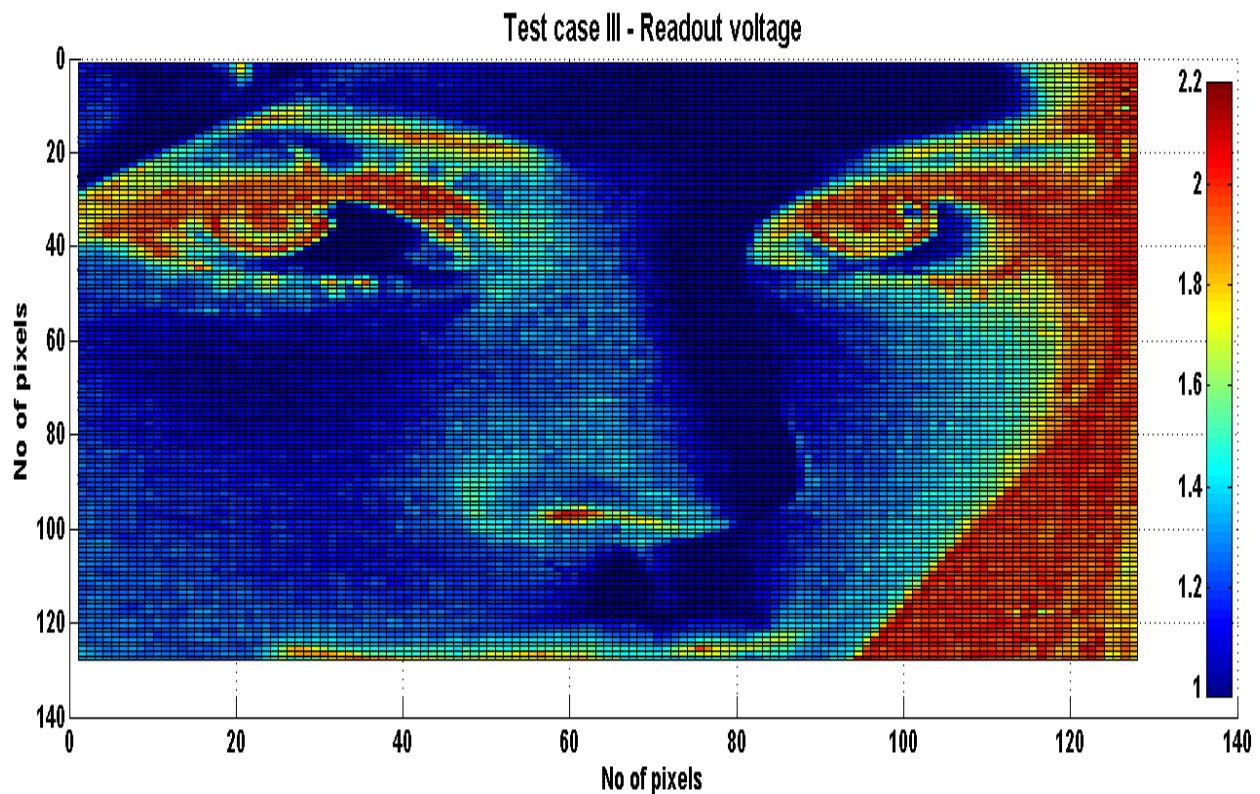


Figure 4.26 Testcase III result – Lena picture – Readout voltage

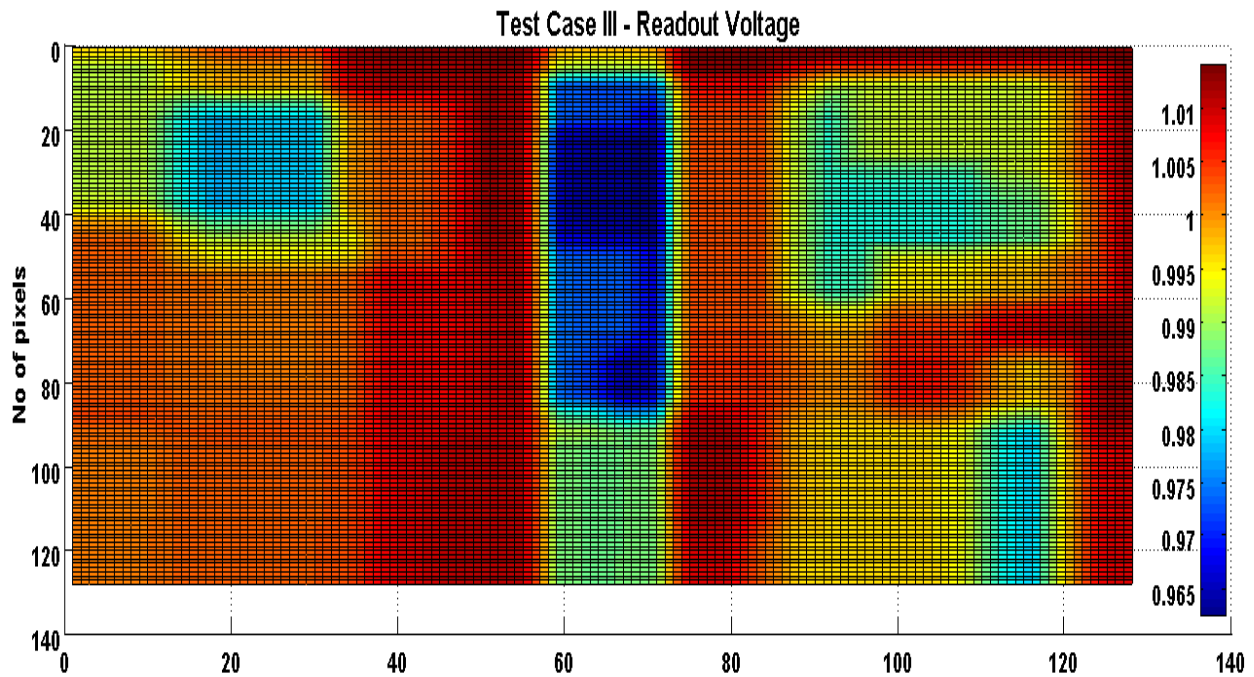


Figure 4.27 Testcase III result – white picture – Readout voltage

Comparative results of the maximum and minimum temperature evolution with reference to the ambient reference simulation is tabulated as in Table 4-7. Temperature distribution is depicted in Figure 4.28. The mean value for this test case is 316.14 K with standard deviation is 3.338 and 3σ value is 10.0140.

Table 4-7 Comparative results (Reference vs Testcase III)

	Temperature (K)		Readout voltage (Volts)	
	Min temp	Max temp	Min Voltage	Max Voltage
Ref.Lena	300	300	1.0072	2.2088
Lena	307.79	323.47	0.986	2.2022
Ref.White	300	300	1.0072	1.0072
White	307.79	323.47	0.9626	1.014

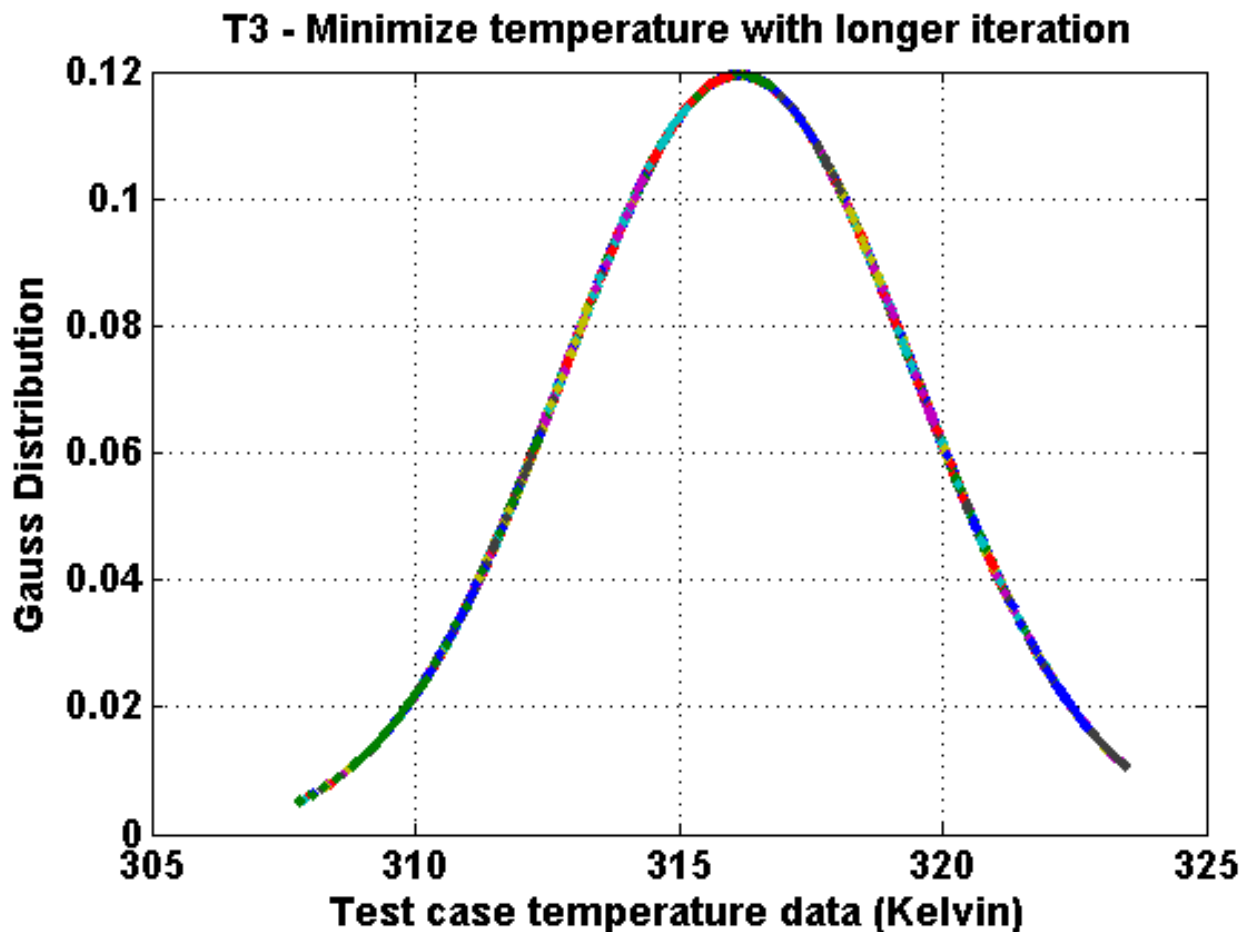


Figure 4.28 Test case III temperature distribution

An average error calculated for the pixel matrix stand at 0.0175V for *lena* picture and 0.0098V for white picture. Based on quanta (Eq 4.7) calculation shift in one level is seen in *lena* picture and no shift of levels in intensity in white picture. From this calculation and the above tabulation there is a clear improvement in performance compared to the previous testcase with longer iteration.

4.5.5 Testcase IV – UseHeuristics

In this testcase we use the compact area along with minimization temperature activated with power density heuristics as explained in section 4.3.1. In this method we try to move blocks based on the power density i.e mean power density of lower layer should be greater than the

top layer to form a pyramidal structure of blocks based on power density. By this process the model generated the following thermal map of each layer as in Figure 4.29

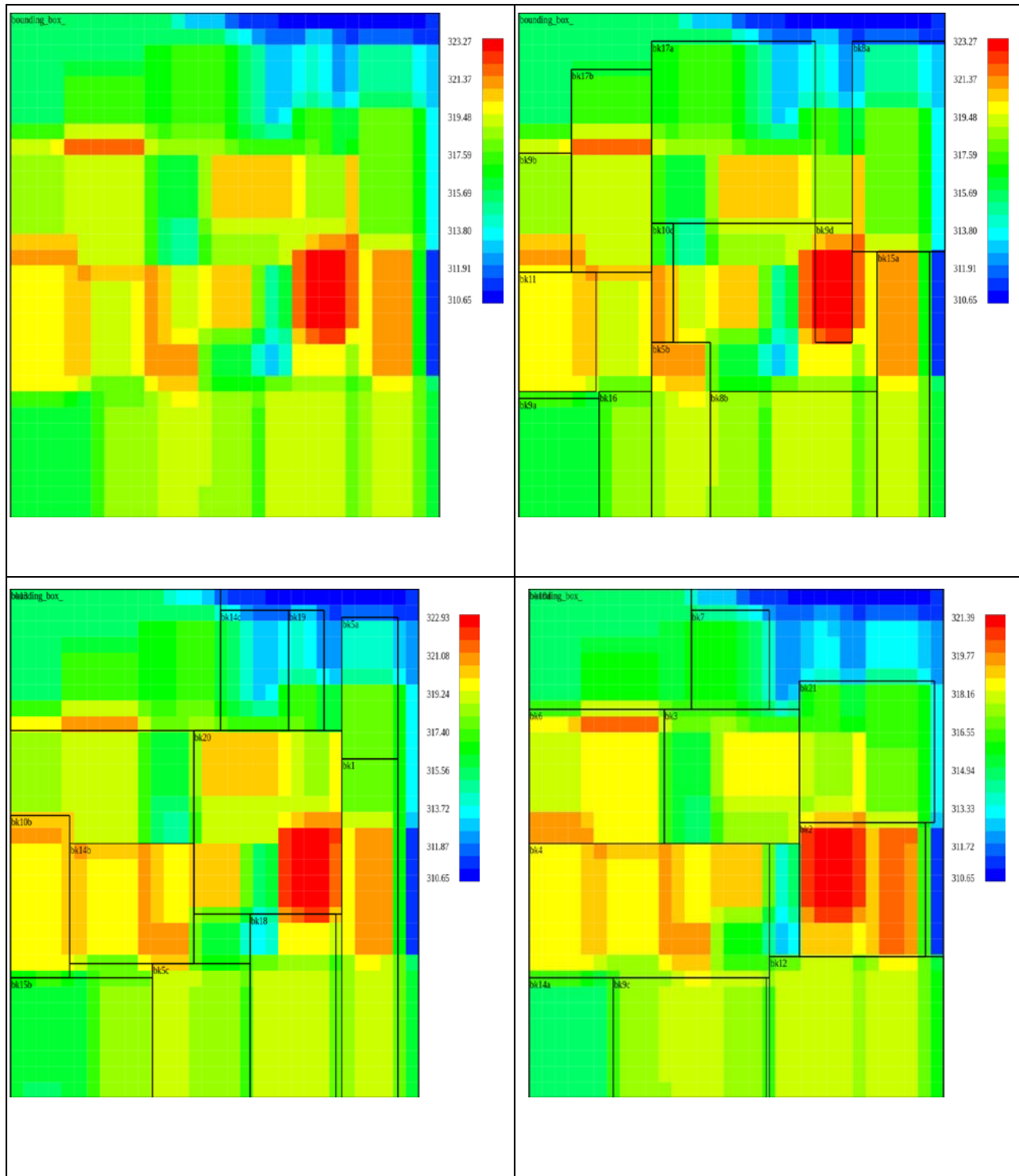


Figure 4.29 Test case IV results – Thermal map
Layer 0 (Top-left), Layer1 (Top-Right), Layer2 (Bottom-left), Layer 3(Bottom-Right)

Reports for various seeds were generated during the process of this optimization and they are tabulated as in Table 4-8. The thermal maps shown in Figure 4.29 is for Seed 1, which resulted in the lowest temperature with use heuristics (objective of the test case).

Table 4-8 Testcase IV – Useheuristics - Report

Seed	Area (um ²)	Height (um)	Width (um)	AR	WL (um)	Temperature (K)	Gradient (K)	Power density (W/m ²)
1	508032	756	672	1.125	71863.1	327.542	10.2031	1384740
2	473536	1057	448	2.35938	75592.4	320.639	11.6932	1485610
3	486080	868	560	1.55	80306.3	325.772	12.5917	1447280
4	465696	672	693	0.9697	62846.7	332.092	11.4651	1510620
5	449330	917	490	1.87143	72238.3	326.594	14.7573	1565650

The layer 0 thermal map obtained after the optimization process is fed into the Imager thermal model. The Imager thermal model produces readout voltage of individual pixels. With the same thermal map two different simulations have been performed, one with intensity distribution coming from *lena* picture and other with white picture. The readout voltage distribution obtained for the *lena* picture is indicated in Figure 4.30 and the readout voltage distribution obtained using white picture is indicated in Figure 4.31.

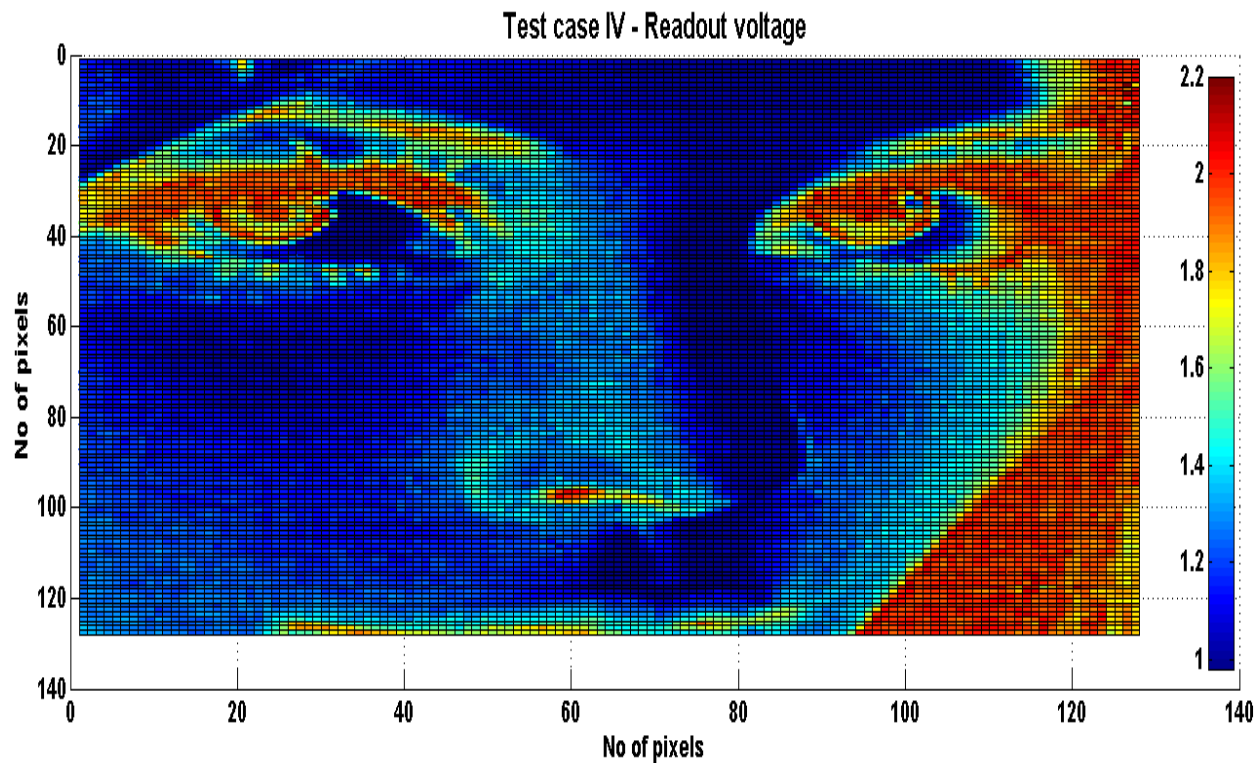


Figure 4.30 Testcase IV results – Lena picture – Readout voltage

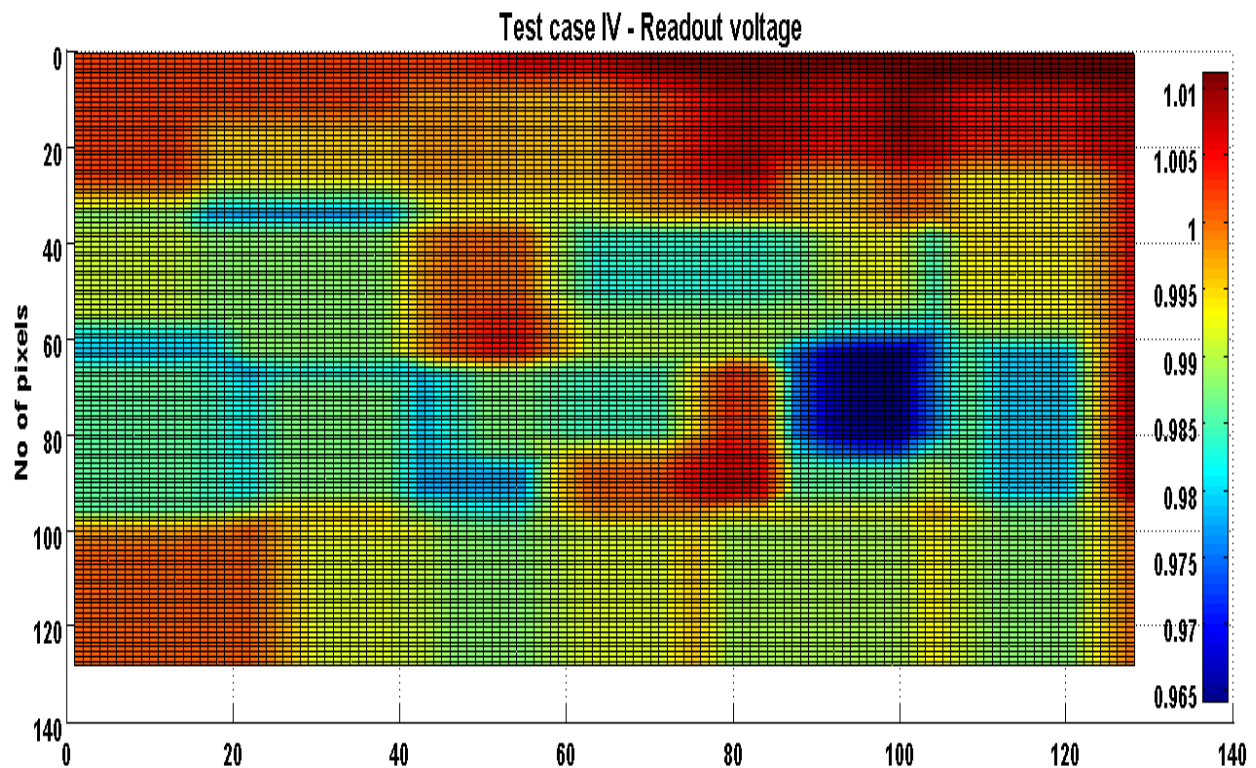


Figure 4.31 Testcase IV – White picture – Readout voltage

Tabulation of the maximum and minimum temperature and their influence in readout voltage is shown in Table 4-10. Temperature distribution is depicted in Figure 4.32. The mean value for this test case is 317.92 K with standard deviation is 2.341 and 3σ value is 7.0229.

Table 4-9 Comparative results (Reference vs Testcase IV)

	Temperature (K)		Readout voltage (Volts)	
	Min temp	Max temp	Min Voltage	Max Voltage
Ref.Lena	300	300	1.0072	2.2088
Lena	310.65	323.27	0.9812	2.2011
Ref.White	300	300	1.0072	1.0072
White	310.65	323.27	0.9642	1.0111

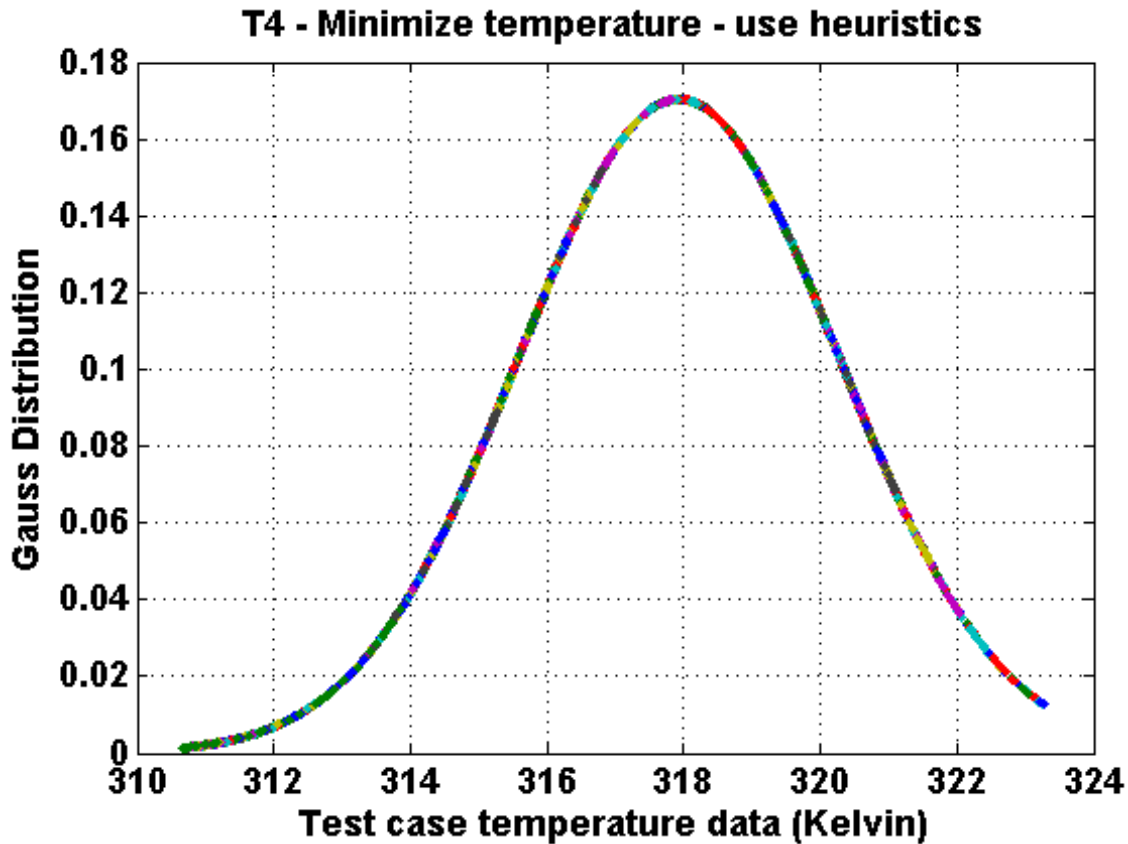


Figure 4.32 Test case IV temperature distribution

An average error seen in the pixel matrix is seen as 0.0229V for *lena* picture and 0.01447V for the white picture test case. The above error when calculated using quanta (Eq 4.7) will lead to shift in intensity level by 2 level for *lena* picture and 1 level for the white picture.

4.6 Conclusion

From the above testcases it is clear that each floorplan influences the output performance of the pixel matrix. Testcase I and Testcase II represent two extremes, where the former targets as compact an area as possible, giving no importance to the temperature aspect, while the latter focuses on better temperature performance but at the cost of area. There is clearly a tradeoff

space to be explored between these scenarios, which is filled partially by testcases III and IV. Testcase III utilized temperature minimization, but allowed the optimization algorithm to run twice as long to see if the results could be improved as compared to previous testcases. Testcase IV used a different scenario, with heuristics realizing power density in a pyramidal structure of blocks.

The average error evaluated in each testcase is tabulated in Table 4.10 compared to the reference ambient temperature simulation. The graph is shown in Figure 4.33

Table 4.10 Average error

Test case	Lena Average error (Volts)	White Average error (Volts)
I	0.1367	0.1138
II	0.0241	0.0163
III	0.0175	0.0098
IV	0.0229	0.0144

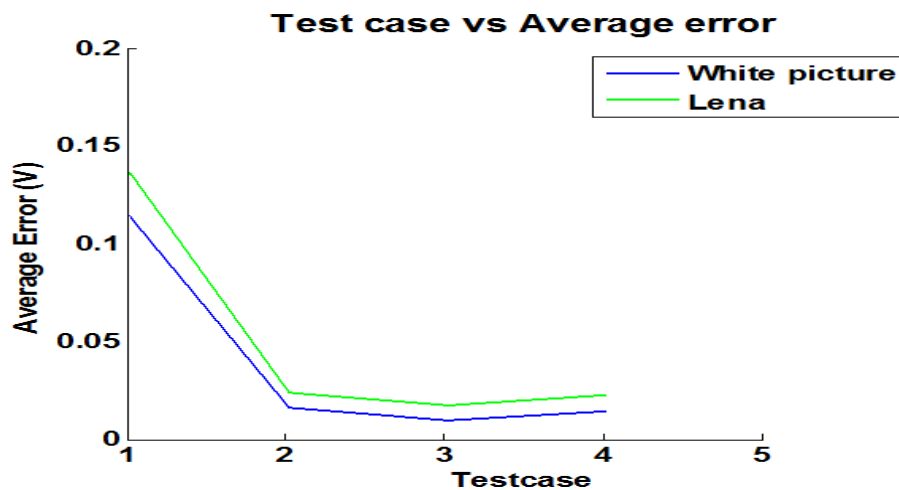


Figure 4.33 Testcase results – Average error

From Figure 4.33, Figure 4.34 and Figure 4.35 we can clearly conclude that test case II or III is efficient in reducing the thermal impact on readout voltage performance. Utilizing these floorplans could translate into a behavior close to output performance under ambient conditions. Area of test case II is 2.7% greater than test case I and test case III area is 5.8%

greater than test case II. In terms of gradient test case II and III remains the same. We choose test case II to achieve the expected performance with meager increase in area. The compact area (test case I), degrades the readout voltage performance of imager, so it has to be avoided.

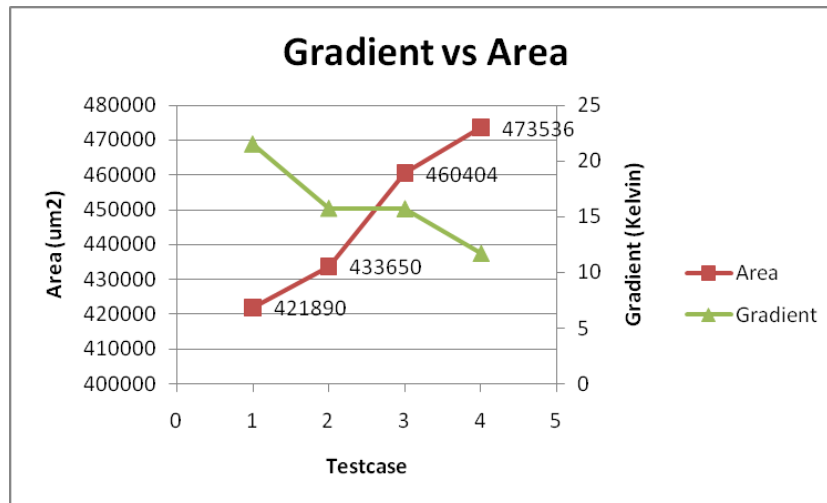


Figure 4.34 Gradient vs Area

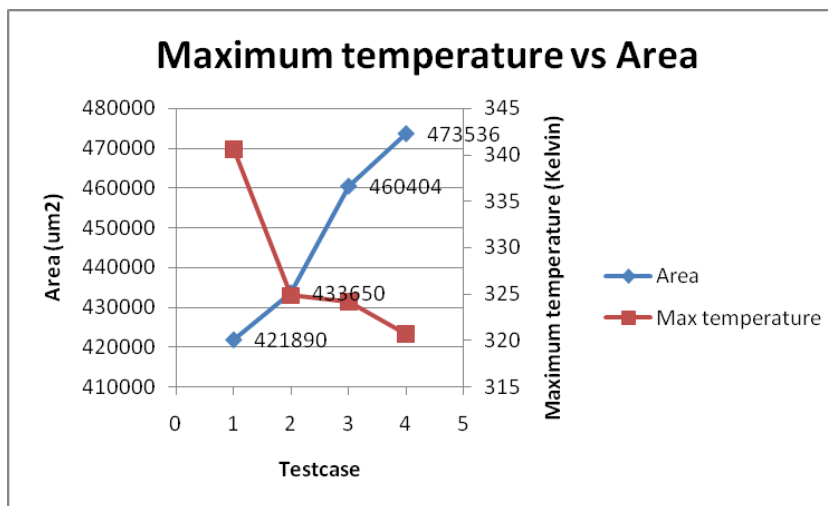


Figure 4.35 Maximum temperature vs Area

Since our interest is mainly on achieving the best readout voltage performance, it is obvious that testcase III achieves the best results.. If the designer has to consider both area and readout voltage performance then Test case II could be selected.

Thus the complete 3D integrated design flow is realized with the following

- 3D Integrated design flow integrating
 - Floorplanner
 - 3D stacked layers
 - Flexible integration of block information
 - Thermal simulation
 - Flexibility in adding material properties
 - Accurate and fast thermal simulation
 - Imager simulation
 - Readout voltage = $f(\text{Temperature}, \text{Light}, \text{Integration time})$
 - Accurate results
 - High speed simulation

This design environment could handle any size of pixel matrix, and groups together floorplanning and thermal simulation, which is missing from existing industrial design flows. The procedure followed in this work could be easily followed to utilize the capability of the model to realize an imager which will meet the performance requirement at early stages of design space exploration. Moving to 3D stacked Imager IC could also be met with this work.

Bibliography

- [1] Meindl, J.D. et al, ” *Beyond Moore's law: the interconnect era.*” Computing in science and engineering, Feb 2003. Vol.5,no.1,p20-24.
- [2] R.S.Patti. et al, ” *Three dimensional integrated circuities and the future of System on chip designs*”. : Proceedings of the IEEE, June 2006. 94, p1214-24.
- [3] S.Tiwar, H.S.Kim et al, ”*Three dimensional integration in silicon electronics*”. :Proceedings IEEE Lester Eastman Conference on High performance Devices, 2002. p24-33.
- [4] W.Davis, E.Oh et al, ” *Application exploration for 3-d integrated circuits: Tcam, fifo, and fft case studies*”. VLSI systems, IEEE Transctions, April 2009. Vol 17, no.4, pp496-506.
- [5] W.Huang, M.Stan et al, ” *Interaction of scaling trends in processor architecture and cooling.*” Semi-therm, Feb 2010. pp.198-204.
- [6] F.Frantz, L.Labrak, I.O'Connor, ”*3D IC Floorplanning: Automating optimization setting and exploring new thermal-aware management techniques*”.: Microelectronics journal, June 2012, Vol. 43. Page 423-432, ISSN 0026-2692.
- [7] S.Adya, I.Markov et al, ” *Fixed-outline floorplanning: enabling hierarchical design*”. VLSI systems, IEEE Transaction, Dec 2003, Vol. 11. pp.1120-1135.
- [8] F.Frantz, ” *Multi objective 3D floorplanner.*” INL internal report, October 2010.
- [9] K.Skadron, K.Sankaranarayanan, S.Velusamy, D.Tarjan, M.R.Stan and W.Huang, ” *Temperature-Aware Microarchitecture: Modeling and Implementation.*” March 2004, ACM Transactions on Architecture and Code Optimization, pp. 1(1):94-125.
- [10] J.Cong, J.Wei, Y.Zhang et al, ” *A thermal- driven floorplanning for 3D ICs*”: ICCAD. IEEE Computer Society / ACM, 2004. pp. 306–313.

- [11] L. Xiao, S. Sinha, J. Xu, and E. Young et al, “Fixed-outline thermal-aware 3d floorplanning.” ASP-DAC, Jan 2010. pp 561-567.
- [12] S.Mendis, S.E.Kemeny, E.Fossum et al, [Online], Bookshelf format. <http://vlsicad.eecs.umich.edu/BK/>.
- [13] The MCNC Benchmark Problems for VLSI Floorplanning [online]. Available <http://www.mcnc.org>

Chapter 5

Conclusion

In recent years, there has been significant focus on the development of CMOS image sensors (CIS) due to their advantages in cost, system size and power consumption, leading to market dominance in consumer applications such as digital cameras, camcorders, mobile phones, web cameras, toys as well as space and security imaging. However, in spite of these rapid developments, market pull towards higher resolution for improving image quality by averaging and for zooming, is increasingly difficult to achieve. On one hand, CMOS technology scaling promises further minimization, higher performance and lower power consumption; on the other hand, it poses additional challenges in achieving good image quality due to the reduced voltage swing, scaling induced noises and the degraded photo-responsivity.

Driven by these concerns, the emergence of 3D integration technology is appropriate for CIS. This technology allows a higher degree of freedom for the designer to move blocks to layers other than that of the pixel matrix. This solution meets the market demand (smaller pixel footprint, increased pixel matrix size, low delay etc.) and further solves scaling issues by allowing various functions to be assigned to appropriate technologies in a heterogeneous stack of layers. However, the shift to 3D technology remains a major problem, due to (i) design challenges due to a lack of methodology and (ii) performance issues due to thermal aspects.

5.1 Summary and discussion of achievements

In this thesis, we address the methodology issue with a top-down modeling approach, subsequently refining the resulting system level model using bottom-up refinement. During the bottom-up refinement procedure we also developed a 3D integrated image sensor thermal design flow to address the thermal issues. The research work (Figure 5.1) is based in the following order:

- Top-down design methodology
- Bottom-Up refinement
 - Image sensor thermal model
- 3D integrated thermal design flow

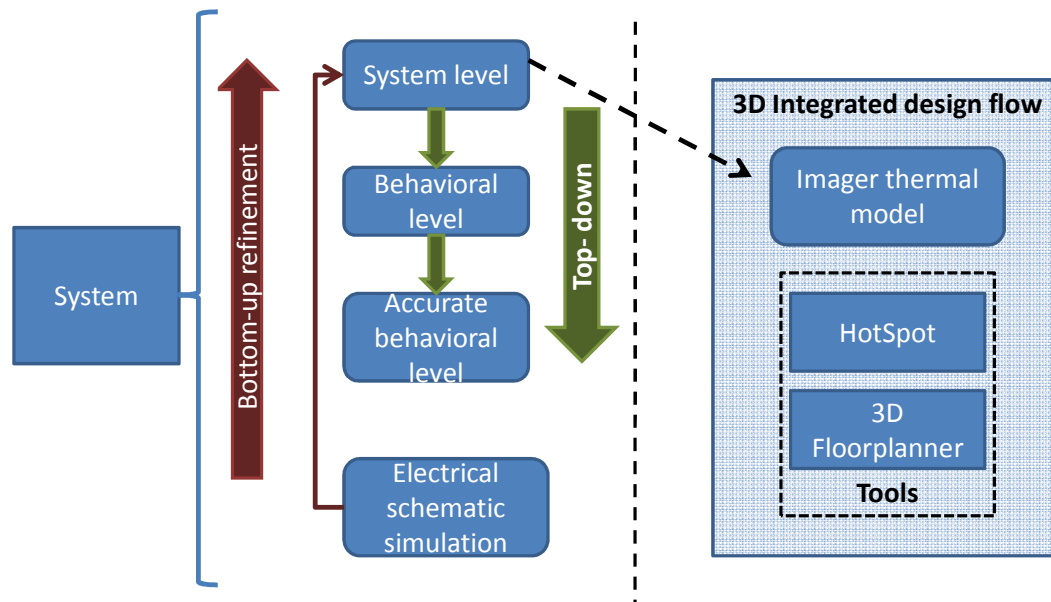


Figure 5.1 High level flow diagram

Top-down design methodology

In this part of the work, we developed flexible models supporting a top-down (TD) design methodology. Models are developed at different abstraction levels in a TD approach in order to analyze the system and for synthesizing the system. These models are optimized with respect to the intended functionality and help in the early stages of design space exploration.

We focused our research work specifically on the pixel matrix and ADC block to prove the hierarchical modeling approach. During this work we formulated the TD approach based on parameter dependency graphs and segregated all the performance/parameter pairs into abstraction levels. The models developed are optimized and can be tuned according to the changes in the system performance requirements. All the models developed from system level down to the lower levels respected the system specifications.

In the top-down design methodology the propagation to each lower level respected a system level performance value. To explore the overall system performance we extended our work with a Pareto-front methodology.

Pareto-front methodology

The drawback of the top-down approach is that the derived requirements may not be feasible (for the available technology). To overcome this limitation, we used the Pareto-front methodology to perform

- Exploration of the entire design space at system level
- Inclusion of limitations at lower levels into system-level design space
- Easy visualization of the tradeoff between various performances

This methodology was successfully proved using the pixel matrix block and we computed the Pareto-front of the pixel matrix design.

Bottom-up refinement

In the top-down approach, the models utilized the ambient (300K) temperature condition. Moving to a 3D stacked IC required a detailed study on the thermal issues and refinement of the system level model using the data extracted from the transistor level to evaluate the system performance degradation due to temperature. This refinement step is used in system validation or system exploration.

Image sensor thermal model

The image sensor thermal model was developed using the following steps:

- **Electrical simulation**

Exhaustive data generation using electrical simulation is performed covering the full range of operation of the imager.

- **Modeling based on surface fitting methodology**

Firstly, realized simple model fitting was carried out with the data obtained from the electrical simulation using two independent variables (temperature and light intensity) to prove the methodology. The work was subsequently extended to volume fitting with three independent variables (temperature, light intensity and integration time) to cover the entire range of operation of image sensor. A pre-validation step was performed to validate the model at random values of temperature and integration time to select the lowest order of fitting capable of achieving the desired accuracy.

- **SystemC Model**

A scalable SystemC based pixel matrix module was developed with an image processing toolbox to decode a picture and convert it into light intensity values. It is also equipped with thermal map reading/writing features. After these initial tool development steps, the pre-validated model was integrated into the SystemC environment to output the readout voltage as a function of temperature, light intensity and integration time. In the current form, the model can simulate from third to sixth order of fitting.

- **Tradeoff analysis**

After integration of the fitted model into SystemC, we performed a post-validation step to analyze the simulation time with respect to various orders of fitting. This part of the work clearly pointed out the tradeoff between simulation time and accuracy. For example: simulation time of 256*256 pixel matrix is 240ms (third order fitting) with relative error of under 1.047% compared to 630ms simulation time (sixth order fitting) with relative error of 0.042%.

- **Validation**

An extensive validation step was performed to prove the robustness of the model with 128*128 and 256*256 pixel *lena* pictures. Furthermore, it was also validated with a uniform (white) picture at 350K temperature to prove the reliability of this model even in extreme (bright light) system operating condition.

- **Simulation time**

Finally, the model was used to simulate at the system level. A first conclusion is that the model has a good simulation speed-up (500,000X) compared to conventional simulation performed using Spice-based simulators at the electrical level. It also adheres to the accuracy criterion (relative error of 4% in 256*256 pixel matrix size) to ensure no change in the intensity level at the output. This model can simulate accurately at system level and take into account inter-pixel variability.

The image sensor thermal model has the capacity to simulate accurately with low simulation time, but used in the initial development a homogeneous temperature distribution. To solve this issue, a 3D integrated thermal design flow was realized with the following features.

3D-Integrated thermal design flow

A 3D integrated thermal design flow was realized in order to couple the thermal map generated from this model as an input to the thermal-aware imager model. The 3D integrated thermal design flow was also used in the design cycle to help adjust the placement of blocks in underlying layers according to their power density and in order to minimize their impact on the imager performance.

This design flow integrated a 3D floorplanner (Parquet) and a thermal simulator (HotSpot) to explore the use of many layers in a 3D stacked imager to support greater freedom of movement. This movement is to enable the movement of high-power blocks away from temperature-sensitive areas or layers in the final placement. At the end of this placement, we generate the thermal map of each layer of the chip.

This generated thermal map is utilized in the image sensor thermal model to simulate the realistic behavior of the imager. This work has been validated with several test cases showing the importance of different scenarios and their impact on imager performance. At the end of this work a tradeoff between area and temperature impact was studied.

Thus this research work has accomplished a hierarchical design approach with an imager as application. As part of the bottom-up refinement, a detailed study of the thermal impact on the imager performance was made along with the development of a fast image sensor thermal simulator.

5.2 Future perspectives

In general, the presented work and results show the feasibility of the top-down approach and further improvements using bottom-up refinement. This does not mean the work is complete. There remains much to be resolved and included in the modeling and design aspects. First and foremost is running the synthesis cycle for different technologies and for different blocks in order to apply the approach more globally. All through this work, AMS 0.35 μm is used. Further extension in the models is necessary in case different technologies are utilized. Pareto-front methodology is realized only for the pixel matrix. This work can be extended to the complete system.

In this work, only a 3T-APS architecture is used to prove our methodology. Future work is necessary to realize different architectures such as 4T, 2.5T, 1.75T and 1.5T APS. Detailed study on readout circuitry, blooming, cross-talk, variability of process parameters specific to imagers is necessary. This work mainly concentrated on the pixel matrix and ADC - other blocks such as CDS, column amplifier and ISP can be modeled.

The image sensor thermal model was developed with a fixed sizing of all three transistors and the photodiode. The model can be extended in terms of variable transistor sizing as function of temperature. Developing such a system-level model will be very useful to analyze performance improvements along with thermal aspects. The existing model can be improved to study High Dynamic Range (HDR) imaging at the system level. Since the model has low simulation time, it can act as a good starting point to analyze the behavior of output image when we combine several images taken at both low light and bright light condition. This model can also be used to realize software-based localized corrections near the region of high temperature. Furthermore this model can be scaled to higher than 8 bits resolution of ADC. According to the thermal model accuracy we have the model could be scaled upto 12 bits (quanta of $552\mu\text{V}$). Moving to higher order of fitting can be investigated to realize 14 bits resolution.

With respect to the 3D integrated thermal design flow, the work has been validated only with ami33 benchmark. It can be validated with other benchmarks, and can further be realized with temperature values measured from a real prototype or with a realistic imager floorplan. Automating the floorplanner flow, HotSpot simulation integrated with the imager sensor thermal model is necessary. In the current state, the best floorplan is chosen manually. This can be extended by automating the design flow to run all the design scenarios to choose the best scenario.

Appendix I

Surface fitting

Linear model Poly55:

$$\begin{aligned} f(x,y) = & p00 + p10*x + p01*y + p20*x^2 + p11*x*y + p02*y^2 + p30*x^3 + p21*x^2*y \\ & + p12*x*y^2 + p03*y^3 + p40*x^4 + p31*x^3*y + p22*x^2*y^2 \\ & + p13*x*y^3 + p04*y^4 + p50*x^5 + p41*x^4*y + p32*x^3*y^2 \\ & + p23*x^2*y^3 + p14*x*y^4 + p05*y^5 \end{aligned}$$

where x is normalized by mean 325 and std 17.21

and where y is normalized by mean 100 and std 63.73

$$\text{Readout voltage} = \begin{pmatrix} \text{Coeff}_1 \\ \vdots \\ \text{Coeff}_m \end{pmatrix} * (\text{Temperature} \quad \text{Light intensity}) \begin{pmatrix} 0 & 0 \\ 1 & 0 \\ 0 & 1 \\ \vdots & \vdots \\ 5 & 5 \end{pmatrix}$$

Coefficients (with 95% confidence bounds):

$$\begin{aligned} p00 &= 1.476 \quad (1.467, 1.485) \\ p10 &= -0.1947 \quad (-0.2186, -0.1707) \\ p01 &= -0.3462 \quad (-0.3642, -0.3283) \\ p20 &= -0.2592 \quad (-0.2768, -0.2416) \\ p11 &= 0.01739 \quad (0.005897, 0.02888) \\ p02 &= 0.04104 \quad (0.02717, 0.05492) \\ p30 &= -0.1561 \quad (-0.1976, -0.1145) \\ p21 &= -0.004089 \quad (-0.0234, 0.01522) \\ p12 &= -0.03417 \quad (-0.05046, -0.01787) \\ p03 &= -0.03004 \quad (-0.05194, -0.008143) \\ p40 &= -0.0286 \quad (-0.03588, -0.02131) \\ p31 &= 0.03224 \quad (0.02743, 0.03705) \\ p22 &= 0.01212 \quad (0.007916, 0.01631) \end{aligned}$$

Appendix

p13 = 0.002916 (-0.001316, 0.007149)
p04 = -0.006102 (-0.01129, -0.0009186)
p50 = 0.002591 (-0.01246, 0.01764)
p41 = 0.0216 (0.01425, 0.02894)
p32 = 0.01899 (0.0135, 0.02448)
p23 = 0.005364 (0.0003773, 0.01035)
p14 = 0.001424 (-0.0038, 0.006647)
p05 = 0.005851 (-0.000859, 0.01256)

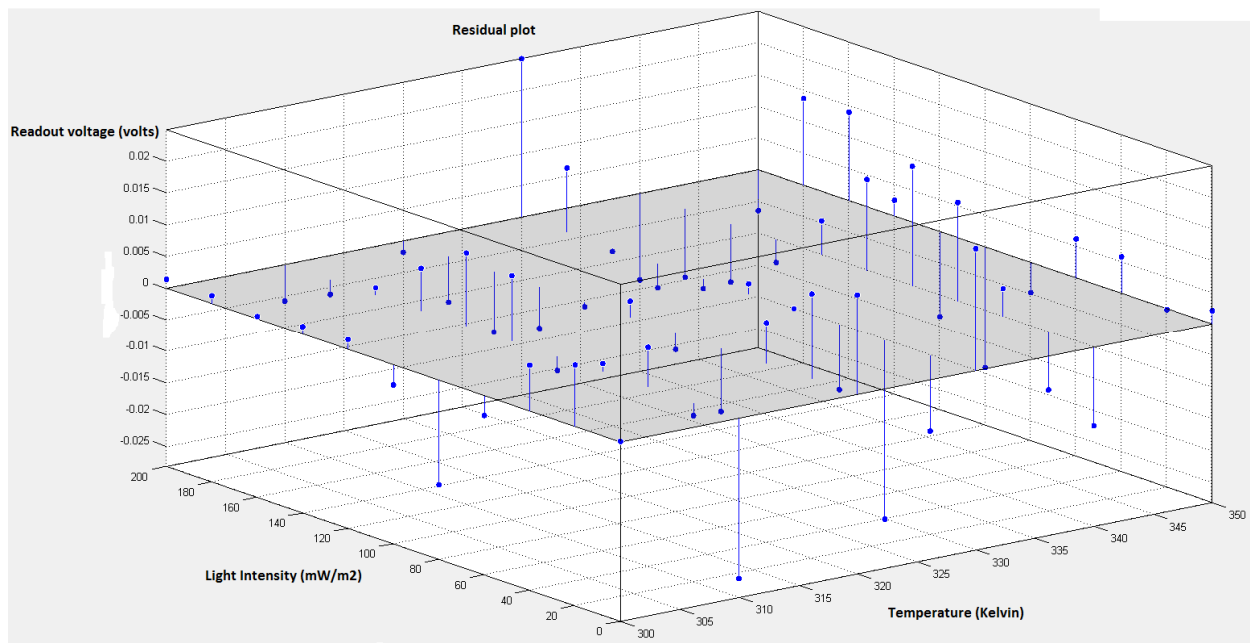
Goodness of fit:

SSE: 0.006929

R-square: 0.9997

Adjusted R-square: 0.9996

RMSE: 0.01241



Appendix II

Volume fitting

```

%% Reshape data for fitting.
% Y vector is the voltage as column.
%To model photo diode discharge voltage output
%Y = [ photoout10ms(:); photoout8ms(:); photoout6ms(:); photoout4ms(:); photoout2ms(:) ];
%To model pixel readout voltage
Y = [ readout10ms(:); readout8ms(:); readout6ms(:); readout4ms(:); readout2ms(:)];
% X vector is [ Tint, Light, Temp ].
NSamples = numel( photoout10ms );
X(:,1) = [ 10*ones( NSamples, 1 ); 8*ones( NSamples, 1 ); 6*ones( NSamples, 1 ); 4*ones(
NSamples, 1 ); 2*ones( NSamples, 1 ) ];
l = 1;
for k=1:5
    for i=1:length(Light)
        for j=1:(length(Temperature))
            X(l,2) = Light(i);
            X(l,3) = Temperature(j);
            l=l+1;
        end
    end
end
end

%% Filter out the points that are too low.
THRESHOLD = 0.1;
X( Y < THRESHOLD, : ) = [];
Y( Y < THRESHOLD ) = [];

%% Try a polynomial fit.
path( path, 'runePoly' );
% Dimensions of the problem.
NVAR = size( X, 2 );
NORDER = 6;           %order of the fitting

% Call the function to fit a polynomial.
[ polyCoeff, output, XPS, YPS ] = doFittingIteration( NORDER, X, Y );
% Get the function to evaluate the polynomial.
[ hPolyEval, ~, ~, ~, orderMatrix ] = getEvaluationFunction( NORDER, NVAR );

%% Do some plots.
Tint = linspace( 2, 10, 5 );
NGRID = 30;
for i=1:length( Tint )

```

Appendix

```

iLight = linspace( 0, 0.2, NGRID );
iTemp = linspace( 300, 370, NGRID );
iTint = Tint(i);
[ iLL, iTT ] = meshgrid( iLight, iTemp );
iY = max( hPolyEval( [ iTint*ones( size(iLL(:)) ) iLL(:) iTT(:) ], polyCoeff, XPS, YPS ), 0
);
% Reshape the output.
iY = reshape( iY, NGRID, NGRID );
surfc( iLL, iTT, iY );hold 'on'
view( 116, 20 ); axis( [ min(iLight) max(iLight) min(iTemp) max(iTemp) 0 3.5 ] );
fr(i) = getframe((gcf) );
end

%% Compute the residuals.
Ypoly = hPolyEval( X, polyCoeff, XPS, YPS );
R = Y - Ypoly;
Rrel = R ./ Y;
% Plot histogram.
figure(1);plot( R );
figure(2);
plot( Y );
hold 'on';
plot( Ypoly, 'm' );

Modeldata=[orderMatrix polyCoeff];
%% Validation of data with low level simulation.
Inputtemperature = 300;
Inputtint = 2;
[ hPolyEval, ~, ~, ~, orderMatrix ] = getEvaluationFunction( NORDER, NVAR );
for j = 1:256
    Readout (j,1) = 0 ;
    Rout_2ms_300K_4thorder_LUT(j,1)=0;
    RGB(j,1)=(j-1);
    Light (j,1) = (j-1)* 0.2/255;
    Readout(j,1) = hPolyEval([Inputtint,Light(j,1),Inputtemperature], polyCoeff, XPS, YPS)
end

```

Appendix

Third order fitting data

Photodiode discharge voltage				Readout voltage			
Tintegrat	Light	Temperature		Tintegrati	Light	Temperatu	Coeff
0	0	0	0.34355	0	0	0	0.3358
1	0	0	-0.07814	1	0	0	-0.0937
2	0	0	0.0671	2	0	0	0.0564
3	0	0	-0.0241	3	0	0	-0.0094
0	1	0	-0.46009	0	1	0	-0.5317
1	1	0	-0.11106	1	1	0	-0.125
2	1	0	0.01339	2	1	0	0.02
0	2	0	0.06725	0	2	0	0.0807
1	2	0	-0.017	1	2	0	-0.0225
0	3	0	-0.0255	0	3	0	-0.0295
0	0	1	-0.36934	0	0	1	-0.3532
1	0	1	-0.23197	1	0	1	-0.2379
2	0	1	0.04714	2	0	1	0.0484
0	1	1	0.10033	0	1	1	0.1083
1	1	1	-0.00205	1	1	1	0.0021
0	2	1	-0.05375	0	2	1	-0.0539
0	0	2	-0.50579	0	0	2	-0.5103
1	0	2	-0.1609	1	0	2	-0.1687
0	1	2	0.02536	0	1	2	0.0242
0	0	3	-0.21771	0	0	3	-0.2176

Appendix

Fourth order fitting data

Photodiode discharge voltage				Readout voltage			
Tintegratio	Light	Temperatu	Coeff	Tintegratio	Light	Temperatu	Coeff
0	0	0	0.340354	0	0	0	0.3292
1	0	0	-0.07404	1	0	0	-0.0843
2	0	0	0.006273	2	0	0	0.0117
3	0	0	-0.02064	3	0	0	-0.0094
4	0	0	0.00943	4	0	0	0.0025
0	1	0	-0.46392	0	1	0	-0.5409
1	1	0	-0.13839	1	1	0	-0.1547
2	1	0	0.019439	2	1	0	0.0218
3	1	0	-0.00142	3	1	0	-0.0037
0	2	0	0.081314	0	2	0	0.1033
1	2	0	-0.01901	1	2	0	-0.0248
2	2	0	0.005346	2	2	0	0.005
0	3	0	-0.02609	0	3	0	-0.0269
1	3	0	0.008619	1	3	0	0.0106
0	4	0	-0.00441	0	4	0	-0.0075
0	0	1	-0.35883	0	0	1	-0.336
1	0	1	-0.09655	1	0	1	-0.0936
2	0	1	0.046441	2	0	1	0.0447
3	0	1	-0.00926	3	0	1	-0.0087
0	1	1	0.089926	0	1	1	0.111
1	1	1	-0.00401	1	1	1	-0.0103
2	1	1	0.001615	2	1	1	0.0003
0	2	1	-0.04846	0	2	1	-0.0525
1	2	1	0.014025	1	2	1	0.013
0	3	1	0.015379	0	3	1	0.0137
0	0	2	-0.37921	0	0	2	-0.3881
1	0	2	-0.17613	1	0	2	-0.1831
2	0	2	0.034536	2	0	2	0.032
0	1	2	0.024246	0	1	2	0.0268
1	1	2	0.013682	1	1	2	0.0104
0	2	2	-0.0047	0	2	2	-0.0074
0	0	3	-0.23402	0	0	3	-0.2339
1	0	3	-0.08455	1	0	3	-0.0911
0	1	3	-0.01114	0	1	3	-0.0168
0	0	4	-0.07518	0	0	4	-0.0729

Appendix III

3D integrated design flow - Tool I/O Configuration

Floorplanner I/O

The GSRC Bookshelf format [12] as used in the Parquet floorplanner is readable and can be used to easily extract information from the text file. This helps to facilitate integration of this tool into another design flow. The following description relates to the writing/reading rules of the each text file. The first line of each file is reserved for version information.

Block declaration (.blocks)

This is defined by the first three lines with the number of hard blocks, soft blocks and terminals.

NumSoftRectangularBlocks : Integer Value

NumHardRectilinearBlocks : Integer value

NumTerminals : Integer value

Each block and its terminals are declared as one per line. For example a hard block is defined by the number of vertices (always 4, since we consider rectangular polygons as is usual in most floorplanners) and the coordinates of these vertices. Each vertex is written in the form (float, float)

<blockName> hardrectilinear 4 <vertex1> ... <vertex 4>

Terminals have no dimension since their role at this level is merely to indicate connectivity:

<terminalName> terminal

Placement information (.pl)

The placement file contains the coordinates of the blocks and terminals. For optimization, the correct position of terminals is needed, since the blocks will be set to random positions. The description resembles as follows

<blockName> <x> <y> [DIMS=(<w>,<l>) : <orient> : <layer>]

where: x x coordinate (lower left corner)

y	y coordinate (lower left corner)
w	width of the block
l	length of the block
orient	orientation of the block (Figure Error! No text of specified style in document.-1)
layer	layer number where the block is placed



Figure **Error! No text of specified style in document.-1** Orientation :
 North (N), Flipped-North (FN), West(W), Flipped-West(FW) (other
 possible orientations are: S,FS,E,FE)

Connectivity information (.nets)

Connectivity information (.nets) is defined as follows with first two lines as

NumNets : Integer value

NumPins : Integer value

Nets are declared in blocks starting with

NetDegree : integer value, number of pins in the net

Followed by one pin declaration per line in the form

```
<blockName> <direction> [: %<xoffset> %<yoffset> : <layer>]
```

where

blockName block or terminal to which pin belongs

direction (I)input, (O)utput or (B)idirectional

xOffset horizontal offset of the pin from the center of the block (%)

yOffset vertical offset of the pin from the centre of the block (%)

layer layer number where the pin (block) is placed

Net weights (.wts)

The length of the net is multiplied by the weight during wirelength computation. Setting a net weight is equivalent to setting a bus width. Each line assigns a weight to a net.

Appendix

<netName> <value>

Power information (.power)

This is defined in first two lines of the file with input values and a scaling factor.

PowerType : (P) for input in W, (D) for power density in W/m²

Scale : multiplication factor

Then the following line assigns a value to each block. Terminals are not considered.

<blockName> <value>

Stack technology (.stack)

Each line links a device technology to an integration technology. Technologies are referenced by their tags.

<deviceTechnologyTag> <integrationTechnologyTag>

HotSpot I/O

Simulator configuration (.config)

For the purpose of optimization the only necessary parameters are:

Parameter	Feature
-ambient	ambient temperature in K
-r convec	convection resistance
-t sink	heatsink thickness
-k sink	heatsink thermal conductivity
-t spreader	spreader thickness
-k spreader	spreader thermal conductivity

Layer Constraint File (.lcf)

Layers are described in block of 7 lines. The parameters are entered in the following order, one per line.

Parameter	Value
layer number	layer index (sequential, starting at 0)

Appendix

lateral heat flow	(Y)es, (N)o
power dissipation	(Y)es, (N)o, yes for active layers
specific heat capacity	not used (transient analysis)
thermal resistivity	in m ² K/W
thickness	in m

PUBLICATIONS (JOURNAL, CONFERENCES, COLLOQUE, WORKSHOPS)

- **Viswanathan.V**, Frantz.F, Feng.Z, Navarro.D, O'Connor.I, 3D-IC: Fast imager thermal modeling, Elsevier Journal of System Architecture (JSA). (*Under review*)
- Feng.Z, **Viswanathan.V**, Navarro.D, O'Connor.I, **Image sensor matrix high speed simulation**, ICECS 2012 , (*Accepted – To be presented on Nov 14-16,2012, Venice, Italy*)
- **Viswanathan.V**, Frantz.F,Feng.Z,Navarro.D,O'Connor.I, **Imager temperature modeling**,WASC Smart Camera, Clermont Ferrand, France, April 5-6,2012
- **Viswanathan.V**,Labrak.L, Frantz.F,Navarro.D,O'Connor.I, “**Model based design of Imager using abstraction segregated parameter dependency graphs**”, NEWCAS 2011, Bordeaux, France, June 26-29,2011.
- Navarro.D, Feng.Z, **Viswanathan.V**,Carrel.L,O'Connor.I, “**Imager tool box for CMOS image sensors in Cadence ADE**”, Demset 2011, Orlando, Florida, USA, November 29th – December 2nd, 2011
- **Viswanathan.V**, Labrak.L, Frantz.F, Navarro.D, O'Connor.I,” **Model based design of Imager pixel matrix**”, GDR SoC SiP colloque 2011, Lyon, France.
- **Viswanathan.V**, Labrak.L, Frantz.F, Navarro.D, O'Connor.I, “**Model based design of Imager pixel matrix**”, GDR Green SoC SiP colloque 2011, Montpellier, France. (*Poster*)
- **Viswanathan.V**, Navarro.D,Labrak.L, O'Connor.I, “**High level modeling of Imager IC**”, GDR SoC SiP 2010, Paris, France.
- **Viswanathan.V**, Navarro.D,Labrak.L, O'Connor.I, “**High level modeling of Imager IC**”, D43D workshop 2010, Lausanne, Switzerland. (*Poster*)
- Frantz.F,Labrak.L,**Viswanathan.V**, O'Connor.I, “**Heterogeneous 3D design methods and tools**”, FETCH 2010, Chamonix, France. (*Poster*)